NASA TECHNICAL MEMORANDUM

NASA TM X-3559

NASA TM X-3559

AERODYNAMIC CHARACTERISTICS AT MACH NUMBERS FROM 0.6 TO 2.16 OF A SUPERSONIC CRUISE FIGHTER CONFIGURATION WITH A DESIGN MACH NUMBER OF 1.8

Barrett L. Shrout

Langley Research Center
Hampton, Va. 23665

NATIONAL AERONAUTICS AND SPACE ADMINISTRATION • WASHINGTON, D. C. • SEPTEMBER 1977

1. Report No.	2. Government Accession No.	3. Recipient's Catalog No.
NASA TM X-3559		

4. Title and Subtitle	5. Report Date
AERODYNAMIC CHARACTERISTICS AT MACH NUMBERS FROM 0.6 TO 2.16 OF A SUPERSONIC CRUISE FIGHTER CONFIGURATION WITH A DESIGN MACH NUMBER OF 1.8	September 1977
	6. Performing Organization Code

7. Author(s)	8. Performing Organization Report No.
Barrett L. Shrout	L-11604
	10. Work Unit No. 505-11-21-03

9. Performing Organization Name and Address	11. Contract or Grant No.
NASA Langley Research Center Hampton, VA 23665	

12. Sponsoring Agency Name and Address	13. Type of Report and Period Covered
National Aeronautics and Space Administration Washington, DC 20546	Technical Memorandum
	14. Sponsoring Agency Code

15. Supplementary Notes

16. Abstract

An investigation was made in the Langley 8-foot transonic pressure tunnel and the Langley Unitary Plan wind tunnel, over a Mach number range of 0.6 to 2.16, to determine the static longitudinal and lateral aerodynamic characteristics of a model of a supersonic-cruise fighter. The configuration, which is designed for efficient cruise at Mach number 1.8, is a twin-engine tailless arrow-wing concept with a single rectangular inlet beneath the fuselage and outboard vertical tails and ventral fins. It had untrimmed values of lift-drag ratio ranging from 10 at subsonic speeds to 6.4 at the design Mach number. The configuration was statically stable both longitudinally and laterally.

17. Key Words (Suggested by Author(s))	18. Distribution Statement
Aerodynamic characteristics Supersonic fighter Wind-tunnel tests	Unclassified - Unlimited Subject Category 02

19. Security Classif. (of this report)	20. Security Classif. (of this page)	21. No. of Pages	22. Price*
Unclassified	Unclassified	77	$5.00

* For sale by the National Technical Information Service, Springfield, Virginia 22161

AERODYNAMIC CHARACTERISTICS AT MACH NUMBERS FROM 0.6 TO 2.16 OF A SUPERSONIC CRUISE FIGHTER CONFIGURATION WITH A DESIGN MACH NUMBER OF 1.8

Barrett L. Shrout
Langley Research Center

SUMMARY

An investigation has been made in the Langley 8-foot transonic pressure tunnel at Mach numbers from 0.6 to 1.2 and in the Langley Unitary Plan wind tunnel at Mach numbers of 1.6, 1.8, and 2.16 to determine the static longitudinal and lateral aerodynamic characteristics of a model of a supersonic-cruise fighter, number four in a series of Langley configurations. This configuration is a twin-engine tailless arrow-wing concept with a single rectangular inlet beneath the fuselage. It has outboard vertical tails and ventral fins and is designed for efficient cruise performance at a Mach number of 1.8. Three inlet-diverter combinations were tested. The results of the investigation show untrimmed values of lift-drag ratio ranging from 10 at subsonic speeds to 6.4 at the design Mach number. The elevons were not very effective as pitch control devices at supersonic speeds. The configuration was statically stable both longitudinally and laterally.

INTRODUCTION

The National Aeronautics and Space Administration, in cooperation with the United States Air Force and with various groups in industry, is involved in a study of the feasibility of supersonic-cruise, fighter-type aircraft. A number of concepts are under study at the Langley Research Center, varying from those designed for low supersonic cruise speeds with good transonic-supersonic maneuver characteristics to those designed for mid to high supersonic cruise speeds with limited maneuver potential. In all the study concepts, however, efficient supersonic cruise is a primary goal. Some indication of the scope and goals of the program and some early experimental results may be found in reference 1.

The present configuration concept is designed with emphasis on efficient supersonic cruise and with little consideration given to maneuver capability. Because it is a point-design supersonic-cruise concept, its aerodynamic design is similar, in many respects, to that of a supersonic transport; thus, much of the technical knowledge and design methodology which evolved during the National Supersonic Transport Program of the 1960's is applicable.

The configuration discussed in this report is number four of a series of supersonic-cruise fighter concepts being studied at the NASA Langley Research Center. This configuration is a twin-engine tailless arrow-wing concept with a single rectangular inlet beneath the fuselage. The engine exits are located

in proximity to the wing trailing edge to utilize the potential benefits of the jet-flap effect of thrust vectoring (ref. 2). The underside of the fuselage aft of the inlet was maintained relatively flat to provide a platform for the carriage of store pallets. The configuration has outboard vertical tails and ventral fins and was designed for efficient cruise performance at a Mach number of 1.8.

An investigation of the static longitudinal and lateral aerodynamic characteristics of this concept at subsonic-transonic speeds and at supersonic speeds was conducted in the Langley 8-foot transonic pressure tunnel and the Langley Unitary Plan wind tunnel, respectively. The test Reynolds number was 6.56×10^6 per meter over the entire speed range. The results of that investigation are presented herein.

SYMBOLS

Force and moment data are referenced to the body axis system except for lift and drag data which are referenced to the stability axis system. The moment reference center for the model is located at 52.222 cm from the model nose and -4.763 cm from the horizontal reference line.

The model was designed and built and data were reduced using the U.S. Customary system of units; however, all data are presented using the SI system of units.

A aspect ratio

b wing span (68.58 cm)

c chord, cm

$\bar{c}$ wing reference chord (42.60 cm)

C_D drag coefficient, $\frac{\text{Drag}}{qS}$

$C_{D,c}$ chamber drag coefficient, $\frac{\text{Chamber drag}}{qS}$

$C_{D,i}$ internal drag coefficient, $\frac{\text{Internal drag}}{qS}$

C_L lift coefficient, $\frac{\text{Lift}}{qS}$

C_{L_α} lift-curve slope at $C_L = 0$, per deg

C_l rolling-moment coefficient, $\frac{\text{Rolling moment}}{qSb}$

C_{l_β} effective dihedral parameter, per deg

C_m pitching-moment coefficient, $\frac{\text{Pitching moment}}{qS\bar{c}}$

$C_{m,o}$ pitching-moment coefficient at $C_L = 0$

$\frac{\partial C_m}{\partial C_L}$ longitudinal stability parameter at $C_L = 0$

$\frac{\partial C_m}{\partial \delta_e}$ pitching-moment effectiveness of elevons at $C_L = 0$, per deg

C_n yawing-moment coefficient, $\frac{\text{Yawing moment}}{qSb}$

C_{n_β} directional stability parameter, per deg

C_Y side-force coefficient, $\frac{\text{Side force}}{qS}$

C_{Y_β} side-force parameter, per deg

L/D lift-drag ratio

M Mach number

m/m_∞ mass-flow ratio

q free-stream dynamic pressure, Pa

S wing reference area (1996 cm^2)

x longitudinal distance from nose of model, cm

α angle of attack, deg

β angle of sideslip, deg

δ_e elevon deflection angle, positive when trailing edge is down, deg

Λ leading-edge sweep angle, deg

Model component symbols:

B body

C canopy

U ventral fins

V vertical tails

W wing

Subscripts:

max maximum

min minimum

DESCRIPTION OF MODEL

A three-view sketch of the model is shown in figure 1, and photographs of the model installed in the Langley Unitary Plan wind tunnel are shown in figure 2. The arrow-type wing planform has a continuously curved leading edge out to the leading-edge break at 60 percent of the semispan, beginning as a strake at the nose of the configuration. Outboard of the break, the leading edge is straight and is swept back 45.6°. The wing-camber plane was designed, using the method of reference 3, to minimize drag due to lift. The design parameters included a lift coefficient of 0.12 and a Mach number of 1.8. Details of the outboard vertical tails and ventral fins are shown in figure 3. The vertical tails are toed to an angle which is approximately one-half the theoretical local sidewash angle on the upper surface of the wing at the design lift coefficient (ref. 4). Similarly, the ventral fins are toed at approximately one-half the theoretical local sidewash angle on the lower wing surface.

By using the method of reference 5, a fuselage area distribution was established to reduce total configuration wave drag at the design Mach number. The normal area distribution for the configuration is shown in figure 4. Because the wing and fuselage are blended together, the fuselage is arbitrarily defined to include all of the wing and fuselage inboard of model span station 6.985 cm. The inlet capture area has been removed from the area distribution.

Three inlet-diverter combinations were tested on the configuration. Details of the internal-flow duct inlets and exits and the inlet boundary-layer diverters are included in the appendix.

The model was equipped with elevons along the outboard trailing-edge portion of the wings. These elevons could be set at various deflection angles with appropriate brackets.

Some of the pertinent geometric characteristics of the model are given in table I. In addition, a listing of the computer cards for the numerical model is given in table II. The format for the listing is described in reference 6. The numerical model is for the wind-tunnel model as constructed, measured on a three-axis dimension recording machine.

TESTS AND INSTRUMENTATION

Tests were conducted in the Langley 8-foot transonic pressure tunnel at Mach numbers from 0.6 to 1.2 and in the Langley Unitary Plan wind tunnel at Mach numbers 1.6, 1.8, and 2.16. The tests were conducted under the following conditions:

Mach number	Stagnation pressure, kPa	Stagnation temperature, K	Reynolds number, per meter
0.6	63.839	322.04	6.56×10^6
.8	53.655	↓	↓
.9	50.883		
.95	49.959		
1.2	47.877		
1.6	54.606	338.71	
1.8	58.399	↓	
2.16	68.430		

Transition-inducing strips of carborundum grit (No. 80 for subsonic-transonic Mach numbers and No. 60 for supersonic Mach numbers) were applied at appropriate distances back from the leading edges to all airfoil-shaped surfaces, the inlet, and the configuration nose. The grit size was selected according to the method of reference 7 to insure fully turbulent flow over the model. Forces and moments on the model were measured by means of a six-component strain-gage balance, which was contained within the model and connected through a supporting sting to the permanent model-actuating systems in the wind tunnels. Corrections were made to the data for both internal flow and chamber drag. Internal mass flow through the engine ducts was measured by means of exit rakes. Details of the internal-flow measurements and corrections made to the data to account for internal flow are included in the appendix. Balance-chamber (base) pressure was measured throughout the test program with a pressure transducer connected to a tube attached to the sting and located in the balance cavity. Typical balance-chamber drag corrections (corrected to free-stream static pressure) are shown in figure 5 as a function of angle of attack for the Mach numbers of this investigation.

RESULTS AND DISCUSSION

All of the data in this section are for the model with the diverter-inlet configuration "C" (see appendix).

The vertical tails, ventral fins, and canopy were all independently removable from the model. The effects of these model components on the longitudinal aerodynamic characteristics of the configuration are shown in figure 6. At subsonic speeds, little or no effect occurs on lift or moment due to the addition of the various components except at the highest angles of attack tested. The drag, and thus L/D, is most affected by the addition of the vertical tails,

which have substantial wetted area and thus substantial skin-friction drag. At supersonic speeds, addition of the canopy results in a slight increase in $C_{m,o}$, except at $M = 2.16$, and a significant increase in drag, the latter attributable to a strong shock at the fuselage-canopy intersection. At the design Mach number of 1.8, addition of the canopy reduced $(L/D)_{max}$ by about 0.7 or about 10 percent. Addition of the vertical tails and ventral fins resulted in little drag increase at the design lift coefficient of 0.12 and no penalty in $(L/D)_{max}$. This result is due to the toeing of the vertical tails and ventral fins to produce a thrust component due to sidewash, thus canceling out the skin friction and wave drag of these components.

The effect of various settings of the elevon pitch controls is shown in figure 7. At subsonic speeds, the variation of pitching moment with lift coefficient tends to be linear except at the highest values of lift coefficient where a pitch-up trend can be seen. The lift-curve slopes are also linear except at high values of C_L where a slight loss of lift with increasing angle of attack can be observed for Mach numbers greater than 0.6. The increments due to control deflection in both pitching moment at constant C_L and lift at constant angle of attack are essentially constant except for an elevon deflection of -15^o at the higher subsonic Mach numbers. At supersonic Mach numbers, within the test angle-of-attack range, the lift and moment curves are well-behaved, with no tendency towards stall or pitch-up, and the increments due to control deflection are essentially constant. It is apparent that, at supersonic Mach numbers, the elevons are not very effective as pitch controls, producing small changes in moment and substantial drag changes as the control deflections are varied.

Some of the longitudinal parameters ($\delta_e = 0^o$) are shown in figure 8 as a function of Mach number. The pitching moment at $C_L = 0$, $C_{m,o}$, is positive at all Mach numbers but decreases above Mach 1.2. The stability parameter $\partial C_m/\partial C_L$ varies by about 10 percent of $\bar{c}$ over the range of Mach numbers. Because the minimum level of static stability shown is 16 percent of $\bar{c}$, the stability level could be considerably reduced, still retaining positive stability and moving the trim points for the various control settings in figure 7 to higher values of C_L.

The maximum lift-drag ratio $(L/D)_{max}$ varies from about 10 at subsonic speeds to about 6.4 at the design Mach number of 1.8. Trimmed values of $(L/D)_{max}$ would be somewhat below the curve shown depending on the stability level selected. The value of minimum drag increases about 50 percent over the transonic Mach number range and decreases slightly with increasing supersonic Mach number. The lift-curve slope C_{L_α} increases at subsonic speeds and, after a rapid increase in the transonic Mach number range, decreases with increasing Mach number above $M = 1.2$.

As mentioned earlier, several analytic methods were used in the design of this configuration. In addition, an analysis was made of the theoretical longitudinal aerodynamic characteristics at supersonic speeds. The method of reference 8 was used to compute wave drag at zero lift, the method of reference 9 was used to compute drag due to lift and moment characteristics, and the method of reference 10 was used to compute skin-friction drag. No accounting was made for grit drag which is small, or drag of the diverter, other than its inclusion

in the volume distribution for computing wave drag. The magnitude of the diverter drag is unknown. In addition, the mass-flow ratio for the duct flow was assumed to be 1.0. Although this assumption is not valid (see appendix), the increment due to spillage is estimated to be a maximum of 3 to 4 drag counts (0.0003-0.0004). Additionally, it was assumed that there was no leading-edge suction on the wing.

The comparison between theory and experiment at supersonic speeds is shown in figure 9. Although the effects of elevon deflection on the longitudinal characteristics were computed, they have been omitted for clarity. The theoretical drag polars are in good agreement with the experimental data at $M = 1.2$ and $M = 1.6$ while, for the higher supersonic Mach numbers, the drag is underpredicted at high values of lift coefficient.

A comparison between experiment and theory for some of the longitudinal parameters is shown in figure 10. The analytic methods tend to overpredict the various moment characteristics over the Mach number range. The stability level $\partial C_m/\partial C_L$ is overpredicted by a maximum of about 3.5 percent of $\bar{c}$. The theoretical values of $C_{m,o}$ and $\partial C_m/\partial \delta_e$ are considerably greater than the values of experimental data, although the differences tend to decrease with increasing Mach number. The theoretical lift-curve slope C_{L_α} and levels of $C_{D,min}$ are in good agreement with experimental values.

LATERAL-DIRECTIONAL AERODYNAMIC CHARACTERISTICS

The effects of components on the lateral-directional aerodynamic characteristics at subsonic-transonic speeds are shown in figure 11. The open symbols are for $\beta = 0^o$, while the filled symbols are for $\beta = 3^o$. For the configuration at $\beta = 3^o$, a stabilizing rolling moment and, as expected, a negative side force were measured for all combinations of components; however, the vertical tails were required to produce a stabilizing yawing moment. Addition of the ventral fins and canopy had little effect on the lateral-directional aerodynamic characteristics at Mach numbers below 1.2.

Figure 12 shows that at supersonic speeds the variation of the lateral-directional aerodynamic characteristics with sideslip angle is essentially linear for both angles of attack shown. The sideslip derivatives as a function of angle of attack at supersonic speeds are shown in figure 13. Positive roll stability and negative side-force derivatives exist regardless of the component configuration. Positive directional stability depends on the addition of the vertical tails, except at Mach number 2.16 where the ventral fins also are required to provide positive stability. It must be noted that an aft movement of the moment reference point, to reduce longitudinal stability and consequently trim drag, may be limited by directional stability considerations because such an aft movement would also reduce directional stability.

CONCLUSIONS

An investigation was conducted in the Langley 8-foot transonic pressure tunnel and the Langley Unitary Plan wind tunnel, over a Mach number range of

0.6 to 2.16, to determine the static longitudinal and lateral aerodynamic characteristics of a model of a supersonic cruise fighter. The following conclusions are indicated:

1. The untrimmed maximum lift-drag ratio varied from 10 at subsonic speeds to 6.4 at the design Mach number of 1.8.

2. At subsonic speeds, the pitching-moment and lift curves were essentially linear, with a slight pitch-up trend and loss of lift, respectively, at the higher values of lift coefficient. At supersonic speeds, the pitching-moment and lift curves were well-behaved, with no tendency towards pitch-up or stall, within the test angle-of-attack range.

3. The longitudinal stability was positive and exhibited a small variation over the Mach number range, so that an aft movement of the moment reference point would reduce trim drag while maintaining adequate longitudinal stability.

4. For the moment center selected, the complete configuration was stable for all the lateral and directional parameters, although marginal in directional stability at a Mach number of 2.16. Aft movement of the moment reference point would adversely affect the lateral-directional parameters.

Langley Research Center
National Aeronautics and Space Administration
Hampton, VA 23665
August 4, 1977

APPENDIX

BOUNDARY-LAYER DIVERTERS AND INTERNAL-FLOW CHARACTERISTICS

The propulsion inlet and exit system was simulated on the model by flow-through ducts. Some of the details of these ducts and the boundary-layer diverters used in conjunction with the duct system are shown in figure A1. The inlet is rectangular, with the sidewall leading edge swept back 50°. A vertical web splits the inlet and is carried back to a transition region where each duct changes to a circular cross section. The inside diameter of each duct was reduced near the exit to choke the flow. A double 6.5° compression wedge, attached to the upper surface inside the inlet, was used during part of the test program.

Three configurations of the diverter shown in figure A1 were tested. Diverter A was a 20° half-angle wedge, which began at the lip of the inlet upper surface. The depth of the diverter was equal to the estimated boundary-layer displacement thickness at the inlet lip for the wind-tunnel test conditions. The compression wedge was used with diverter A.

A schlieren photograph of the configuration with diverter A is shown in figure A2. This photograph, taken at the design Mach number 1.8, shows a strong shock ahead of the inlet. It was thought that this shock was the result of a detached shock at the diverter or choking of the flow in the diverter channels.

Diverter B was designed to eliminate both problems. The wedge was cut back 1.27 cm from the lip of the inlet. Although this modification increased the initial wedge angle, it was felt that the detached shock would remain aft of the inlet lip and thus not affect the duct flow. In addition, the boundary-layer gutter was considerably enlarged to prevent the flow from choking in the channels. Some recontouring of the underside of the forebody was done to smooth the loft lines in the vicinity of the inlet. The schlieren photograph of configuration B in figure A2 shows that there was still a strong shock ahead of the inlet. The compression ramp was also used for this configuration.

The third diverter configuration used on the model is identified as diverter C in figure A1. This diverter was developed in the shape of a cusp with the starting angle small enough to prevent shock detachment, although the included angle in the middle part of the diverter is greater than the original wedge angle. Because of a lack of structural support, the compression ramp was removed for configuration C. Schlieren photographs of configuration C in figure A2 show that a strong shock was still present in front of the inlet. The schlieren photograph taken at $M = 1.2$ in the Langley 8-foot transonic pressure tunnel shows a normal shock well ahead of the inlet. Further modifications would have required a major redesign of the inlet; thus the test program was conducted with the C diverter-inlet configuration. The data presented in the main body of this report are for the C configuration.

Although the problem with the inlet shock was not solved through diverter modifications, some differences in the internal-flow characteristics between

the three configurations were observed. Internal-flow data were obtained for configurations A and C at subsonic-transonic speeds and for configurations A, B, and C at supersonic speeds. The data were taken by means of a rake at each duct exit. Each rake consisted of 13 total head tubes and 4 static tubes arranged so that each tube was centered in a proportional segment of the total duct area. Approximately 2 percent of the exit area was occupied by the rake tubes. The rakes were attached to the sting and model to minimize relative movement between the rake and duct exit under aerodynamic loads. Because the arrangement fouled the balance, tunnel runs separate from the force-test runs were required to measure internal flow.

Results from the internal-flow test runs are presented in figures A3 through A5. The mass-flow ratio for the various configurations as a function of angle of attack is shown in figure A3. At subsonic and transonic speeds configuration C, without the internal compression ramp, had slightly higher values of mass-flow ratio. There was little variation with angle of attack in this Mach number range. At supersonic Mach numbers, there were again only slight differences, with configuration C generally having slightly lower mass-flow ratios than the other configurations. At supersonic speeds mass-flow ratio increased with increased angle of attack, undoubtedly due to precompression of the inlet flow by the forebody.

Internal-drag coefficients are shown in figure A4. There are small differences in the internal-drag coefficients for the various configurations, and these differences tend to decrease with increasing Mach number. There were also small variations of internal drag with angle of attack. The zero angle-of-attack internal drag and total-configuration drag are summarized in figure A5. The cross-hatched curve shows the calculated turbulent skin-friction drag for the internal-duct wetted area at free-stream conditions. At subsonic-transonic speeds, the measured internal-flow drag is less than half of the calculated skin-friction drag.

The total-configuration drag, corrected for internal flow and chamber drag, is shown in the lower half of the figure. Note that configuration C, with the cusped diverter, has about 5 percent more drag than configuration B at the design Mach number. At least part of this drag increase for configuration C can be attributed to spillage, indicated by a slight decrease in mass-flow ratio; however, the cusped diverter itself probably produces more drag because of its larger effective wedge angle.

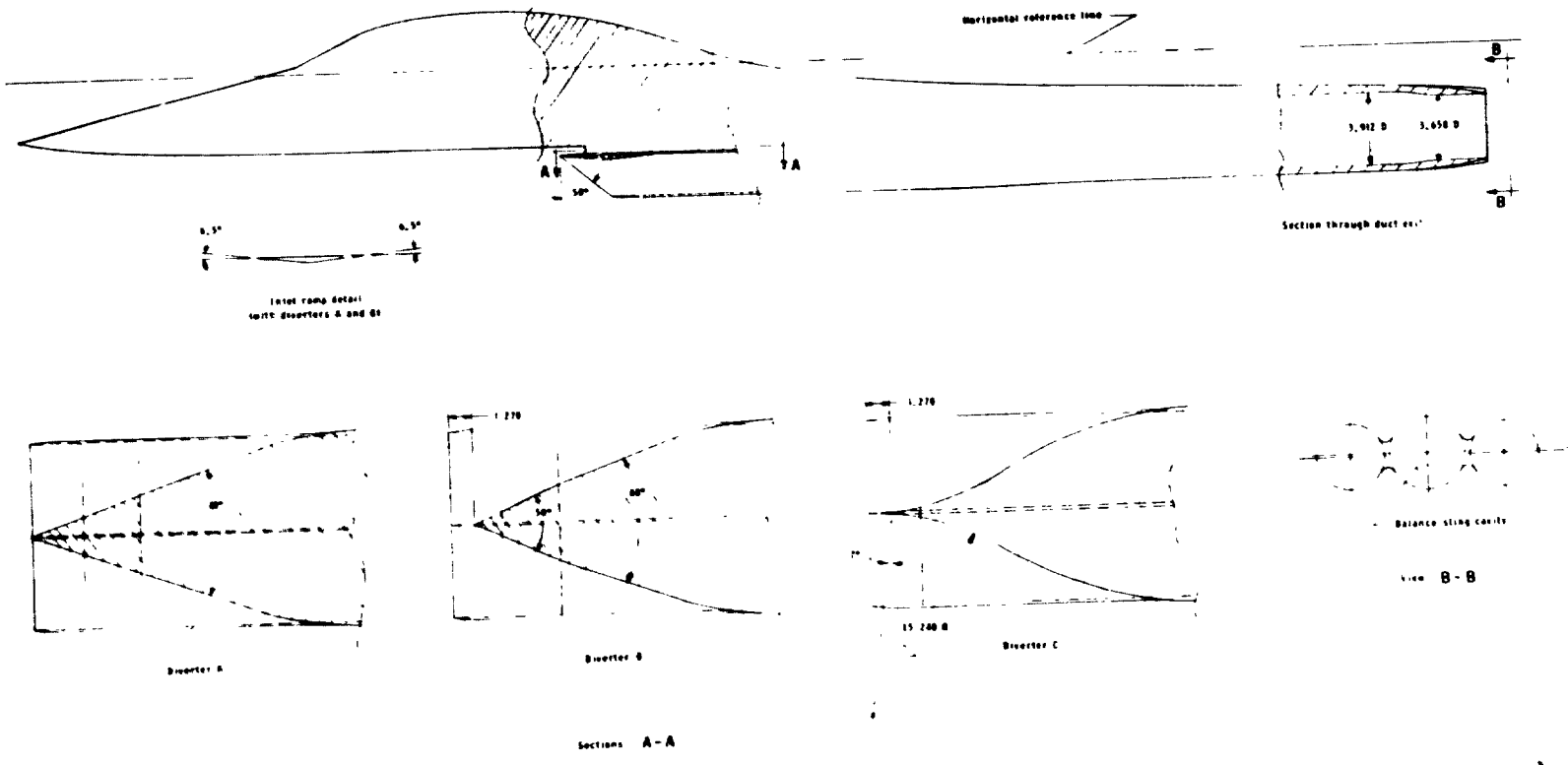

Figure A1.- Details of duct inlet, duct exit, and diverters. (All linear dimensions are in cm.)

APPENDIX

APPENDIX

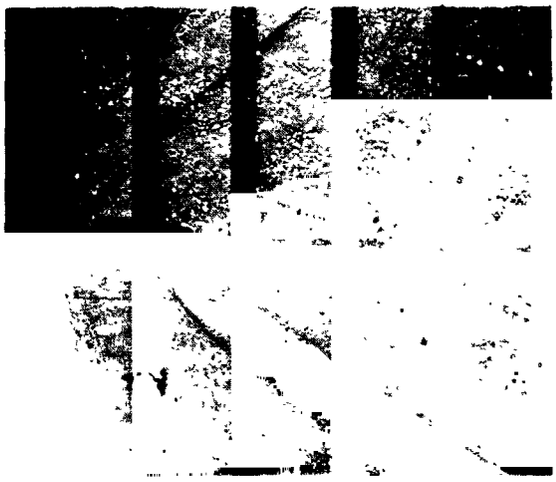

Configuration A; M = 1.8

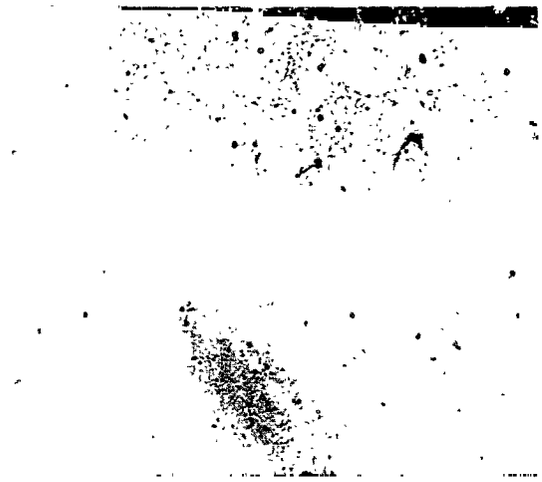

Configuration C; M = 1.2

Configuration B; M = 1.8

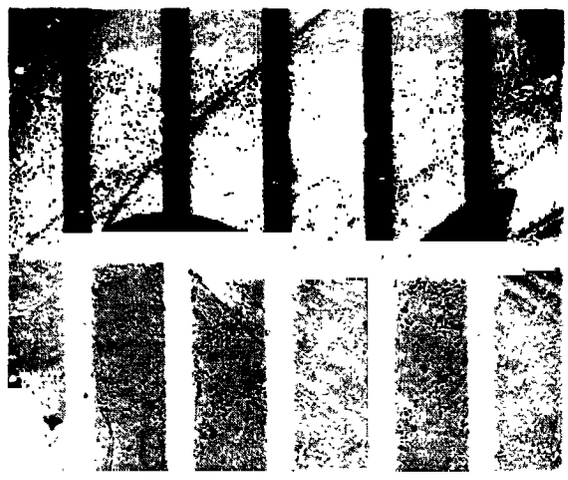

Configuration C; M = 1.8

L-77-267

Figure A2.- Schlieren photographs of the three configurations at $\alpha = 0^{\circ}$.

APPENDIX

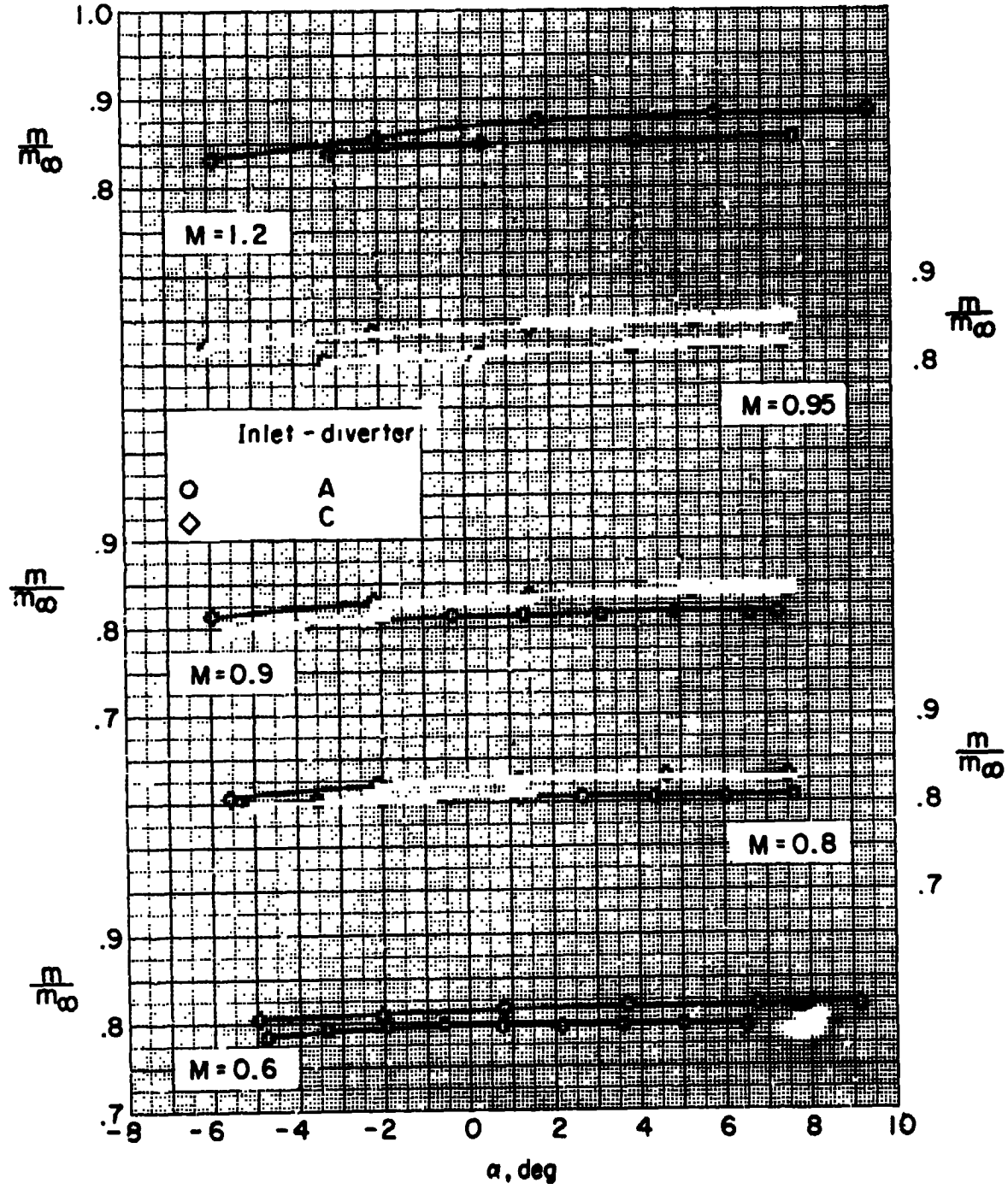

Figure A3.- Variation of mass-flow ratio with angle of attack for various Mach numbers.

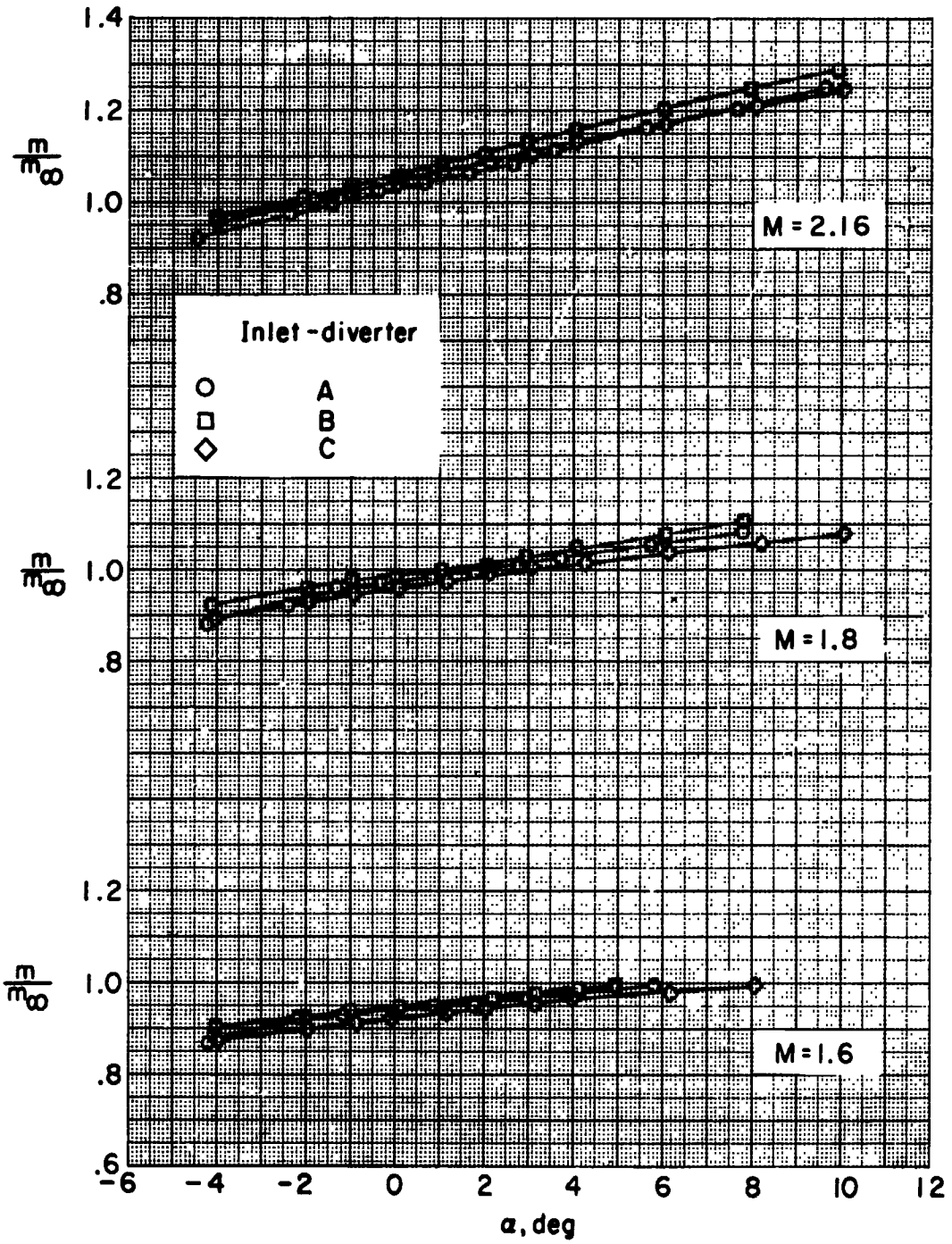

Figure A3.- Concluded.

APPENDIX

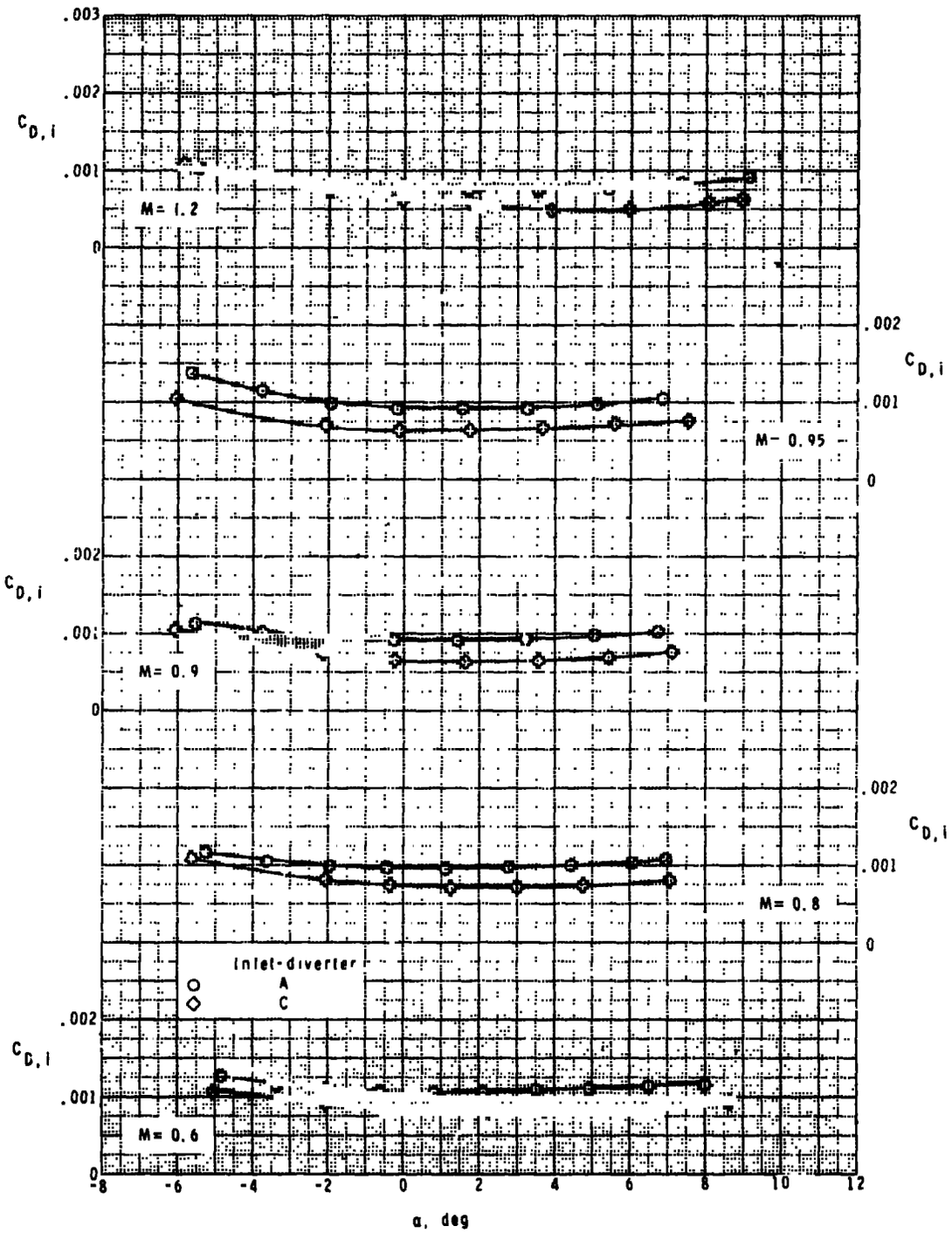

Figure A4.- Variation of internal-flow drag correction with angle of attack for various Mach numbers.

APPENDIX

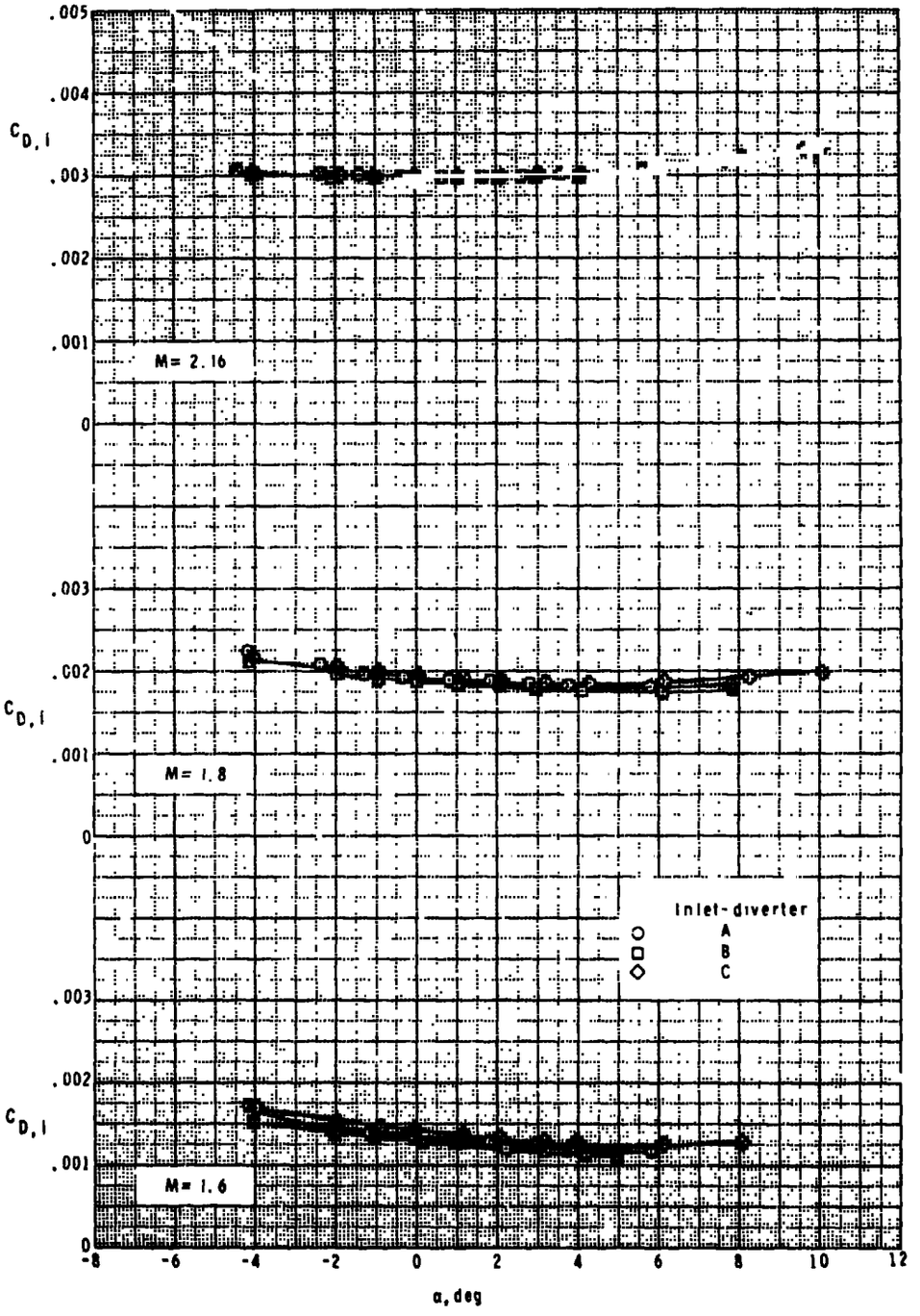

Figure A4.- Concluded.

APPENDIX

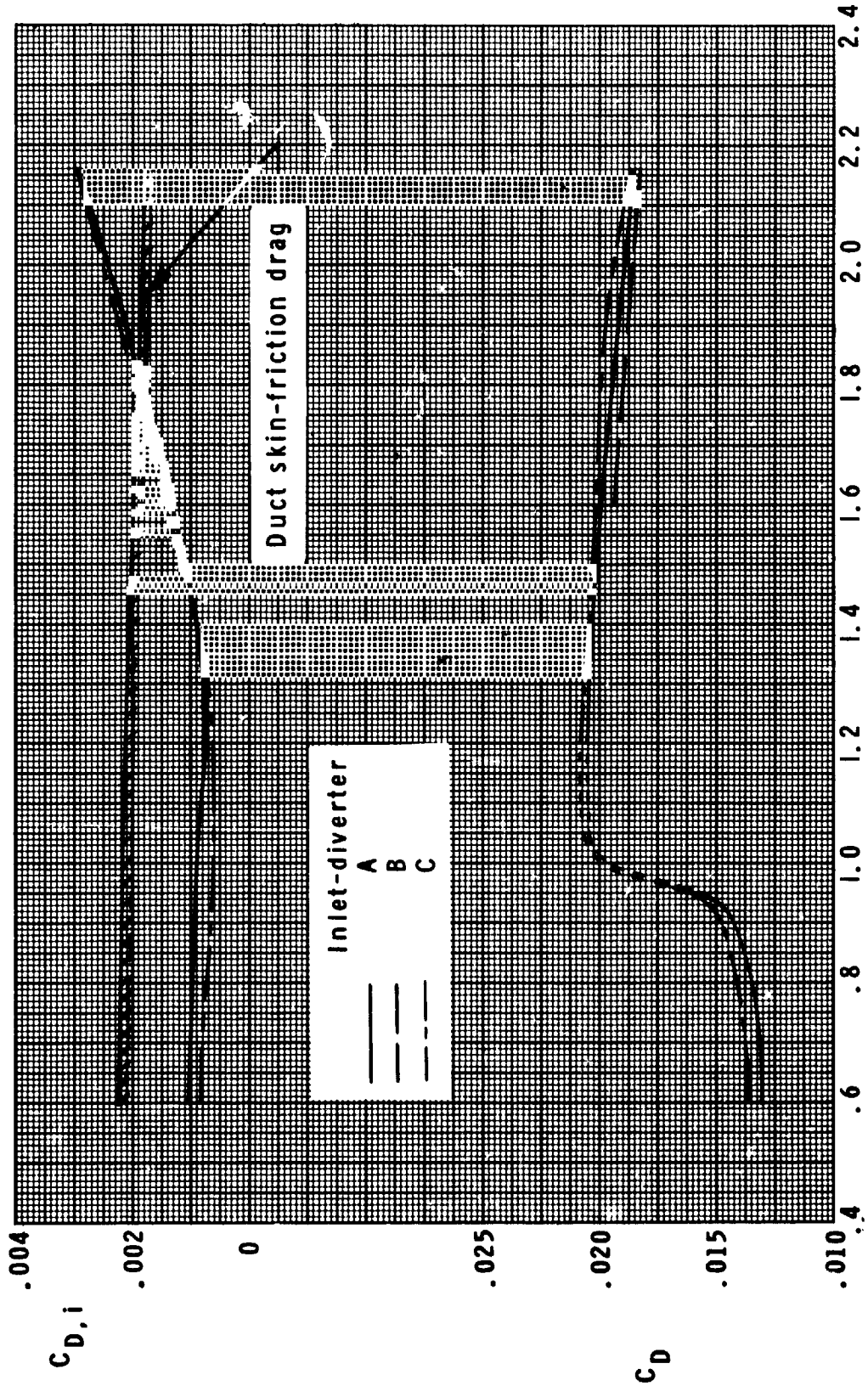

Figure A5.- Variation of duct internal drag and total-configuration drag, at zero angle of attack, with Mach number.

TABLE I.- GEOMETRIC CHARACTERISTICS OF MODEL

Wing:	
A (total planform)	2.356
Leading edge (main wing panel)	Curved
Λ (outboard panel), deg	45.6
$\bar{c}$, cm	42.60
b, cm	68.58
S, cm^2	1996
Airfoil section, main wing panel	See table II
Airfoil section, outboard panel (circular arc), maximum thickness, percent c	3.36
Vertical tail (each):	
A (exposed)	1.905
Λ, deg	54.45
Mean geometric chord, cm	10.0
Semispan, cm	9.528
Area, cm^2	95.29
Airfoil section (circular arc) maximum thickness, percent c	2.5
Ventral fin (each):	
A (exposed)	0.39
Λ, deg	54.45
Mean geometric chord, cm	13.08
Semispan, cm	2.54
Area, cm^2	33.23
Airfoil section (circular arc) maximum thickness, percent c	2.5
Miscellaneous:	
Inlet capture area (total), cm^2	23.486
Exit area (total), cm^2	21.015
Chamber area, cm^2	21.46

TABLE II.- NUMERICAL MODEL (SEE REF. 6)

```
SUPERSONIC CRUISE FIGHTER NUMBER 4
  1  1  1      1          8 18  4 16 10 20  8 23  8 25  8          2 10
1996.00                                                                    REFA
0.0     .5     1.5     5.0     10.     20.     30.     40.     50.     60.  YAF10
65.     70.     75.     80.     85.     90.     95.     100.                XAF18
 27.178  6.985 -1.715 52.118                                               WORG 1
 32.421  8.572 -1.999 47.112                                               WORG 2
 43.244 12.001 -2.667 36.860                                               WORG3
 52.995 15.430 -3.104 27.681                                               WORG4
 57.473 17.145 -3.277 23.490                                               WORG5
 65.626 20.554 -3.429 17.051                                               WORG6
 65.626 20.574 -3.429 17.051                                               WORG7
 79.057 34.290 -3.335 10.478                                               WORG8
  0.000   .023   .081   .211   .221  -.051  -.470  -.975 -1.377 -1.908  TZ 1
 -2.129 -2.324 -2.504 -2.687 -2.858 -3.020 -3.183 -3.315                  TZ 1
  0.000   .028   .086   .234   .251   .030  -.348  -.787 -1.242 -1.681  TZ2
 -1.892 -2.096 -2.286 -2.477 -2.647 -2.799 -2.972 -3.104                  TZ2
  0.000   .023   .069   .206   .279   .216   .020  -.239  -.528  -.836  TZ3
  -.988 -1.138 -1.288 -1.435 -1.575 -1.712 -1.844 -1.968                  TZ3
  0.000   .018   .048   .165   .239   .262   .185   .063  -.089  -.264  TZ4
  -.356  -.450  -.544  -.640  -.734  -.825  -.917 -1.003                  TZ4
  0.000   .013   .041   .124   .216   .264   .231   .163   .063  -.053  TZ5
  -.117  -.180  -.246  -.310  -.376  -.439  -.505  -.566                  TZ5
  0.000   .005   .013   .041   .081   .109   .104   .081   .046   .005  TZ6
  -.015  -.041  -.066  -.091  -.119  -.147  -.173  -.201                  TZ6
  0.000   .005   .013   .041   .081   .109   .104   .081   .046   .005  TZ7
  -.015  -.041  -.066  -.091  -.119  -.147  -.173  -.201                  TZ7
  0.000  -.003  -.008  -.028  -.056  -.074  -.079  -.074  -.061  -.041  TZ8
  -.023  -.008   .013   .030   .051   .071   .094   .117                  TZ8
0.0     .338   .509   .628   .750   .944  1.078  1.166  1.220  1.244    WORD 1
1.216  1.15   1.049   .912   .738   .528   .283   0.0                     WORD 1
0.0     .354   .534   .658   .786   .990  1.130  1.222  1.278  1.304    WORD2
1.274  1.206  1.099   .956   .774   .554   .296   0.0                     WORD2
0.0     .400   .602   .743   .888  1.118  1.276  1.379  1.442  1.472    WORD3
1.438  1.362  1.241  1.079   .873   .626   .334   0.0                     WORD3
0.0     .462   .694   .857  1.022  1.287  1.470  1.589  1.662  1.696    WORD4
1.657  1.569  1.430  1.243  1.006   .721   .385   0.0                     WORD4
0.0     .470   .706   .873  1.042  1.311  1.498  1.619  1.694  1.728    WORD5
1.688  1.598  1.457  1.266  1.025   .734   .392   0.0                     WORD5
0.0     .457   .687   .849  1.013  1.275  1.457  1.574  1.646  1.680    WORD6
1.642  1.554  1.416  1.231   .996   .714   .382   0.0                     WORD6
0.0     .034   .098   .319   .605  1.075  1.411  1.613  1.680  1.613    WORD7
1.529  1.411  1.260  1.075   .857   .605   .319   0.0                     WORD7
0.0     .034   .098   .319   .605  1.075  1.411  1.613  1.680  1.613    WORD8
1.529  1.411  1.260  1.075   .857   .605   .319   0.0                     WORD8
  0.000   .953  1.905  3.810  5.649  7.620  9.525 11.430 14.605 15.240  XFUS  10
  0.000  0.000  0.000  0.000  0.000  0.000  0.000  0.000  0.000  0.000  Y     1
  0.000  0.000  0.000  0.000  0.000  0.000                               Y     1
 -3.310 -3.310 -3.310 -3.310 -3.310 -3.310 -3.310 -3.310 -3.310 -3.310  Z     1
 -3.310 -3.310 -3.310 -3.310 -3.310 -3.310                               Z     1
  0.000   .094   .196   .272   .323   .399   .450   .475   .503   .503  Y     2
   .503   .376   .272   .145   .043  0.000                               Y     2
 -3.640 -3.614 -3.538 -3.487 -3.386 -3.284 -3.233 -3.208 -3.157 -3.106  Z     2
 -3.056 -3.056 -3.056 -3.056 -3.078 -3.078                               Z     2
  0.000   .178   .305   .434   .460   .536   .615   .640   .716   .792  Y     3
   .640   .513   .335   .183   .056  0.000                               Y     3
 -3.716 -3.665 -3.566 -3.439 -3.312 -3.185 -3.109 -3.033 -2.957 -2.908  Z     3
 -2.880 -2.855 -2.852 -2.878 -2.875 -2.875                               Z     3
```

TABLE II.- Continued

0.000	.178	.406	.559	.663	.790	.866	.942	1.146	1.222	Y	4
1.120	.841	.584	.330	.127	0.000					Y	4
-3.995	-3.945	-3.816	-3.716	-3.538	-3.155	-2.977	-2.926	-2.774	-2.697	Z	4
-2.621	-2.545	-2.520	-2.494	-2.494	-2.469					Z	4
0.000	.406	.739	.917	.993	1.120	1.171	1.247	1.425	1.476	Y	5
1.374	1.019	.688	.406	.229	0.000					Y	5
-4.199	-4.097	-3.868	-3.716	-3.538	-3.002	-2.901	-2.799	-2.596	-2.520	Z	5
-2.393	-2.342	-2.215	-2.139	-2.088	-2.062					Z	5
0.000	.518	.978	1.133	.311	1.491	1.516	1.570	1.697	1.798	Y	6
1.671	1.316	.935	.655	.249	0.000					Y	6
-4.326	-4.176	-3.896	-3.747	-3.442	-2.753	-2.652	-2.576	-2.423	-2.322	Z	6
-2.195	-2.068	-1.913	-1.732	-1.605	-1.577					Z	6
0.000	.493	1.001	1.435	1.615	1.847	1.900	1.976	2.205	2.230	Y	7
2.106	1.671	1.214	.782	.427	0.000					Y	7
-4.376	-4.277	-4.051	-3.772	-3.442	-2.603	-2.451	-2.400	-2.197	-2.096	Z	7
-1.968	-1.814	-1.582	-1.351	-1.199	-1.171					Z	7
0.000	.841	1.450	1.755	1.935	2.164	2.266	2.367	2.621	2.697	Y	8
2.621	1.882	1.374	.866	.406	0.000					Y	8
-4.481	-4.300	-3.995	-3.767	-3.437	-2.520	-2.393	-2.266	-2.139	-1.986	Z	8
-1.831	-1.501	-1.222	-.917	-.765	-.739					Z	8
0.000	1.095	2.012	2.240	2.367	2.799	2.901	3.028	3.437	3.564	Y	9
3.360	2.672	1.831	1.196	.610	0.000					Y	9
-4.455	-4.326	-3.995	-3.919	-3.767	-2.443	-2.164	-2.062	-1.961	-1.755	Z	9
-1.552	-1.196	-.765	-.330	-.076	0.000					Z	9
0.000	1.029	1.971	2.250	2.431	2.791	2.944	3.200	3.658	3.683	Y	10
3.609	3.025	2.060	1.323	.663	0.000					Y	10
-4.427	-4.305	-4.079	-3.876	-3.647	-2.504	-2.200	-2.047	-1.872	-1.768	Z	10
-1.539	-1.283	-.770	-.259	.048	.178					Z	10
15.240	16.192	17.145	19.050	21.438	25.717	27.178	29.528			XFUS	8
0.000	1.001	1.948	2.233	2.441	2.791	2.924	3.101	3.282	3.668	Y	1
3.721	3.647	3.266	2.154	1.146	.968	.765	.485	.231	0.000	Y	1
-4.437	-4.326	-4.061	-3.861	-3.609	-2.494	-2.215	-2.116	-2.042	-1.895	Z	1
-1.768	-1.590	-1.405	-.851	-.198	-.091	-.013	.094	.124	.152	Z	1
0.000	.958	2.007	2.289	2.522	2.896	3.028	3.157	3.310	3.823	Y	2
3.955	3.780	3.475	2.261	1.351	1.125	.925	.546	.213	0.000	Y	2
-4.437	-4.374	-4.110	-3.934	-3.734	-2.515	-2.314	-2.187	-2.088	-1.867	Z	2
-1.715	-1.483	-1.300	-.696	-.097	.213	.498	.681	.737	.739	Z	2
0.000	.032	1.979	2.492	2.751	3.099	3.231	3.490	3.693	4.155	Y	3
4.262	4.135	3.731	2.642	1.554	1.410	1.135	.782	.401	0.000	Y	3
-4.488	-4.399	-4.237	-4.013	-3.686	-2.596	-2.291	-2.090	-2.017	-1.819	Z	3
-1.593	-1.463	-1.227	-.701	-.099	.516	.902	1.161	1.321	1.377	Z	3
0.000	1.128	2.329	2.766	2.974	3.376	3.533	3.741	3.947	4.587	Y	4
4.742	4.694	4.188	3.025	1.836	1.621	1.349	.947	.417	0.000	Y	4
-4.437	-4.379	-4.194	-3.973	-3.747	-2.527	-2.301	-2.101	-1.976	-1.732	Z	4
-1.608	-1.402	-1.138	-.584	.020	.841	1.356	1.796	2.111	2.195	Z	4
0.000	1.468	2.720	3.104	3.366	3.764	3.973	4.178	4.564	5.204	Y	5
5.337	5.210	4.628	3.513	2.093	1.826	1.580	1.102	.599	0.000	Y	5
-4.488	-4.356	-4.221	-4.049	-3.696	-2.527	-2.200	-1.996	-1.798	-1.580	Z	5
-1.402	-1.273	-.983	-.533	.071	1.069	1.763	2.278	2.644	2.781	Z	5
0.000	1.844	3.581	3.813	3.970	4.557	4.790	5.151	5.611	6.477	Y	6
6.530	6.457	5.646	3.868	2.144	1.877	1.585	1.186	.559	0.000	Y	6
-4.463	-4.338	-4.188	-4.089	-3.787	-2.189	-1.913	-1.689	-1.646	-1.608	Z	6
-1.430	-1.250	-.907	-.444	.094	1.041	1.811	2.428	3.000	3.213	Z	6

TABLE II.- Continued

0.000	1.974	3.658	4.018	4.252	4.681	4.994	5.405	5.941	6.833	Y	7
6.990	6.916	6.132	4.049	2.169	1.979	1.709	1.237	.658	0.000	Y	7
-4.463	-4.366	-4.214	-4.067	-3.739	-2.367	-1.913	-1.689	-1.674	-1.737	Z	7
-1.562	-1.306	-.988	-.470	.119	.937	1.681	2.403	2.949	3.137	Z	7
0.000	2.090	3.901	4.310	4.564	5.202	5.354	5.636	6.195	6.988	Y	8
6.988	6.988	6.325	4.232	2.065	1.862	1.504	1.021	.485	0.000	Y	8
-4.437	-4.336	-4.190	-4.090	-3.601	-2.180	-1.970	-1.836	-1.785	-1.811	Z	8
-1.478	-1.199	-.942	-.587	.254	1.123	1.811	2.398	2.830	2.931	Z	8
29.528	30.798	33.337	35.560	38.100	40.640	43.815	48.578			XFUS	8
0.000	4.920	5.000	5.090	5.090	4.890	0.000	0.000	3.848	4.305	Y	1
4.536	5.258	5.946	6.965	6.967	5.977	4.450	3.104	2.062	1.763	Y	1
1.283	.574	0.000								Y	1
-7.260	-7.250	-7.150	-7.090	-5.030	-4.920	-4.900	-4.427	-4.194	-4.094	Z	1
-3.739	-2.037	-1.760	-1.816	-1.181	-.871	-.658	-.168	.244	1.417	Z	1
2.131	2.720	2.901								Z	1
0.000	5.052	5.230	5.283	5.304	5.077	.025	.030	4.318	4.702	Y	A1
4.851	5.436	6.025	6.995	7.000	5.908	4.506	3.211	1.966	1.671	Y	A1
1.194	.587	0.000								Y	A1
-7.346	-7.295	-7.244	-7.066	-4.976	-4.821	-4.872	-4.437	-4.125	-3.950	Z	A1
-3.302	-2.096	-1.847	-1.831	-1.118	-.902	-.683	-.236	.259	1.333	Z	A1
2.002	2.469	2.601								Z	A1
0.000	5.095	5.250	5.304	5.324	5.095	.592	.594	5.154	5.283	Y	2
5.342	5.552	6.012	6.955	6.962	5.946	4.473	3.101	1.732	1.511	Y	2
1.110	.630	0.000								Y	2
-7.381	-7.379	-7.305	-7.051	-4.938	-4.732	-4.740	-4.359	-4.021	-3.716	Z	2
-2.977	-2.370	-2.093	-1.951	-1.161	-1.074	-.780	-.310	.239	1.105	Z	2
1.694	2.004	2.113								Z	2
0.000	5.055	5.260	5.314	5.342	5.116	1.417	1.422	5.253	5.382	Y	A2
5.443	5.679	6.066	7.010	6.998	5.850	4.450	3.104	1.633	1.359	Y	A2
1.031	.551	0.000								Y	A2
-7.396	-7.386	-7.287	-7.056	-4.889	-4.735	-4.737	-4.277	-3.970	-3.795	Z	A2
-2.979	-2.497	-2.273	-2.106	-1.189	-1.173	-.950	-.500	.005	.544	Z	A2
.930	1.242	1.326								Z	A2
0.000	4.956	5.210	5.314	5.331	5.128	2.761	2.766	5.263	5.441	Y	3
5.446	5.756	6.165	6.980	6.988	5.867	4.572	3.150	1.549	1.171	Y	3
.815	.411	0.000								Y	3
-7.381	-7.419	-7.295	-7.117	-4.854	-4.750	-4.729	-4.171	-3.988	-3.861	Z	3
-3.178	-2.718	-2.492	-2.347	-1.328	-1.369	-1.232	-.787	-.267	-.036	Z	3
.173	.404	.406								Z	3
0.000	4.994	5.276	5.382	5.387	5.184	3.937	3.970	5.375	5.479	Y	A3
5.484	5.745	6.132	7.003	7.018	5.817	4.569	3.045	1.445	1.143	Y	A3
.787	.406	0.000								Y	A3
-7.396	-7.417	-7.295	-7.041	-4.821	-4.717	-4.699	-4.138	-4.031	-3.853	Z	A3
-3.396	-3.015	-2.741	-2.550	-1.453	-1.539	-1.443	-1.039	-.582	-.399	Z	A3
-.216	-.081	.025								Z	A3
0.000	4.910	5.291	5.420	5.428	5.250	5.072	5.075	5.354	5.456	Y	4
5.484	5.662	6.020	6.988	6.993	5.720	4.448	2.438	1.346	1.041	Y	4
.658	.251	0.000								Y	4
-7.432	-7.450	-7.325	-6.995	-4.780	-4.679	-4.676	-4.117	-4.092	-3.914	Z	4
-3.686	-3.381	-3.051	-2.878	-1.732	-1.829	-1.722	-1.257	-.947	-.818	Z	4
-.691	-.612	-.584								Z	4
0.000	5.100	5.306	5.484	5.819	5.819	5.819	5.845	5.870	5.870	Y	5
5.895	6.025	6.279	7.018	6.995	5.951	4.780	2.416	1.092	.838	Y	5
.582	.277	0.000								Y	5
-7.432	-7.341	-7.188	-7.010	-4.719	-4.567	-4.567	-4.415	-4.389	-4.211	Z	5
-4.211	-3.780	-3.551	-3.373	-2.177	-2.225	-2.197	-1.786	-1.427	-1.402	Z	5
-1.402	-1.349	-1.349								Z	5

TABLE II.- Concluded

48.578	53.340	60.960	68.580	72.009	75.057	79.296	80.010			XFUS	8
0.000	.638	1.323	2.062	2.774	3.411	4.072	4.912	5.370	5.545	Y	1
5.842	6.325	6.985	6.982	6.574	6.116	5.479	4.768	4.003	3.366	Y	1
2.731	2.093	1.354	.615	0.000						Y	1
-7.407	-7.429	-7.402	-7.399	-7.396	-7.394	-7.391	-7.363	-7.132	-6.393	Z	1
-4.178	-3.515	-3.360	-2.189	-2.192	-2.217	-2.220	-2.172	-2.073	-1.948	Z	1
-1.849	-1.671	-1.471	-1.397	-1.349						Z	1
0.000	.691	1.303	1.989	2.753	3.261	3.846	4.762	5.728	5.979	Y	2
6.431	6.657	7.041	7.036	6.474	5.941	5.329	4.516	3.828	3.241	Y	2
2.553	1.943	1.280	.643	0.000						Y	2
-7.305	-7.277	-7.300	-7.272	-7.267	-7.267	-7.264	-7.234	-6.772	-6.134	Z	2
-4.453	-3.970	-3.815	-2.543	-2.545	-2.548	-2.550	-2.527	-2.428	-2.304	Z	2
-2.154	-1.976	-1.801	-1.676	-1.577						Z	2
0.000	.457	1.095	1.857	2.672	3.284	3.995	4.938	5.674	6.058	Y	3
6.388	6.693	7.026	7.026	6.541	5.804	5.116	4.582	4.097	3.360	Y	3
2.850	2.215	1.374	.688	0.000						Y	3
-7.254	-7.254	-7.254	-7.229	-7.254	-7.254	-7.280	-7.178	-6.820	-6.363	Z	3
-5.039	-4.557	-4.506	-3.155	-3.155	-3.002	-2.799	-2.647	-2.520	-2.342	Z	3
-2.266	-2.139	-2.012	-1.882	-1.857						Z	3
0.000	.782	1.521	2.233	2.667	3.251	3.861	4.674	5.441	5.977	Y	4
6.363	6.594	7.054	7.031	6.345	5.839	5.255	4.569	4.008	3.195	Y	4
2.736	1.999	1.313	.625	0.000						Y	4
-7.178	-7.054	-6.904	-6.779	-6.833	-7.066	-7.247	-7.224	-6.871	-6.391	Z	4
-5.705	-5.070	-4.895	-3.876	-3.696	-3.259	-2.850	-2.565	-2.537	-2.662	Z	4
-2.685	-2.657	-2.398	-2.217	-2.189						Z	4
0.000	.800	1.440	2.027	2.710	3.393	4.234	5.151	5.819	6.236	Y	5
6.472	6.680	6.985	6.995	6.515	6.111	5.735	4.978	4.140	3.172	Y	5
2.456	1.897	1.087	.531	0.000						Y	5
-7.254	-7.137	-6.764	-6.619	-6.906	-7.196	-7.308	-7.092	-6.591	-5.933	Z	5
-5.428	-5.100	-5.103	-4.214	-4.054	-3.693	-3.231	-2.710	-2.573	-2.687	Z	5
-2.934	-2.850	-2.535	-2.350	-2.266						Z	5
0.000	.884	1.656	2.093	2.700	3.406	4.219	5.316	5.756	6.144	Y	6
6.355	6.617	6.972	6.980	6.525	6.251	5.753	5.022	4.237	3.368	Y	6
2.319	1.633	1.054	.472	0.000						Y	6
-7.280	-7.115	-6.667	-6.421	-6.660	-7.051	-7.191	-6.927	-6.553	-6.076	Z	6
-5.517	-5.141	-5.146	-4.610	-4.450	-4.013	-3.294	-2.824	-2.659	-2.799	Z	6
-3.266	-3.028	-2.637	-2.426	-2.393						Z	6
0.000	.914	1.575	2.261	2.794	3.429	4.267	5.029	5.588	5.969	Y	6A
6.198	6.223	6.985	6.985	6.223	6.147	5.817	5.156	4.242	3.226	Y	6A
2.286	1.753	1.270	.610	0.000						Y	6A
-7.220	-7.000	-6.590	-6.360	-6.452	-6.756	-6.909	-6.731	-6.350	-5.893	Z	6A
-5.334	-4.826	-4.826	-4.826	-4.826	-4.293	-3.683	-3.073	-2.896	-3.073	Z	6A
-3.492	-3.201	-2.896	-2.591	-2.515						Z	6A
0.000	.818	1.506	2.245	2.804	3.439	4.176	4.889	5.451	5.784	Y	7
6.010	6.170	6.190	6.120	6.009	5.830	5.359	4.877	4.163	3.221	Y	7
2.304	1.745	1.212	.551	0.000						Y	7
-7.200	-7.040	-6.570	-6.340	-6.420	-6.756	-6.901	-6.801	-6.520	-6.220	Z	7
-5.669	-5.314	-4.933	-4.577	-4.427	-3.912	-3.454	-3.172	-3.090	-3.402	Z	7
-3.603	-3.203	-2.819	-2.591	-2.515						Z	7
67.628	20.574	-3.335	15.240	80.963	20.574	6.193	4.762			FINORG	
0.0	20.	30.	40.	50.	60.	70.	80.	90.	100.	XFIN	
0.0	.695	.938	1.111	1.215	1.250	1.172	.938	.547	0.0	FINORD	
70.564	19.406	-5.918	10.922	67.008	19.406	-3.378	15.240			FINORG	
0.0	20.	30.	40.	50.	60.	70.	80.	90.	100.	XFIN	
0.0	.70	.933	1.116	1.216	1.250	1.167	.933	.55	0.0	FINORD2	

REFERENCES

1. Design Conference Proceedings - Technology for Supersonic Cruise Military Aircraft. Volume I, AFFDL/FX, U.S. Air Force, [1976].

2. Parlett, Lysle P.; and Shivers, James P.: Low-Speed Wind-Tunnel Tests of a Large-Scale Blended-Arrow Advanced Supersonic Transport Model Having Variable-Cycle Engines and Vectoring Exhaust Nozzles. NASA TM X-72809, 1976.

3. Sorrells, Russell B.; and Miller, David S.: Numerical Method for Design of Minimum-Drag Supersonic Wing Camber With Constraints on Pitching Moment and Surface Deformation. NASA TN D-7097, 1972.

4. Landrum, Emma Jean: Effect of Nacelle Orientation on the Aerodynamic Characteristics of an Arrow Wing-Body Configuration at Mach Number 2.03. NASA TN D-3284, 1966.

5. Baals, Donald D.; Robins, A. Warner; and Harris, Roy V., Jr.: Aerodynamic Design Integration of Supersonic Aircraft. J. Aircr., vol. 7, no. 5, Sept.-Oct. 1970, pp. 385-394.

6. Craidon, Charlotte B.: Description of a Digital Computer Program for Airplane Configuration Plots. NASA TM X-2074, 1970.

7. Braslow, Albert L.; Hicks, Raymond M.; and Harris, Roy V., Jr.: Use of Grit-Type Boundary-Layer-Transition Trips on Wind-Tunnel Models. Conference on Aircraft Aerodynamics, NASA SP-124, 1966, pp. 19-36. (Also available as NASA TN D-3579.)

8. Harris, Roy V., Jr.: An Analysis and Correlation of Aircraft Wave Drag. NASA TM X-947, 1964.

9. Middleton, Wilbur D.; and Carlson, Harry W.: Numerical Method of Estimating and Optimizing Supersonic Aerodynamic Characteristics of Arbitrary Planform Wings. J. Aircr., vol. 2, no. 4, July-Aug. 1965, pp. 261-265.

10. Sommer, Simon C.; and Short, Barbara J.: Free-Flight Measurements of Turbulent-Boundary-Layer Skin Friction in the Presence of Severe Aerodynamic Heating at Mach Numbers From 2.8 to 7.0. NACA TN 3391, 1955.

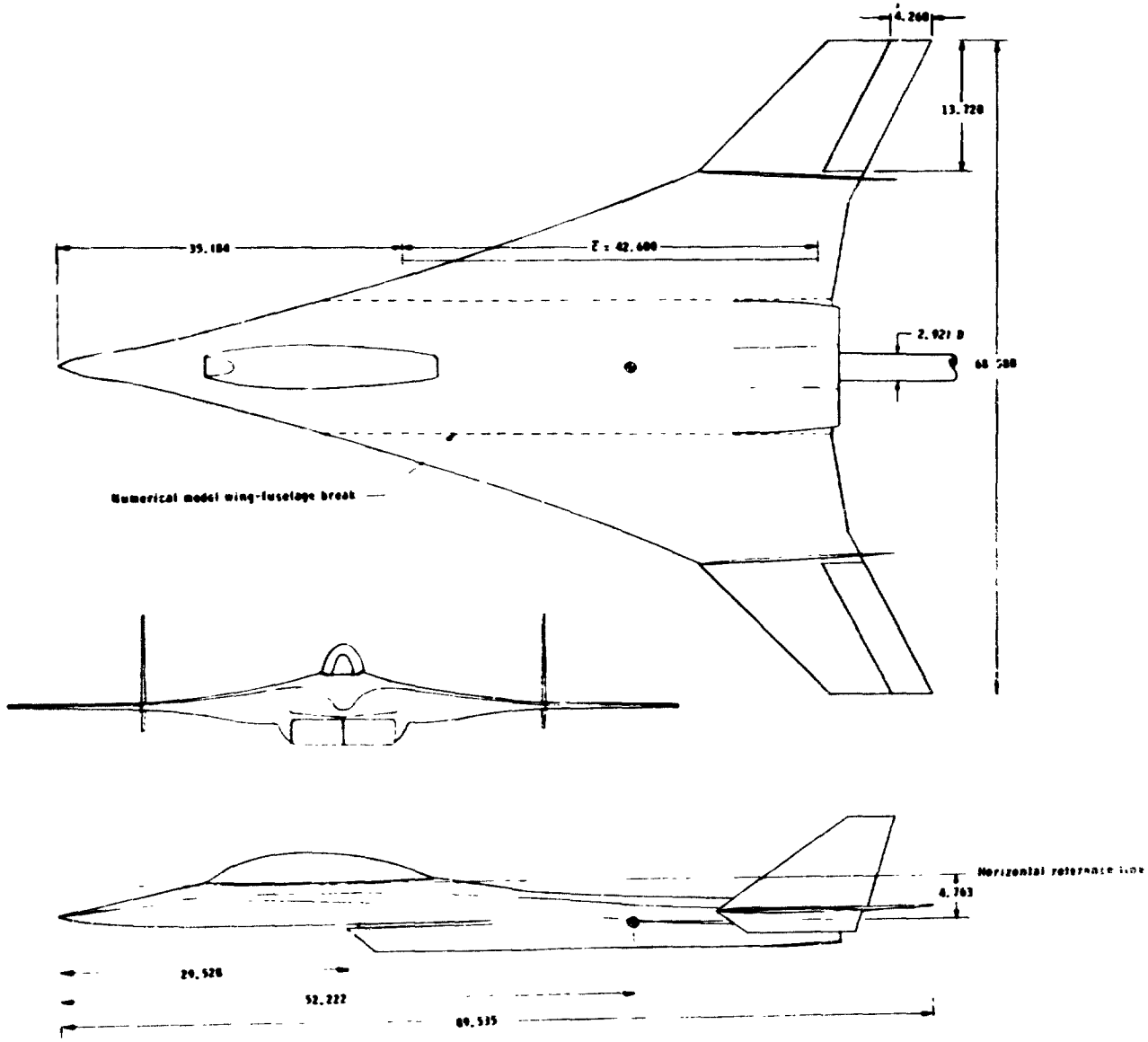

Figure 1.- Three-view sketch of model. (All linear dimensions are in cm.)

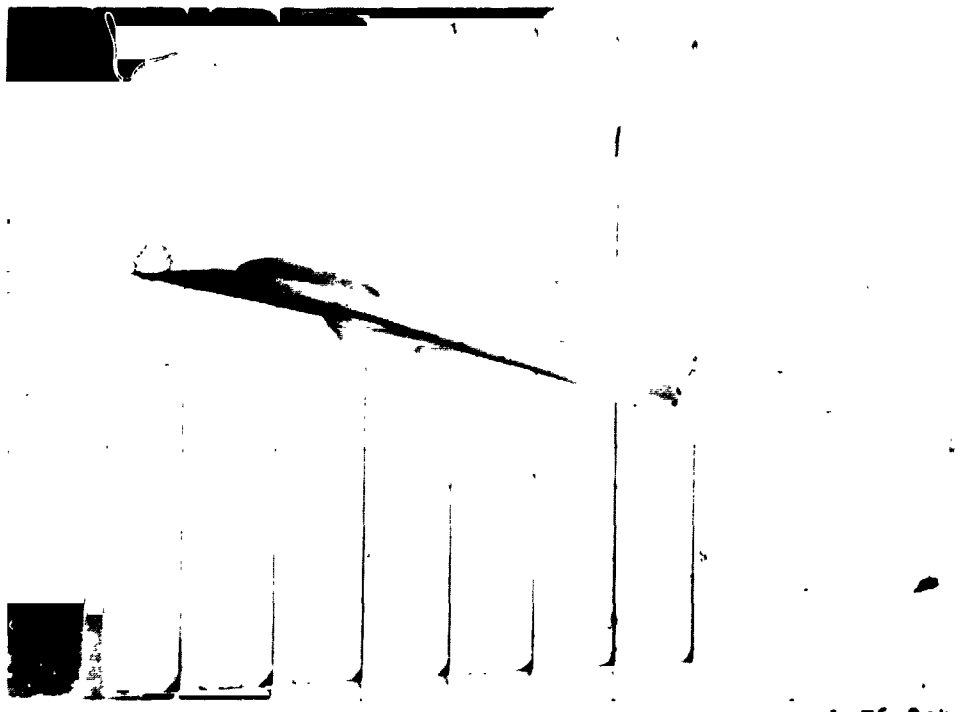

L-76-814

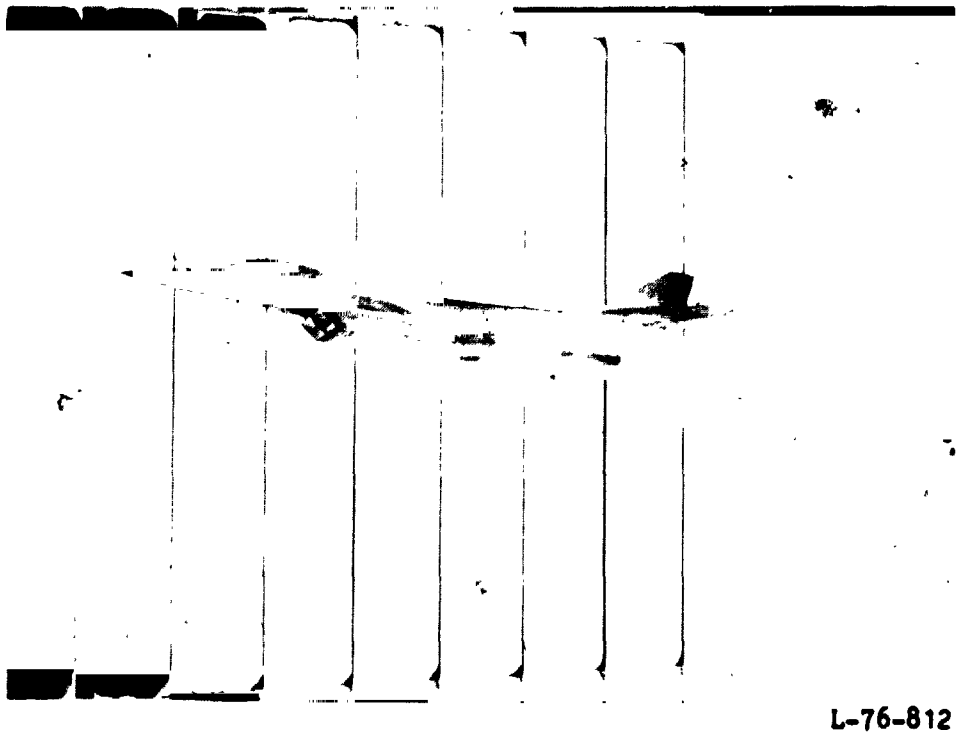

L-76-812

Figure 2.- Photographs of model without ventral fins installed in Langley Unitary Plan wind tunnel.

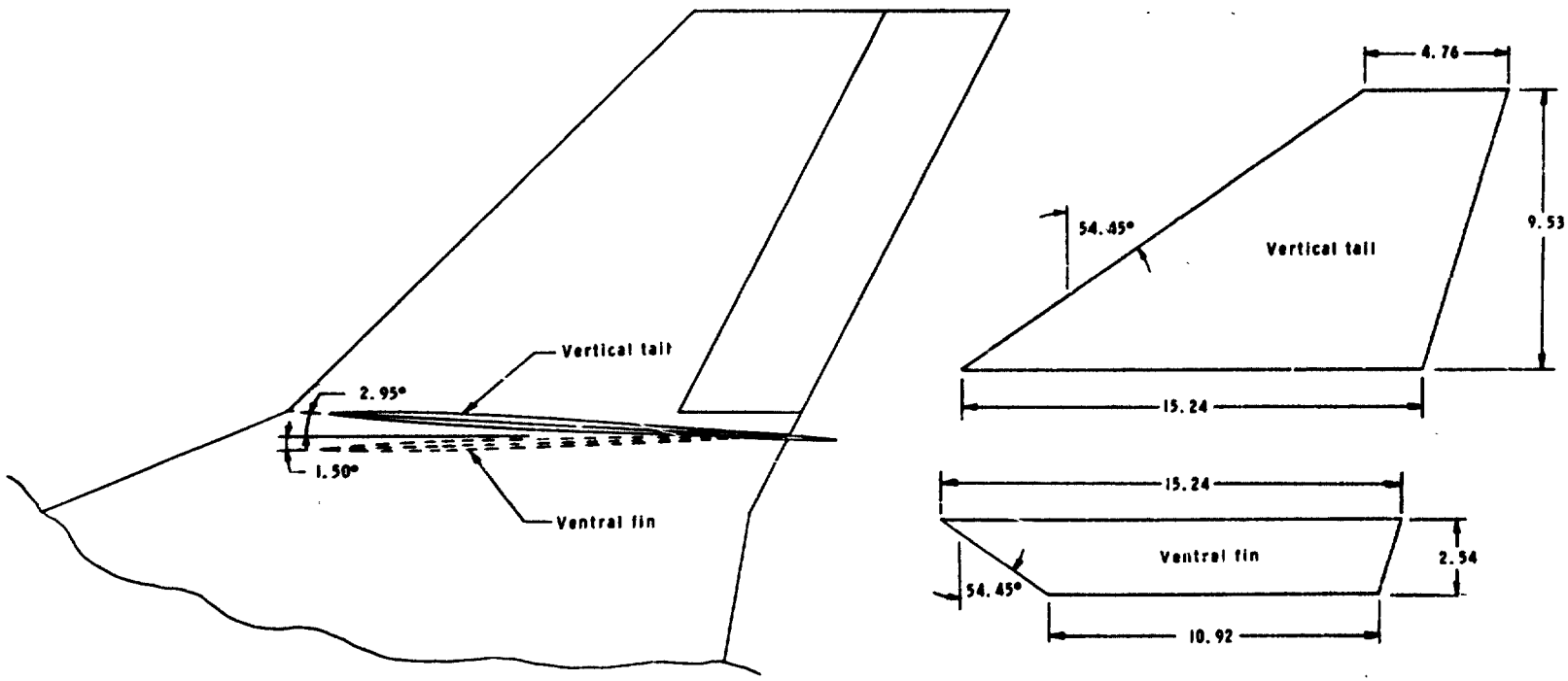

Figure 3.- Details of vertical tail and ventral fin. (All linear dimensions are in cm.)

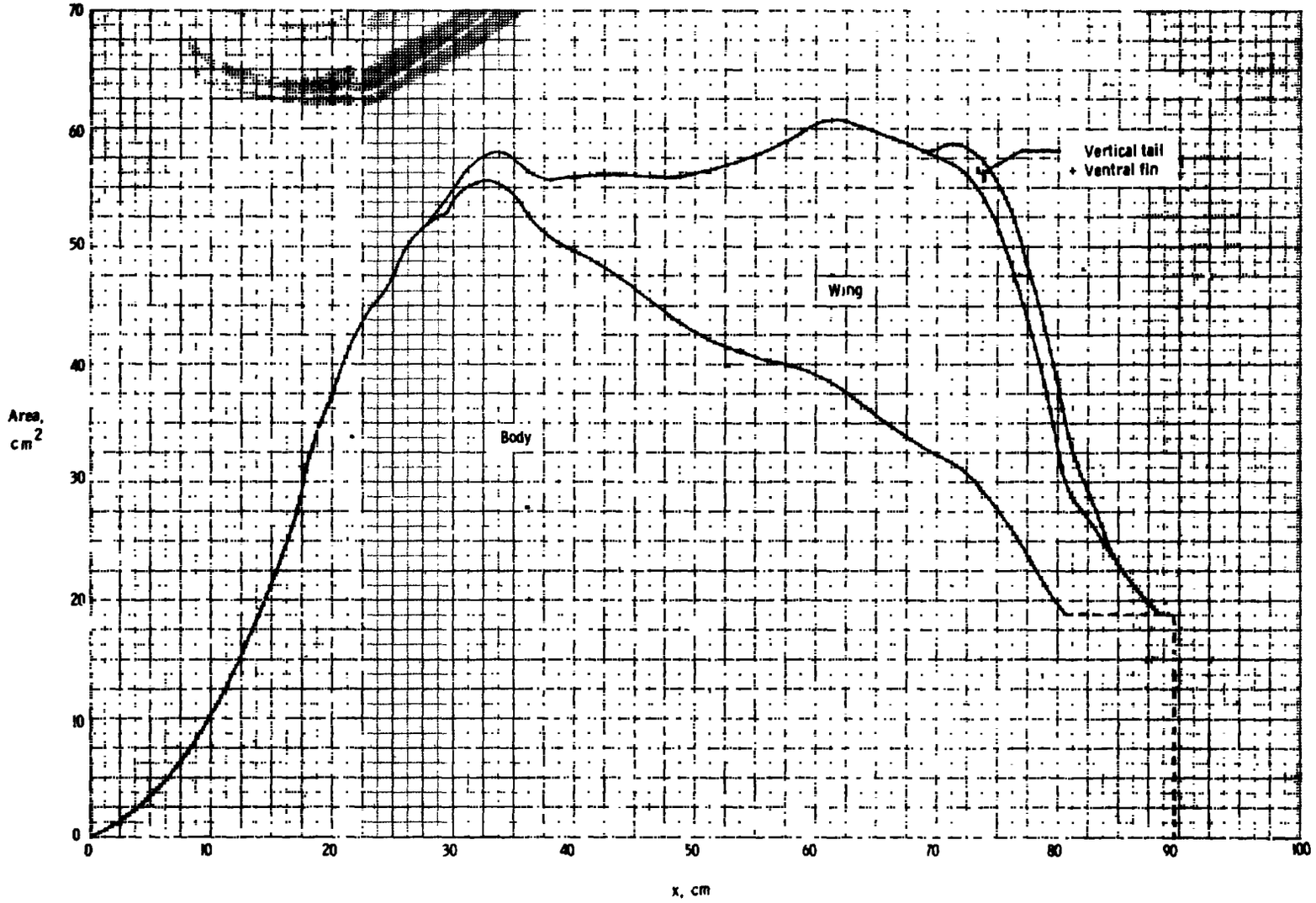

Figure 4.- Normal area distribution for complete model. Capture area removed.

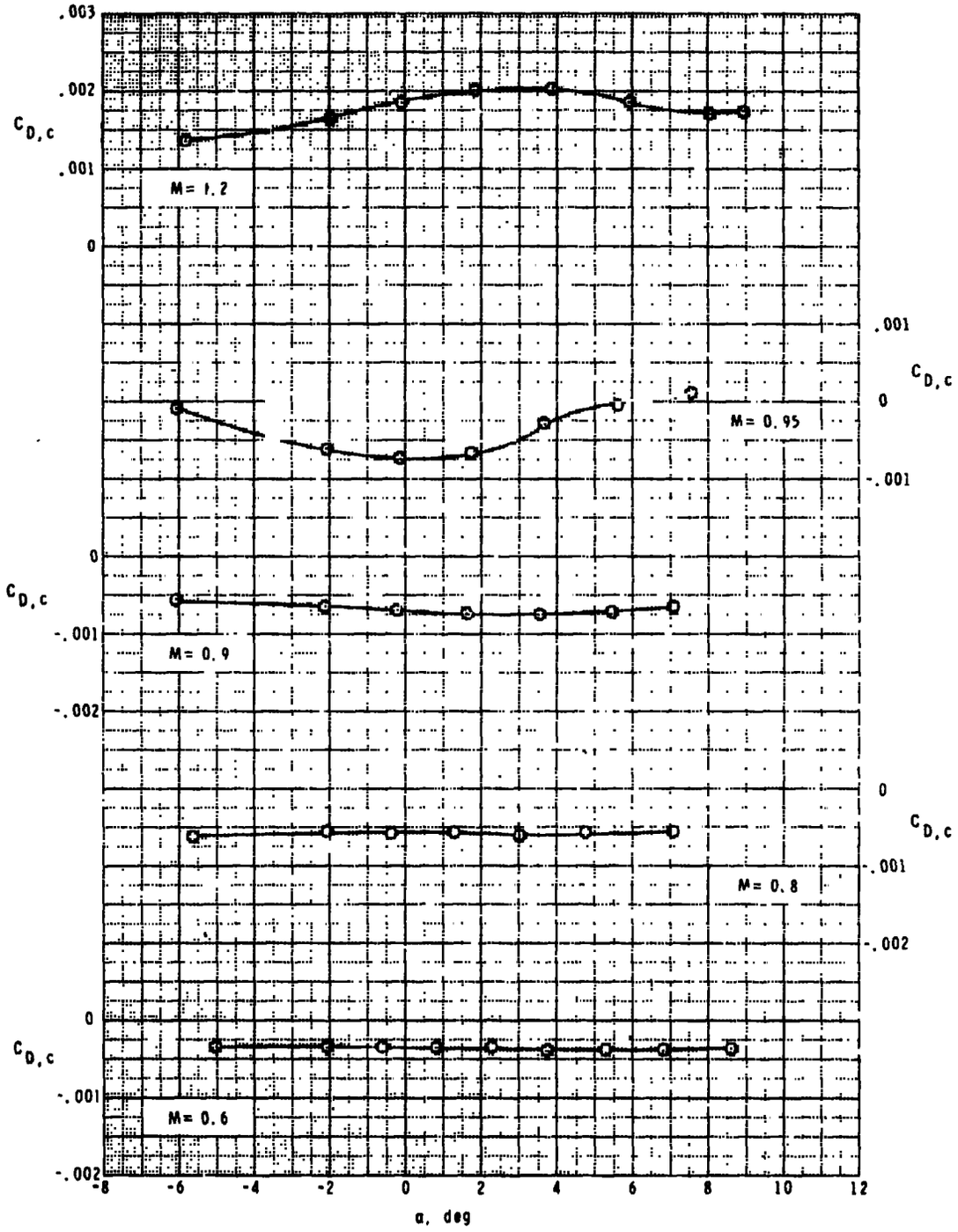

Figure 5.- Typical balance-chamber drag corrections.

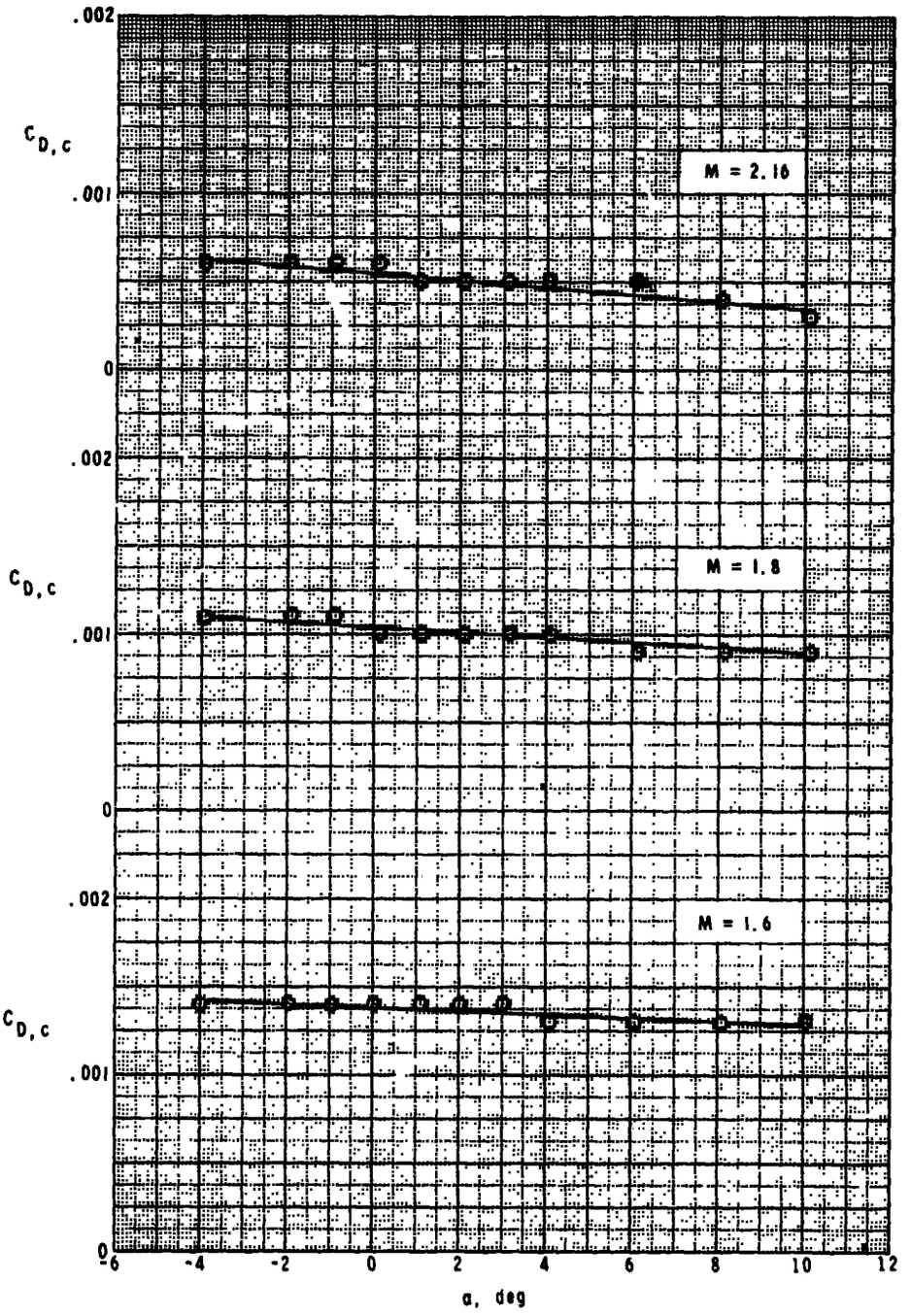

Figure 5.- Concluded.

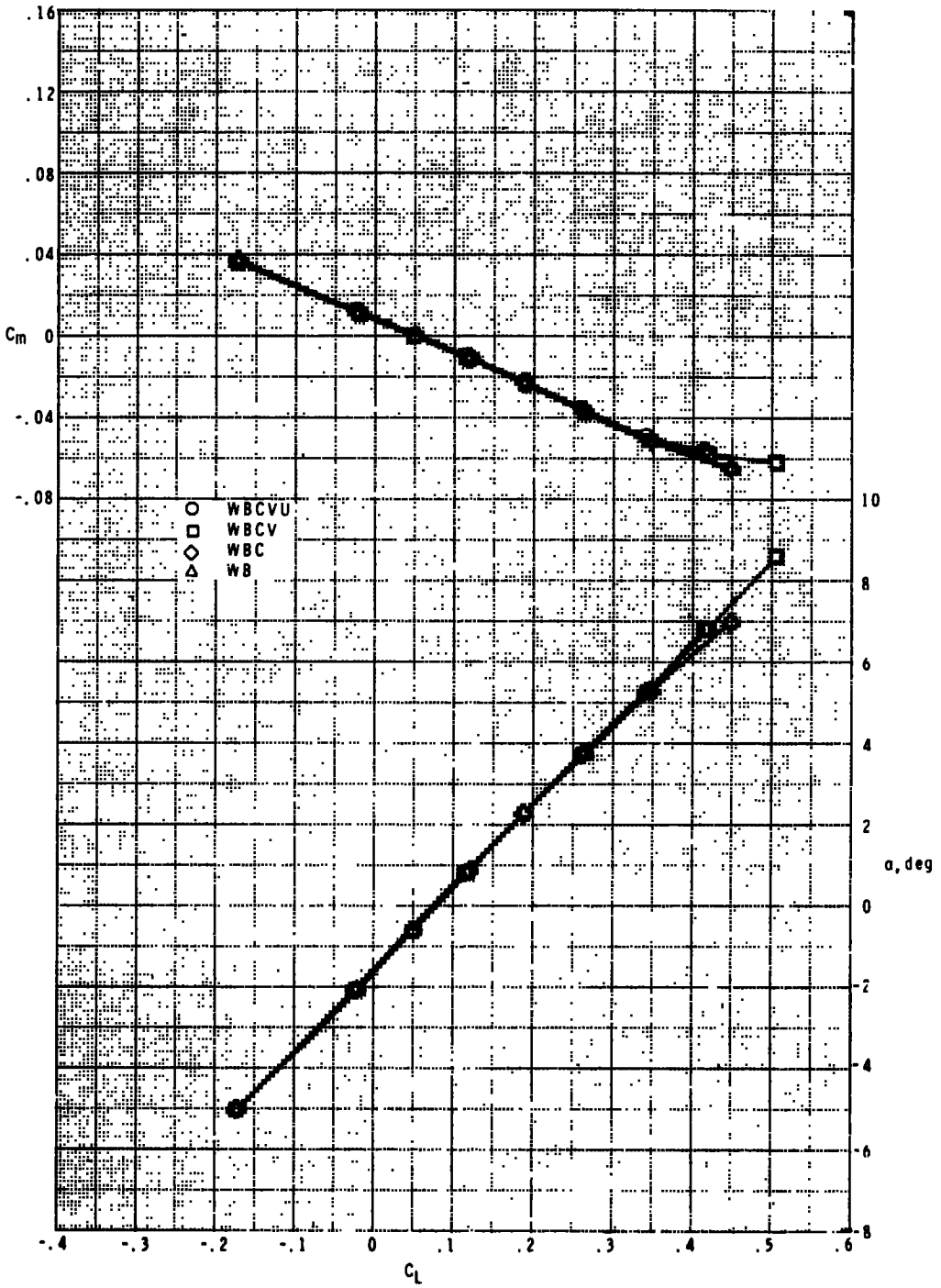

(a) M = 0.6.

Figure 6.- Effects of components on longitudinal aerodynamic characteristics of model. $\delta_e = 0^o$.

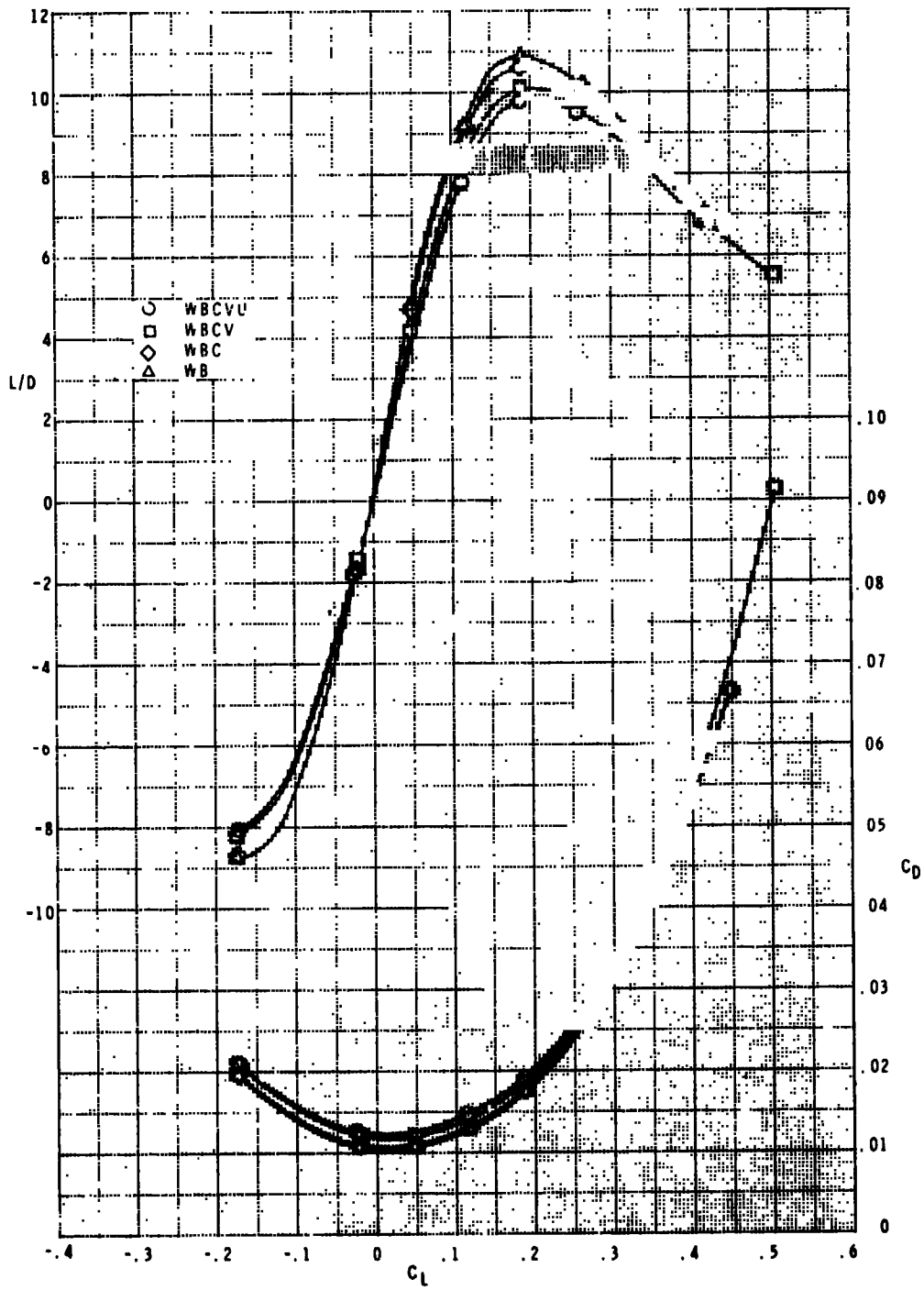

(a) Concluded.

Figure 6.- Continued.

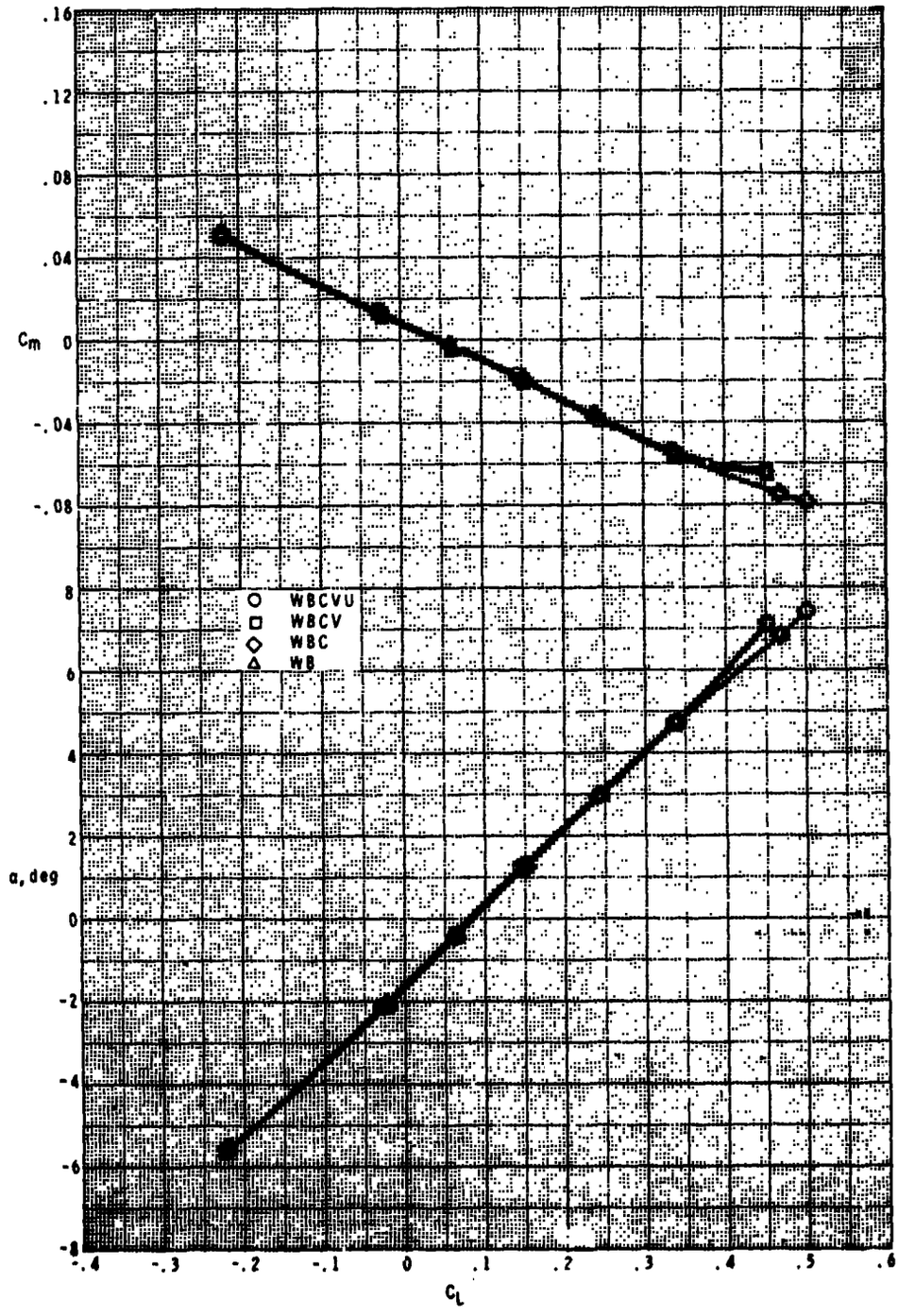

(b) M = 0.8.

Figure 5.- Continued.

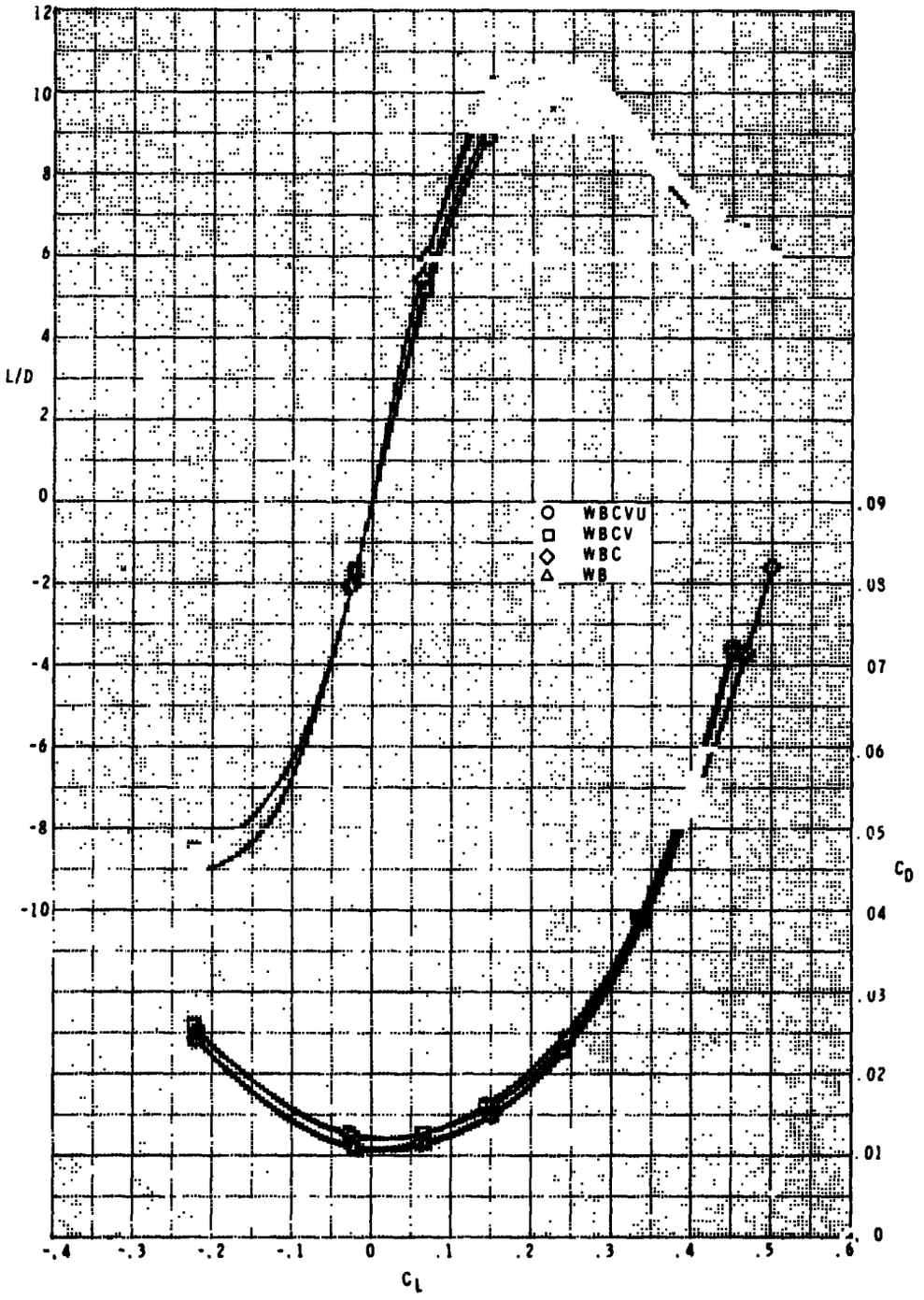

(b) Concluded.

Figure 6.- Continued.

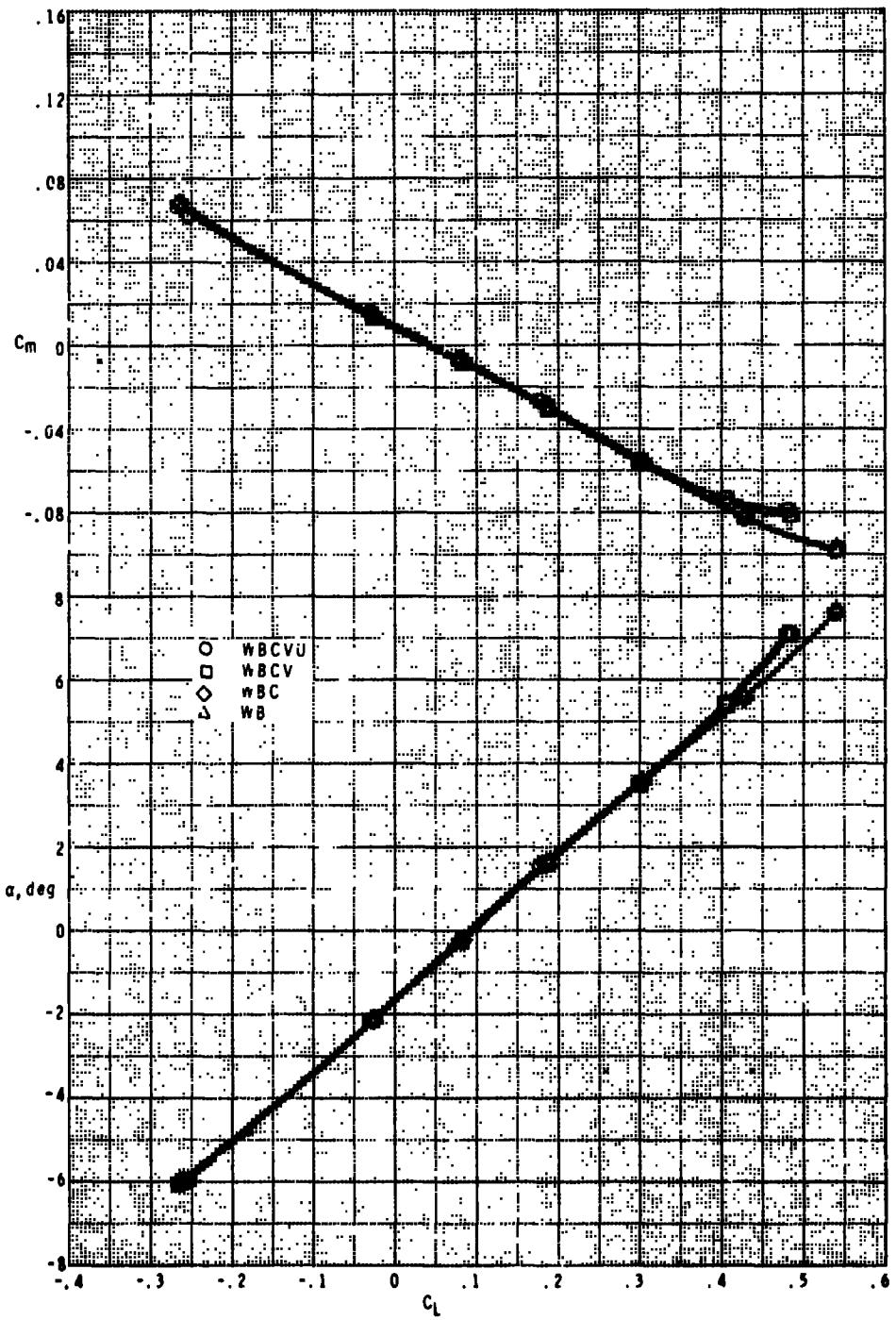

(c) M = 0.9.

Figure 6.- Continued.

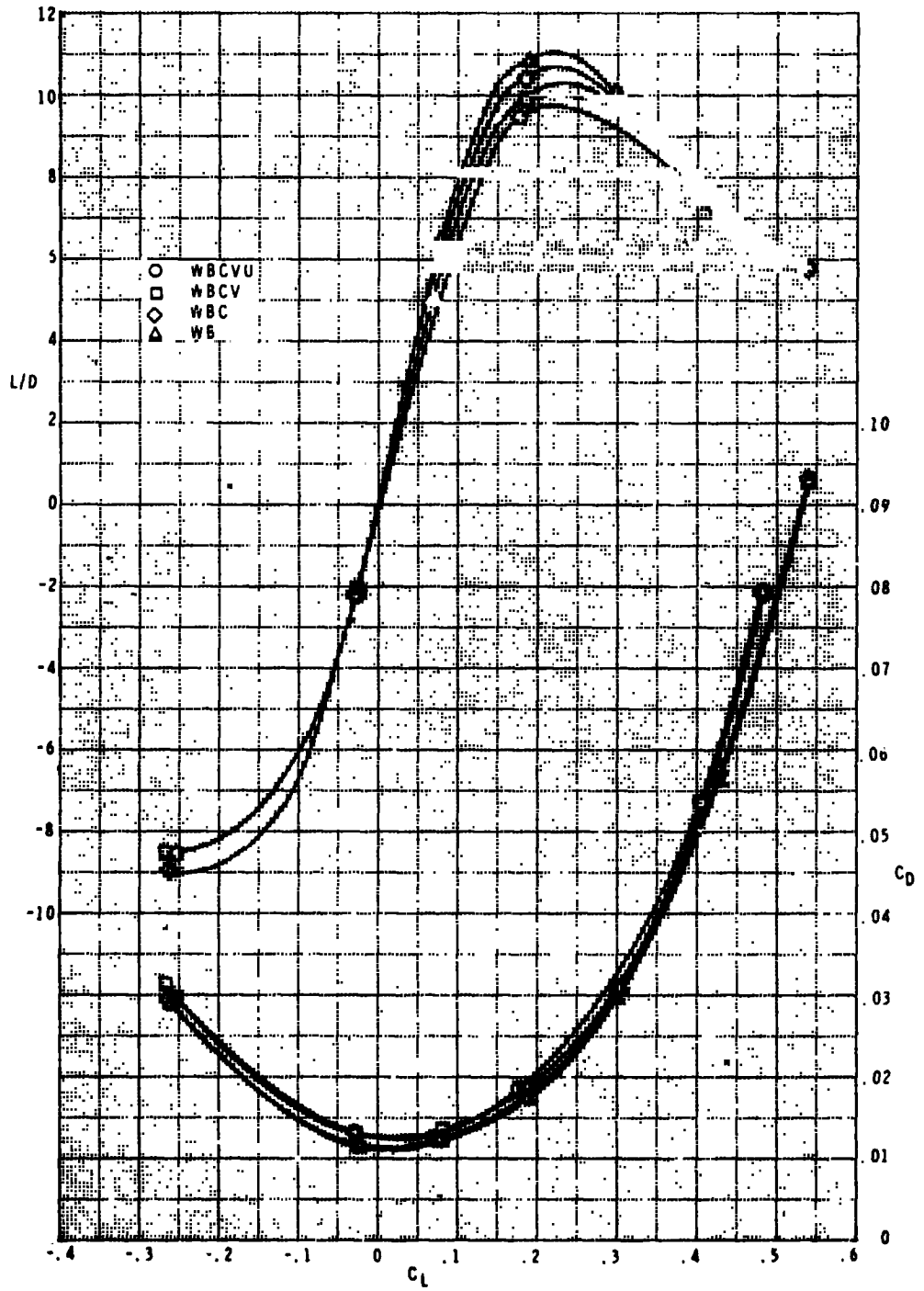

(c) Concluded.

Figure 6.- Continued.

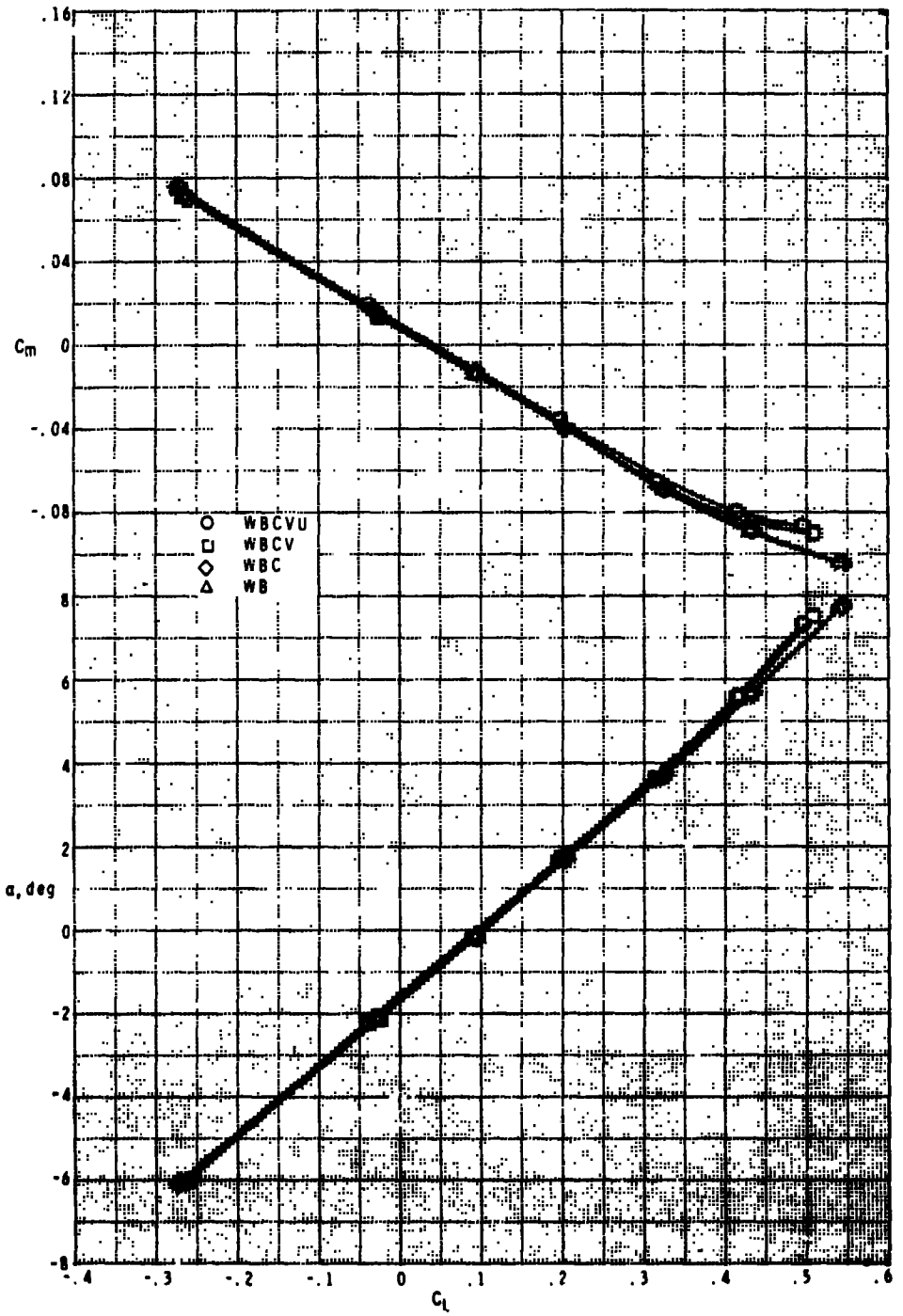

(d) M = 0.95.

Figure 6.- Continued.

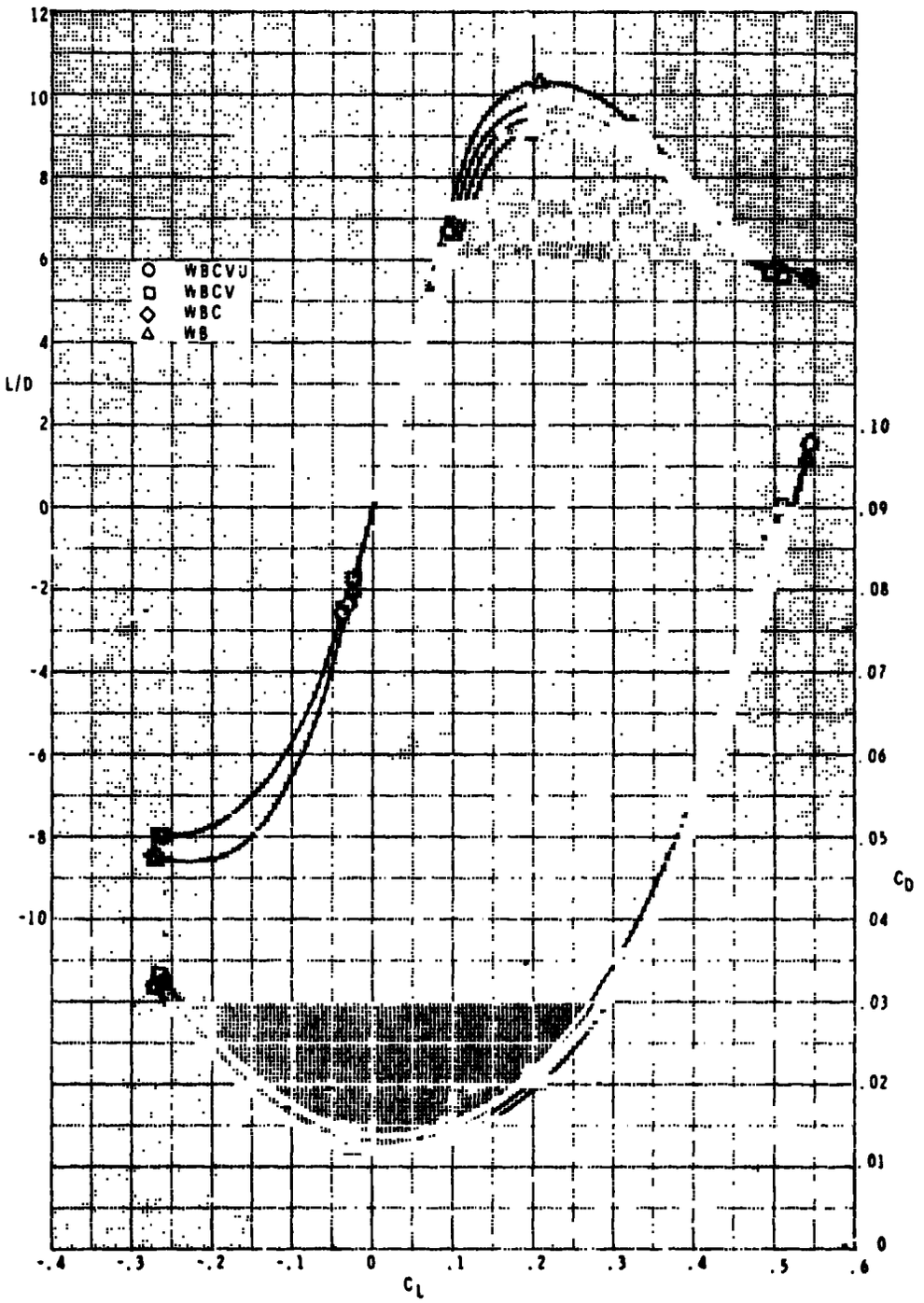

(d) Concluded.

Figure 6.- Continued.

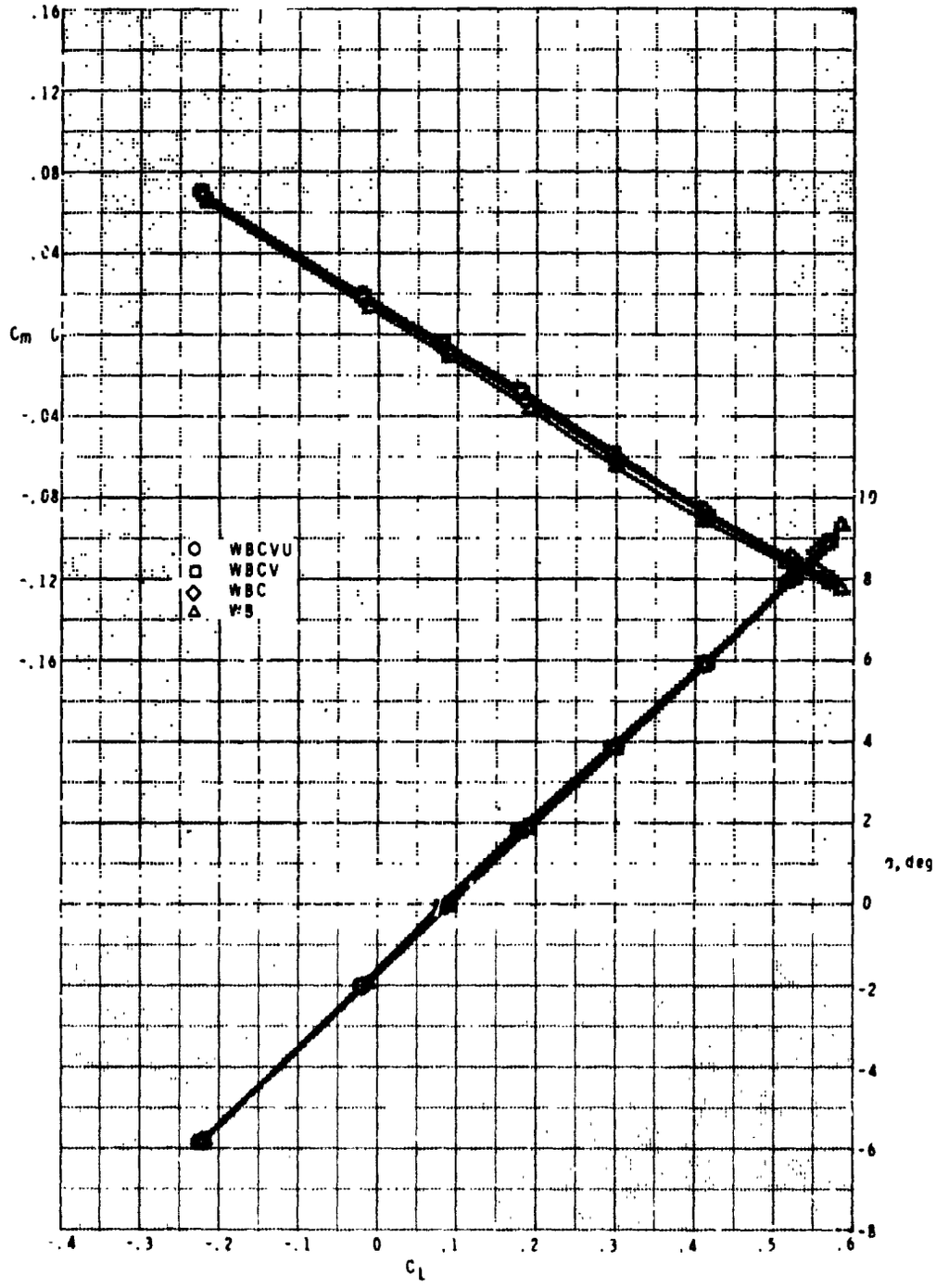

(e) M = 1.2.

Figure 6.- Continued.

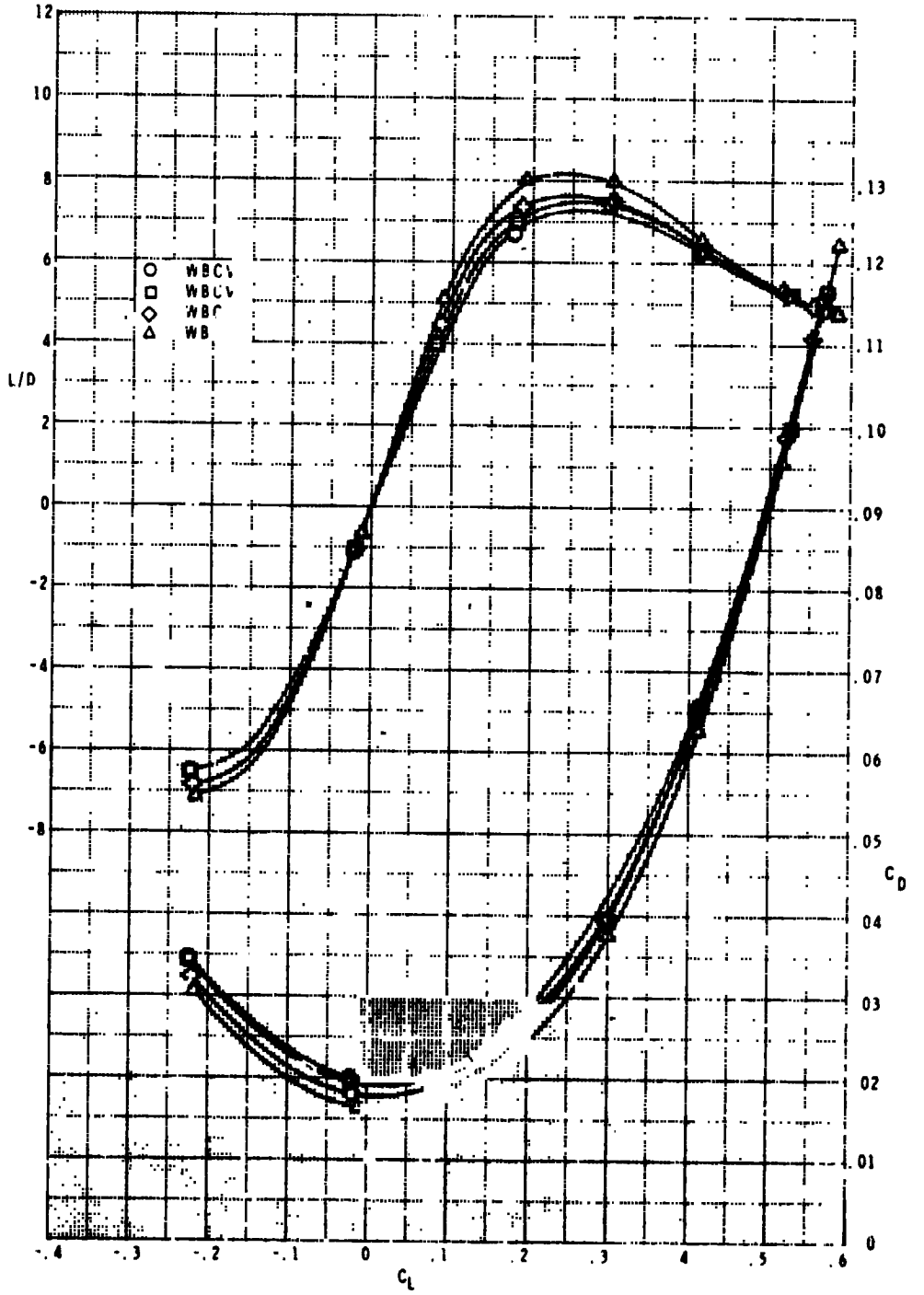

(e) Concluded.

Figure 5.- Continued.

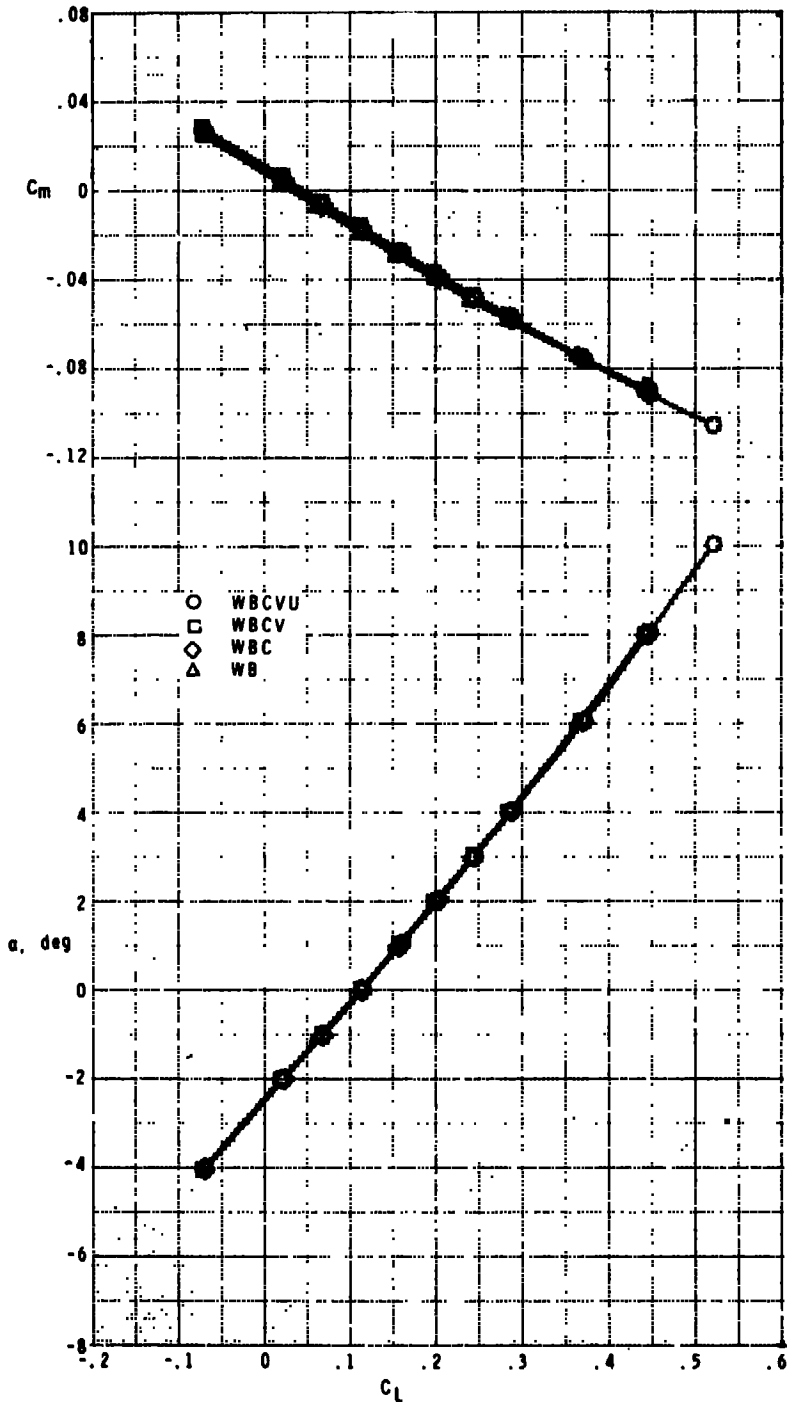

(f) M = 1.6.

Figure 6.- Continued.

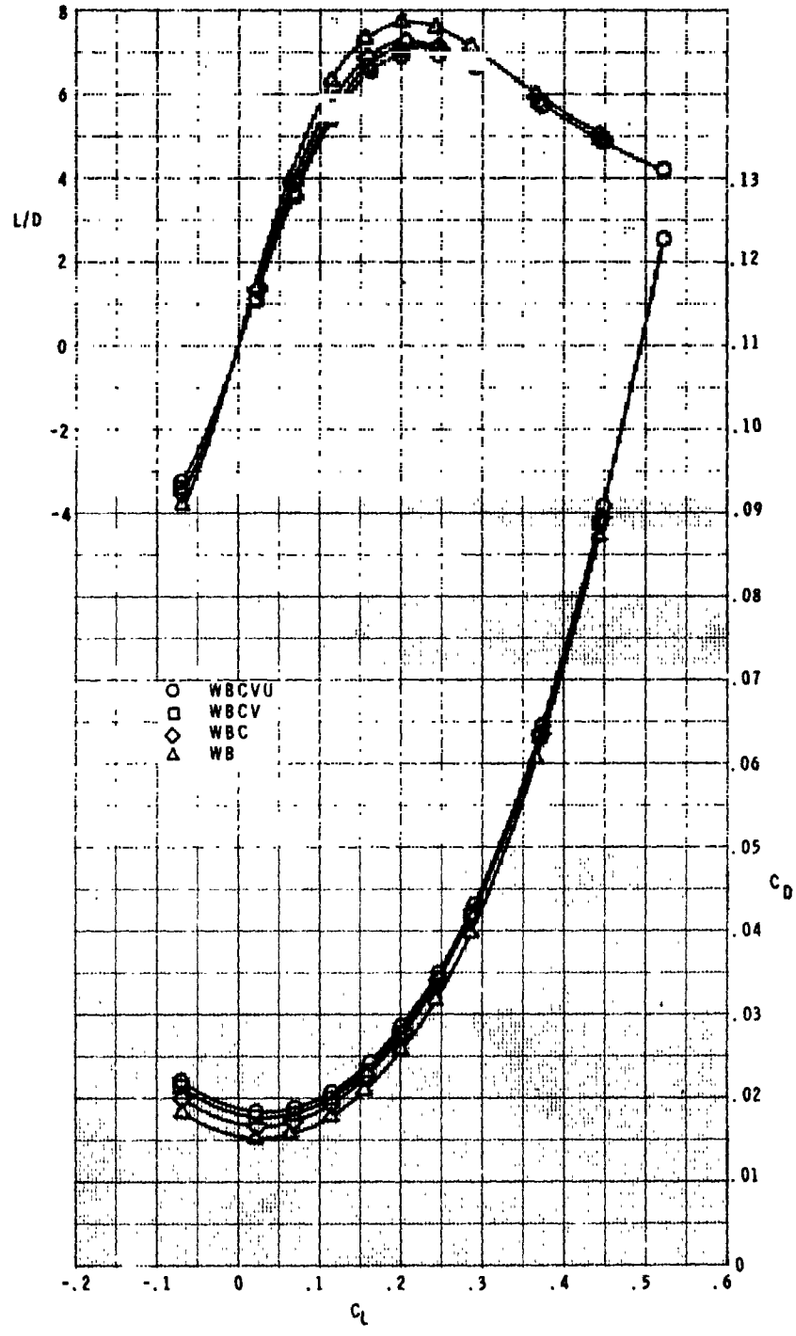

(f) Concluded.

Figure 6.- Continued.

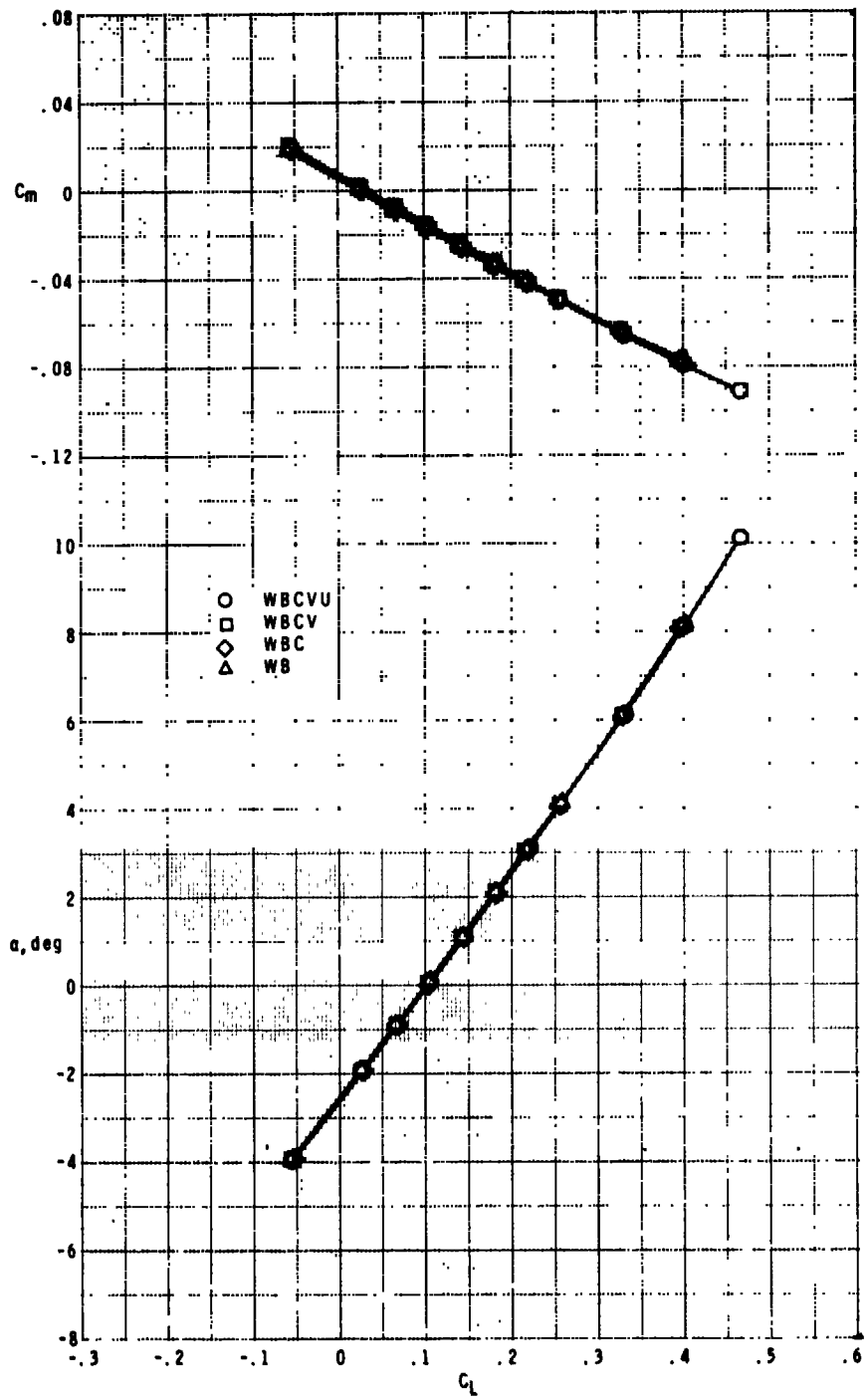

(g) M = 1.8.

Figure 6.- Continued.

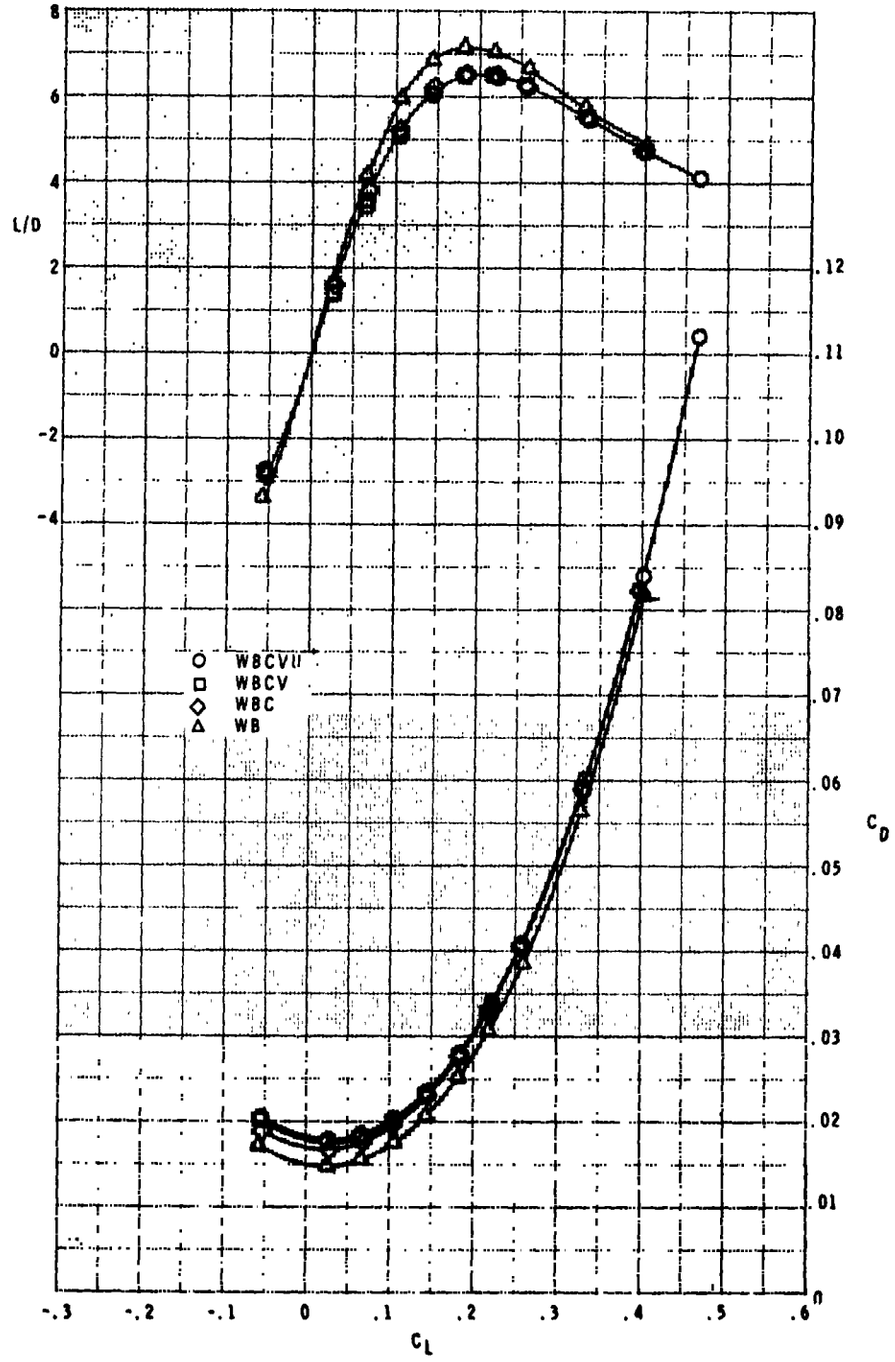

(g) Concluded.

Figure 6.- Continued.

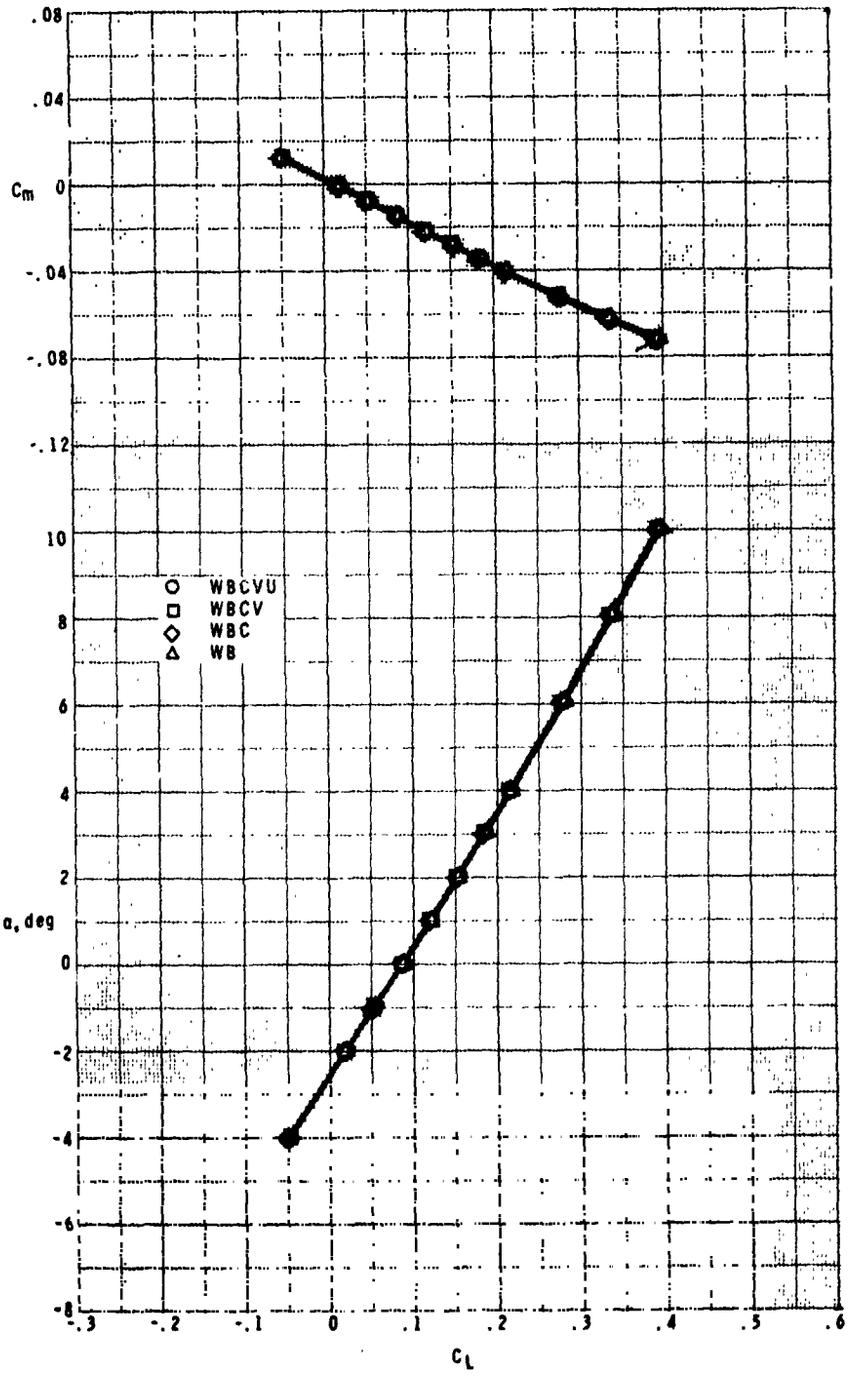

(h) M = 2.16.

Figure 6.- Continued.

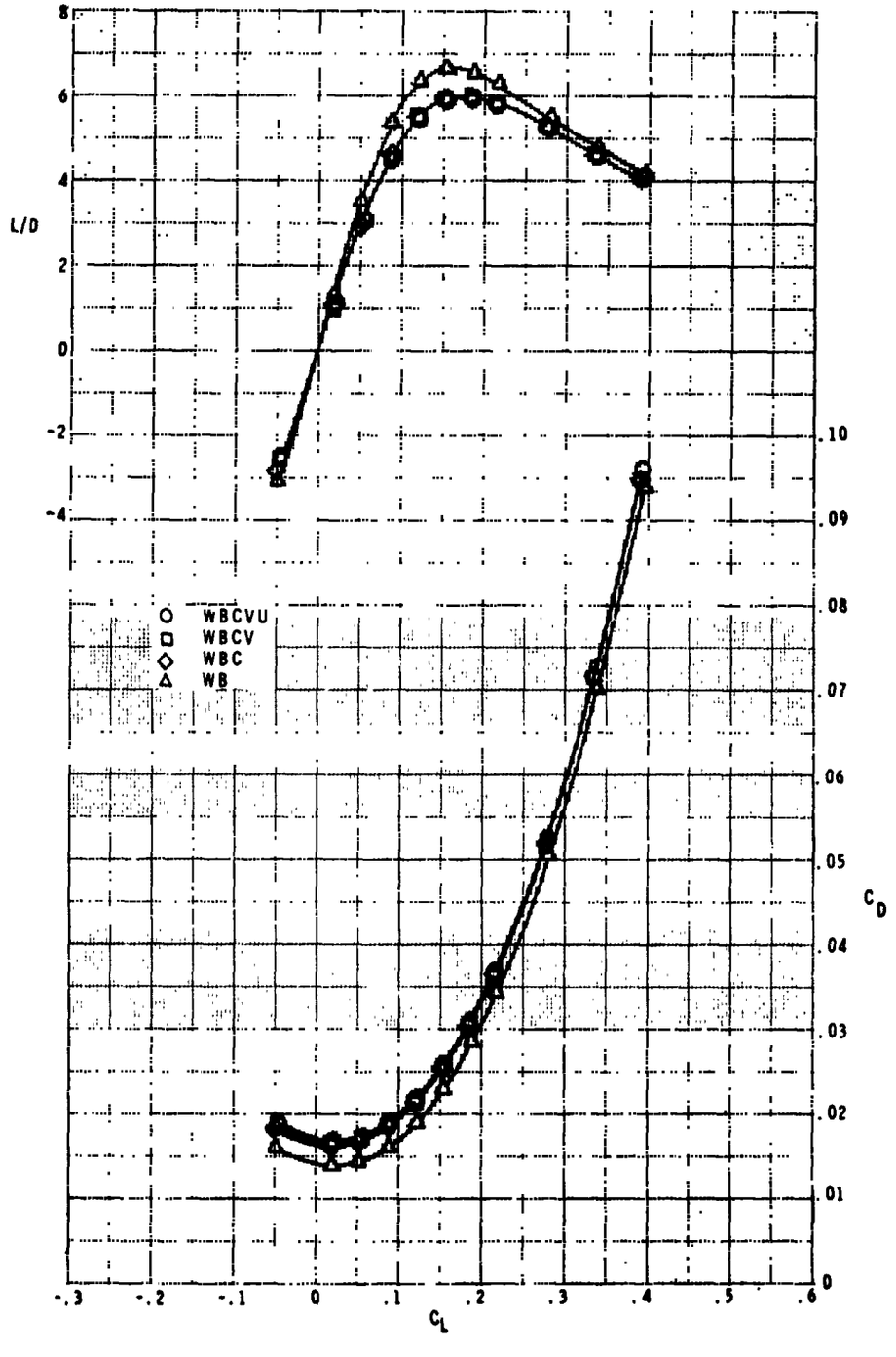

(h) Concluded.

Figure 6.- Concluded.

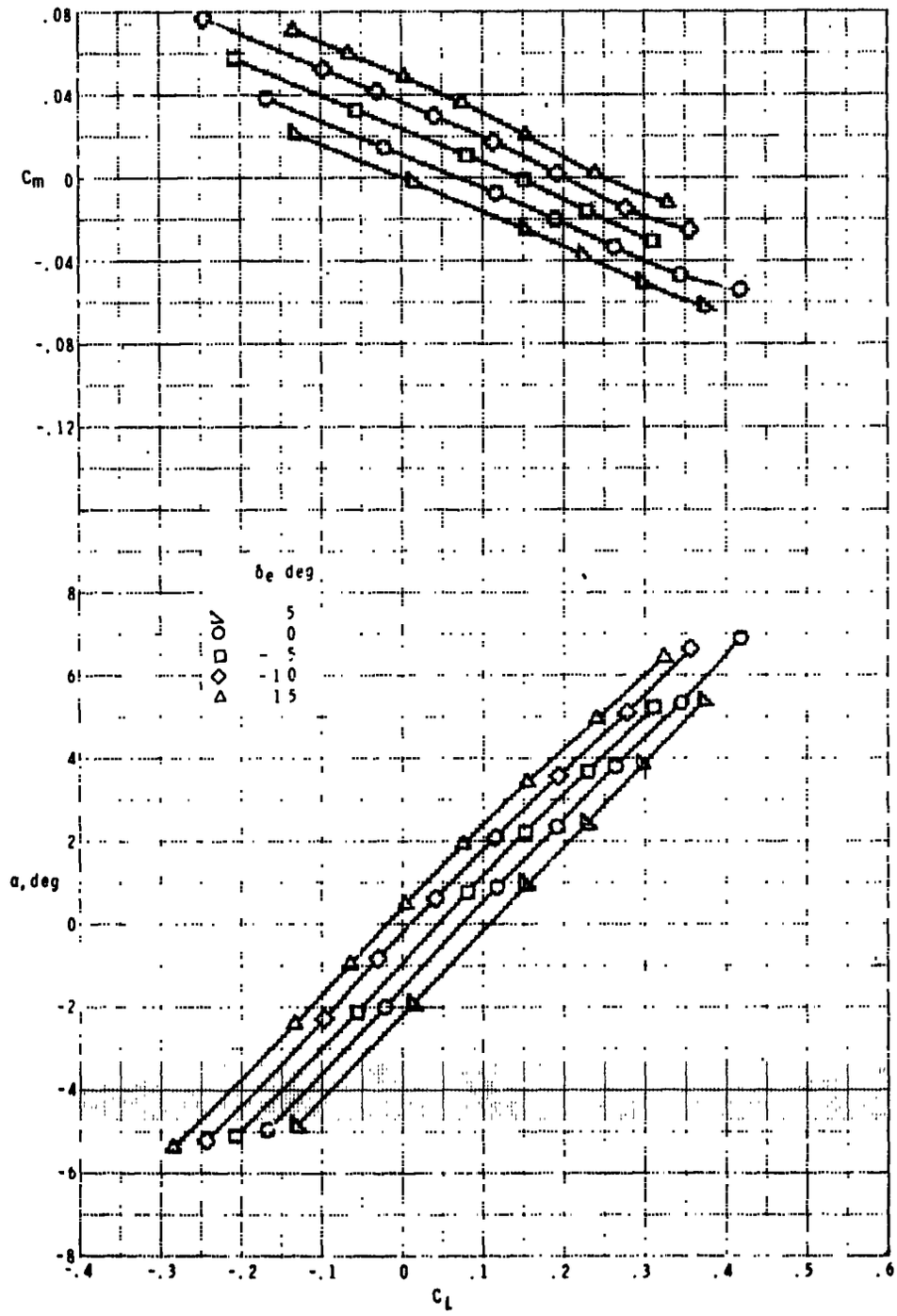

(a) M = 0.6.

Figure 7.- Effects of control deflections on longitudinal aerodynamic characteristics of model. WBCVU.

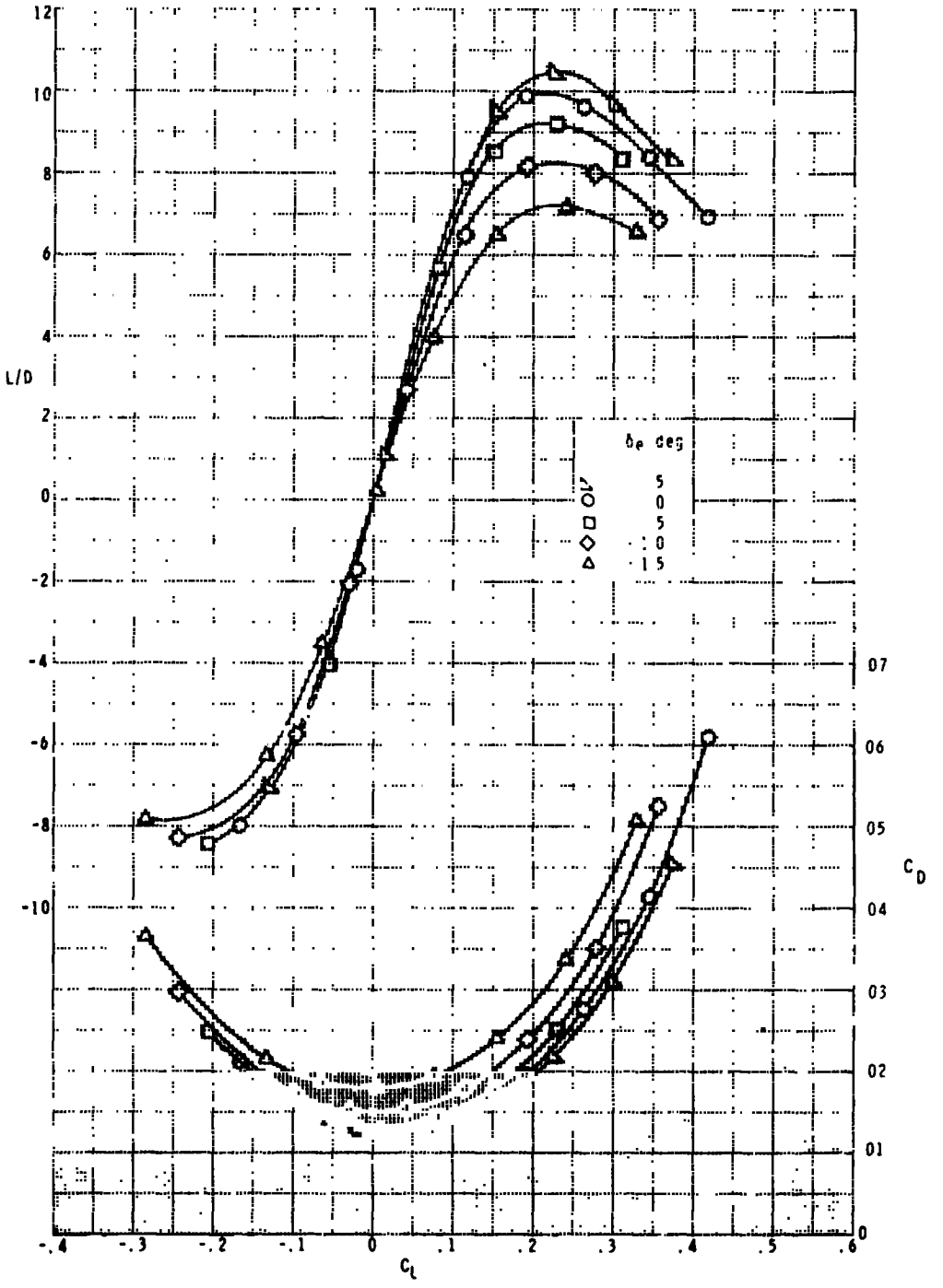

(a) Concluded.

Figure 7.- Continued.

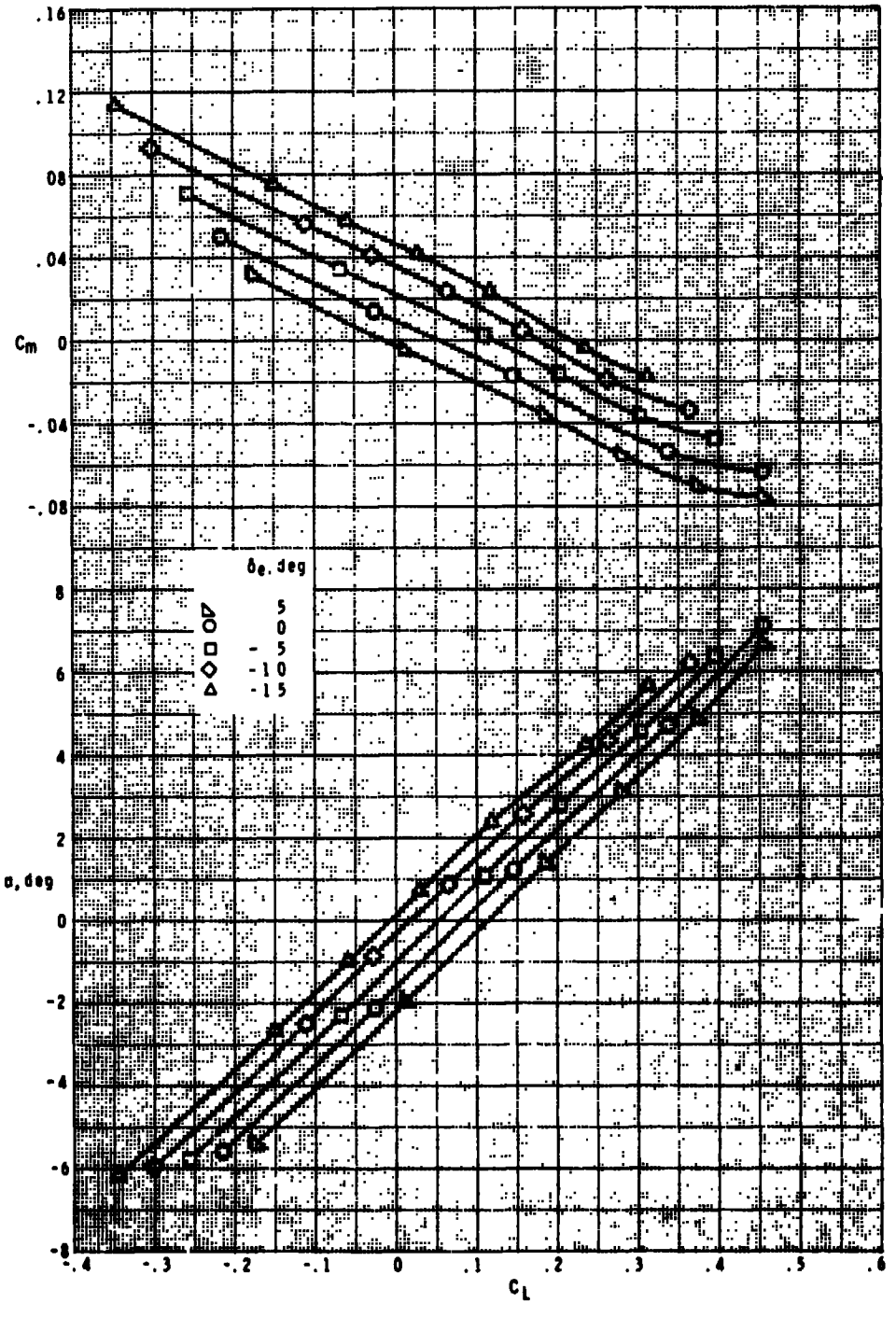

(b) M = 0.8.

Figure 7.- Continued.

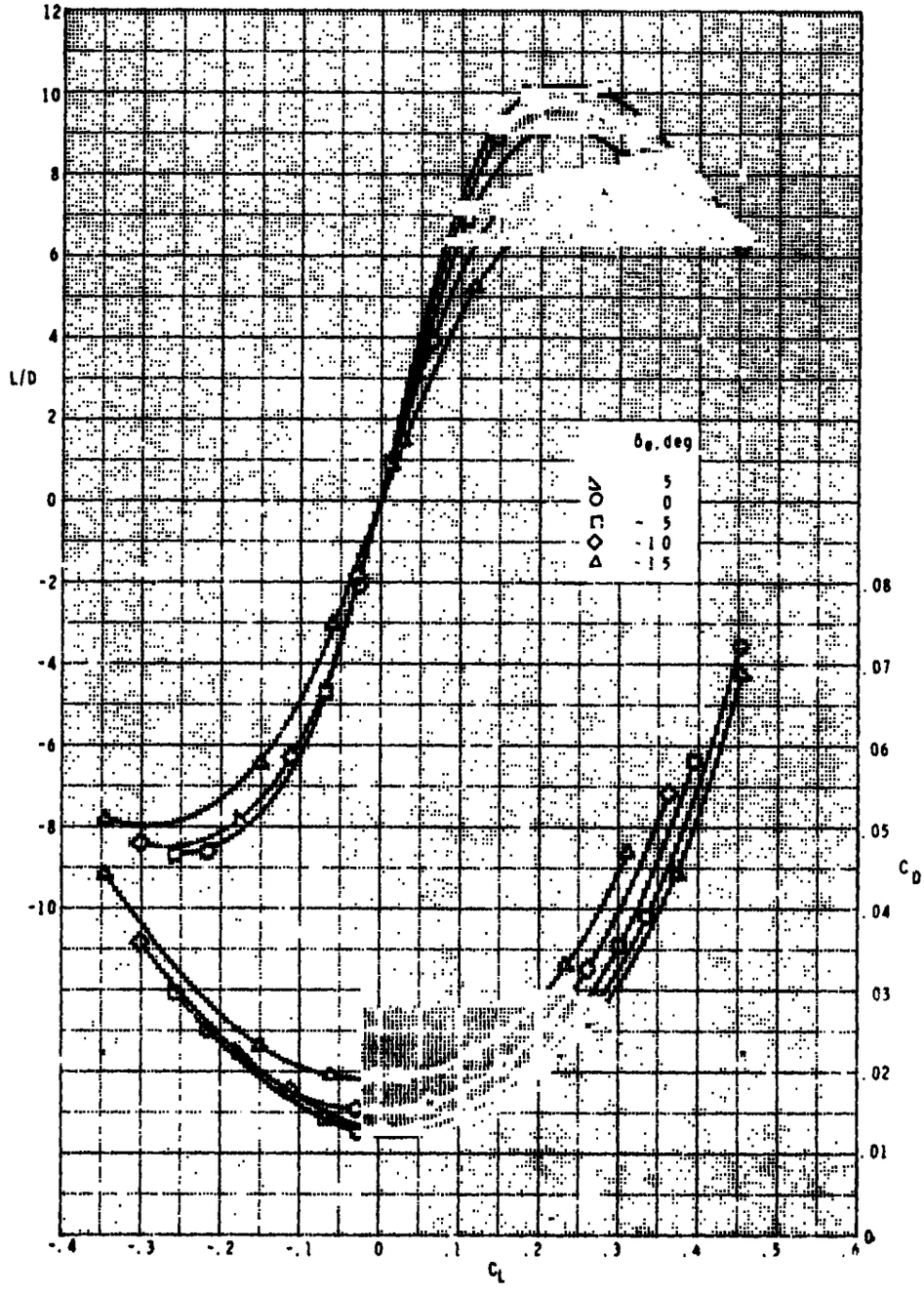

(b) Concluded.

Figure 7.- Continued.

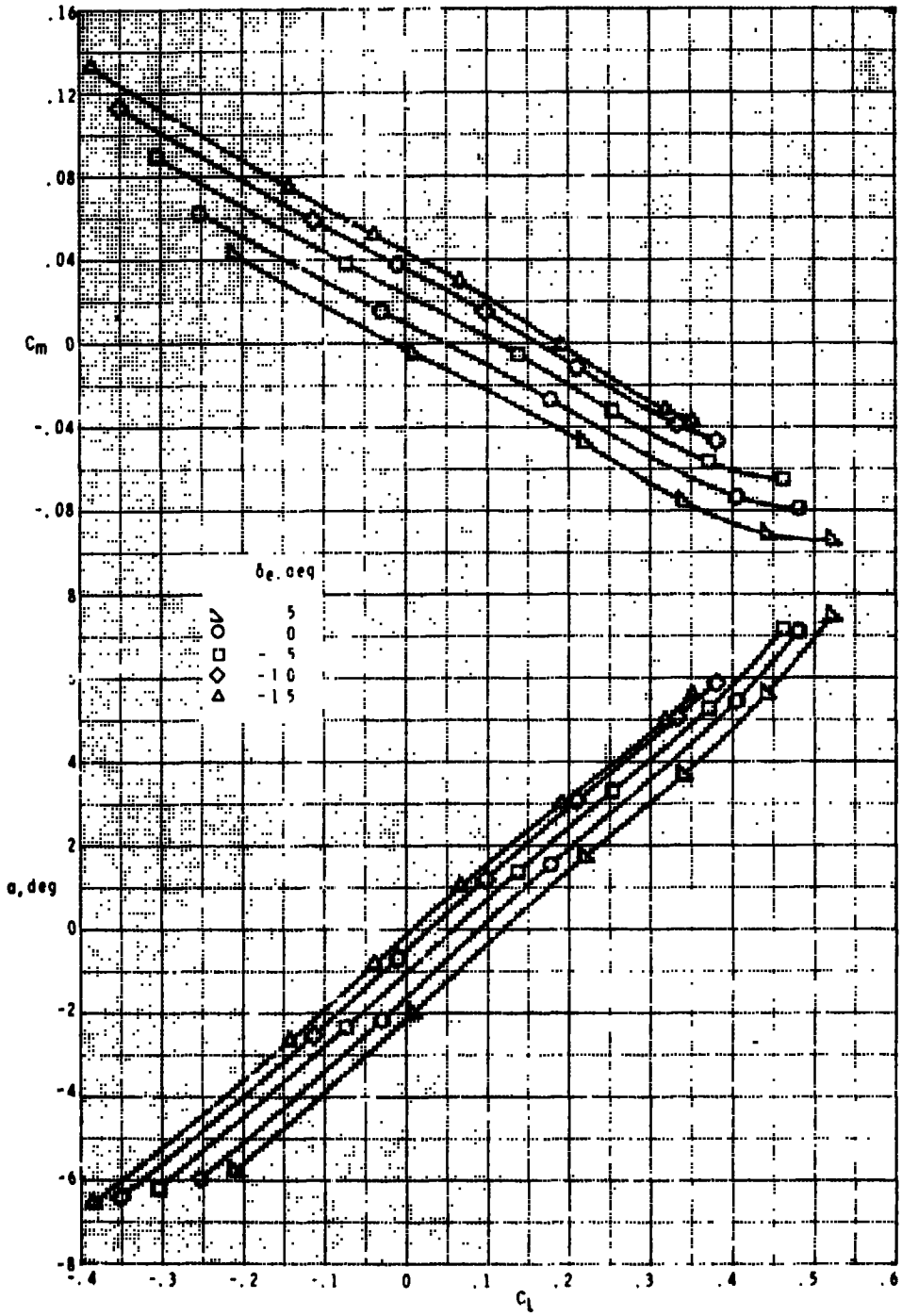

(c) M = 0.9.

Figure 7.- Continued.

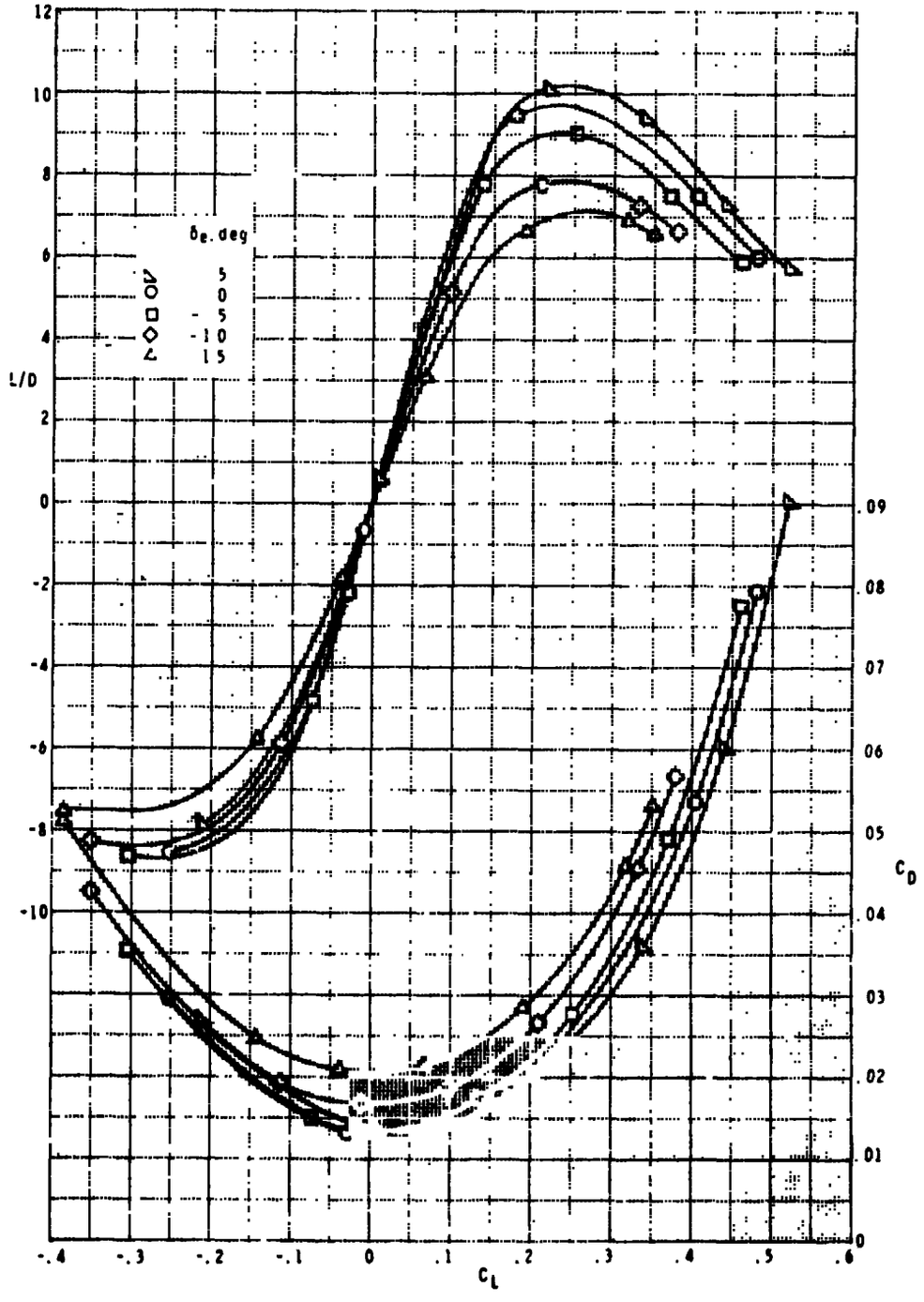

(c) Concluded.

Figure 7.- Continued.

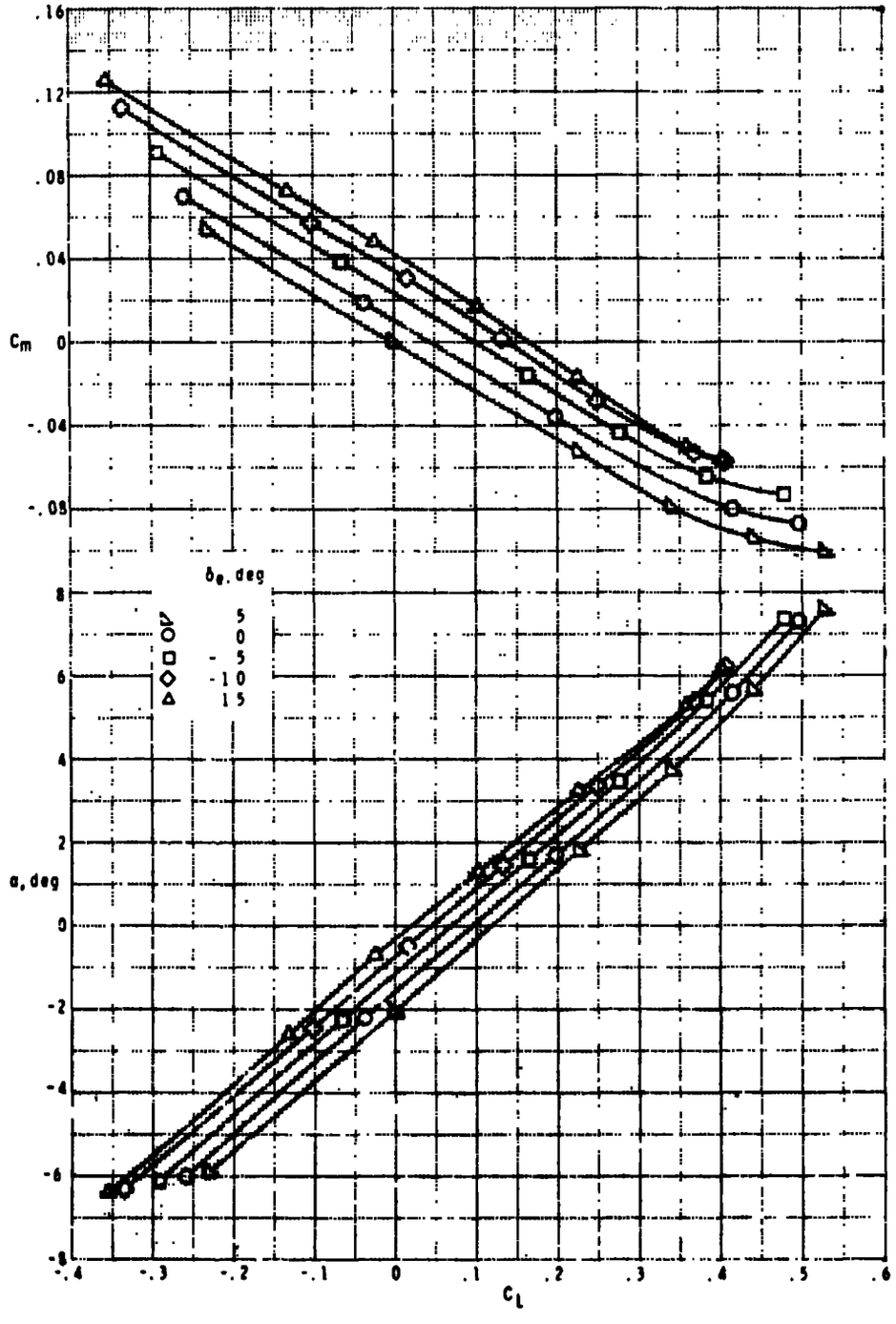

(d) M = 0.95.

Figure 7.- Continued.

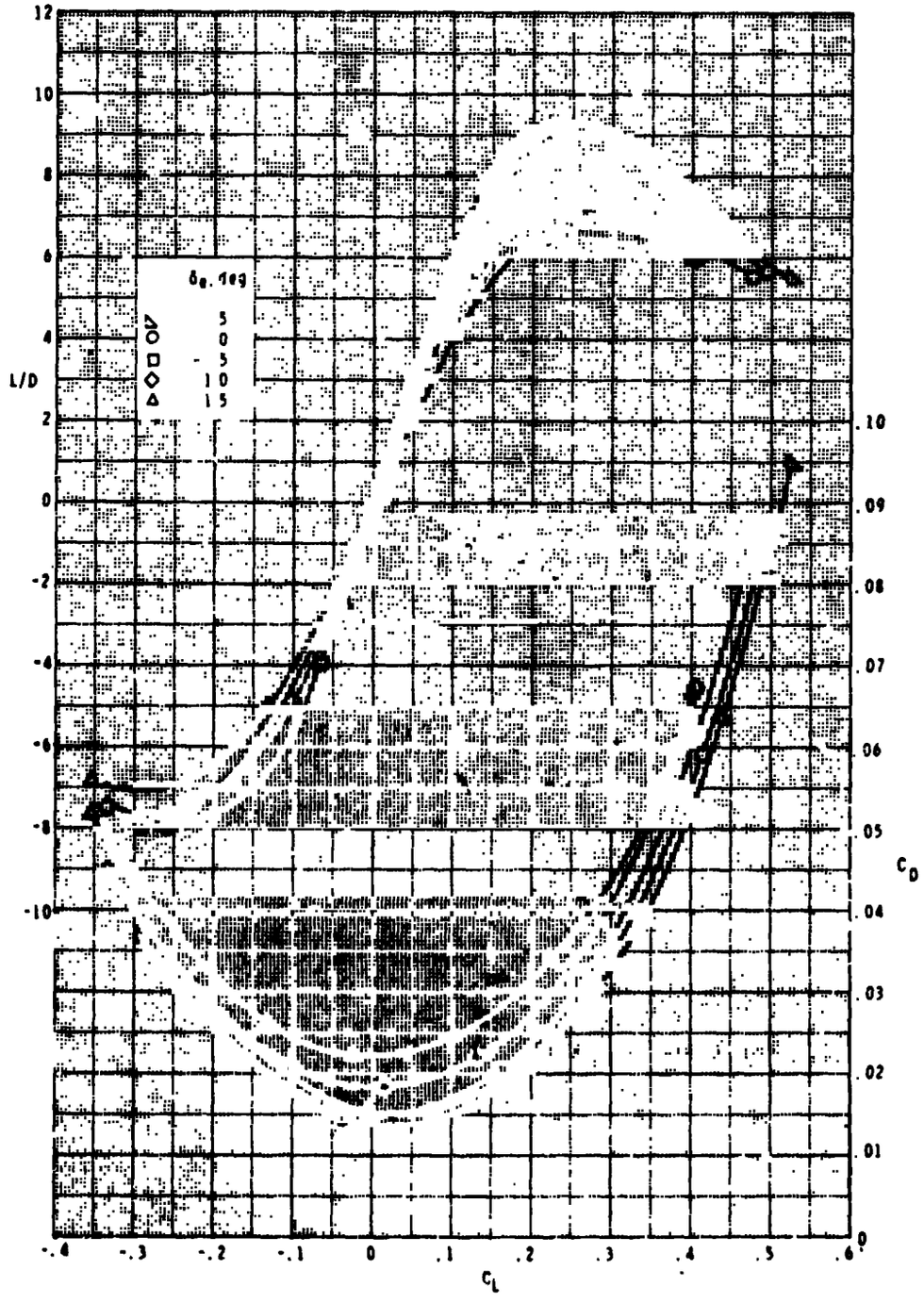

(d) Concluded.

Figure 7.- Continued.

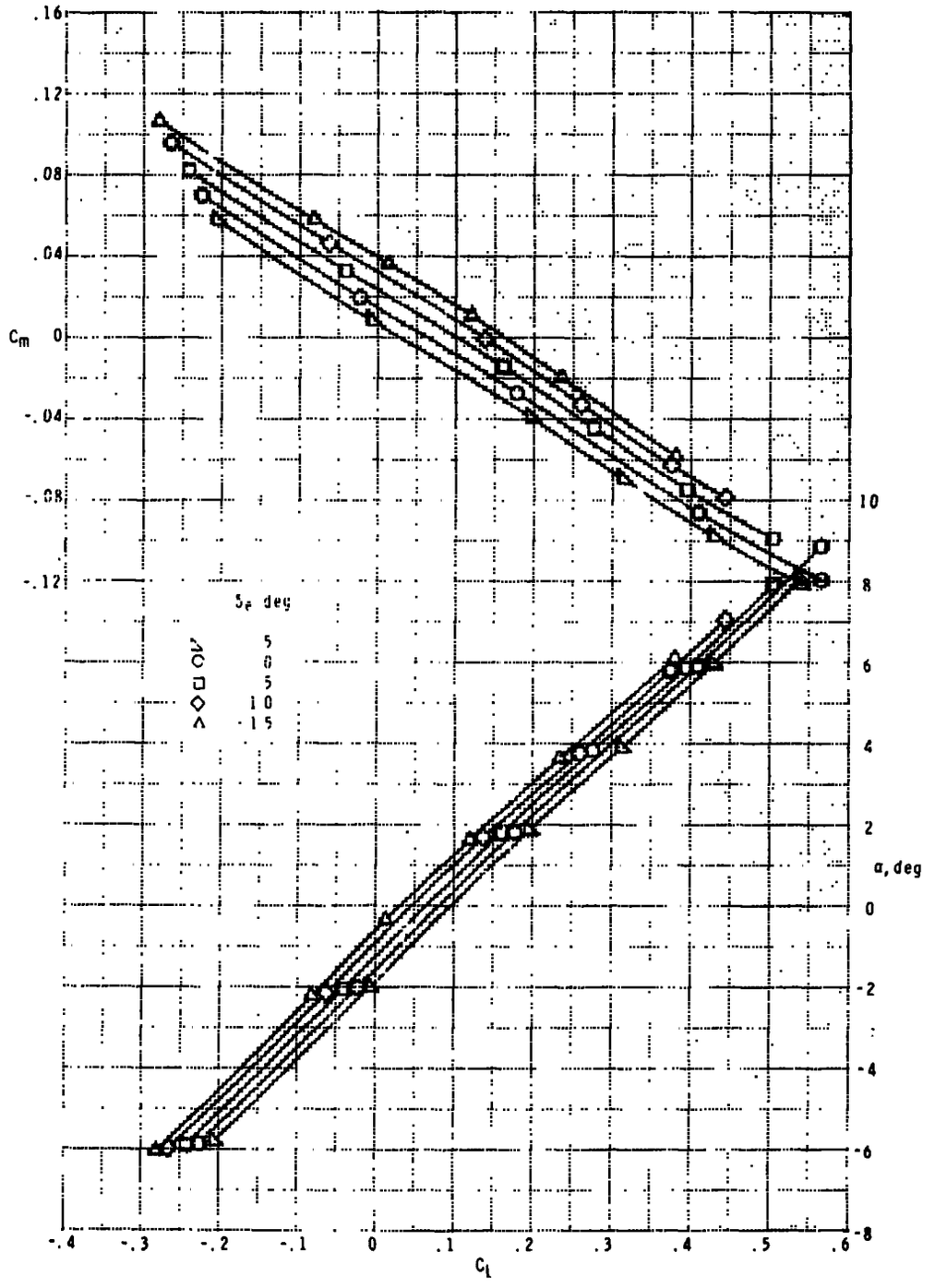

(e) M = 1.2.

Figure 7.- Continued.

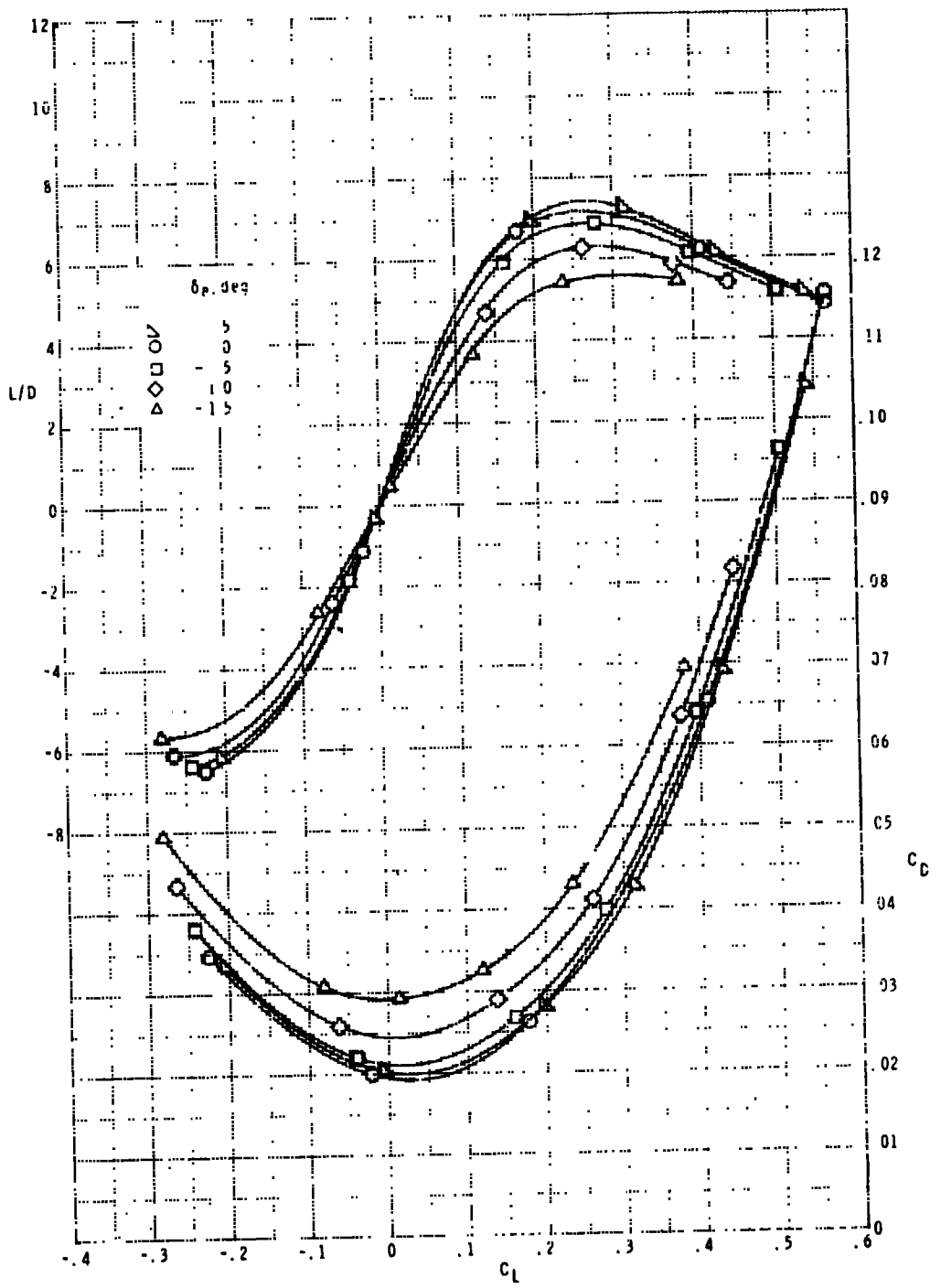

(e) Concluded.

Figure 7.- Continued.

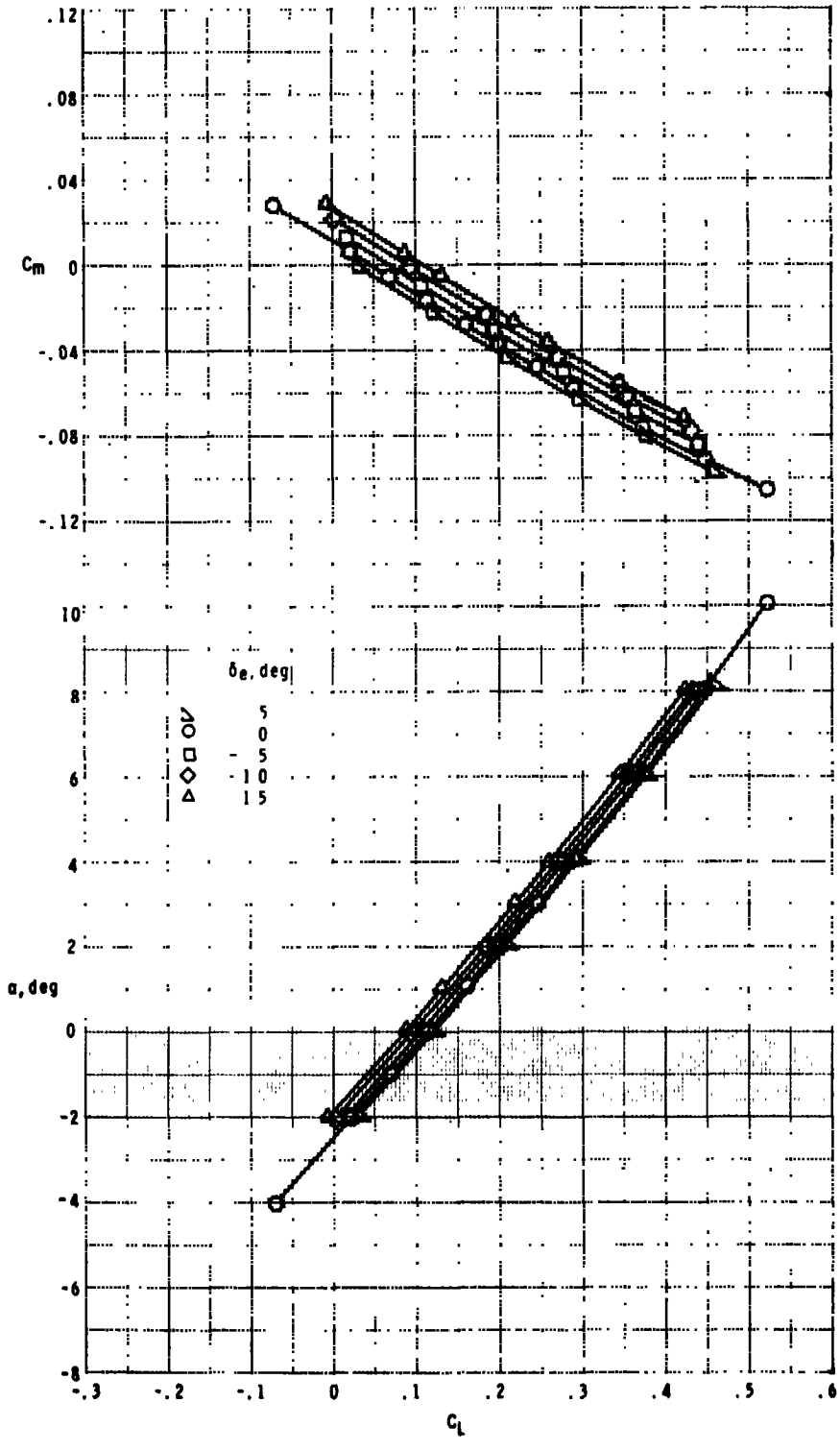

(f) M = 1.6.

Figure 7.- Continued.

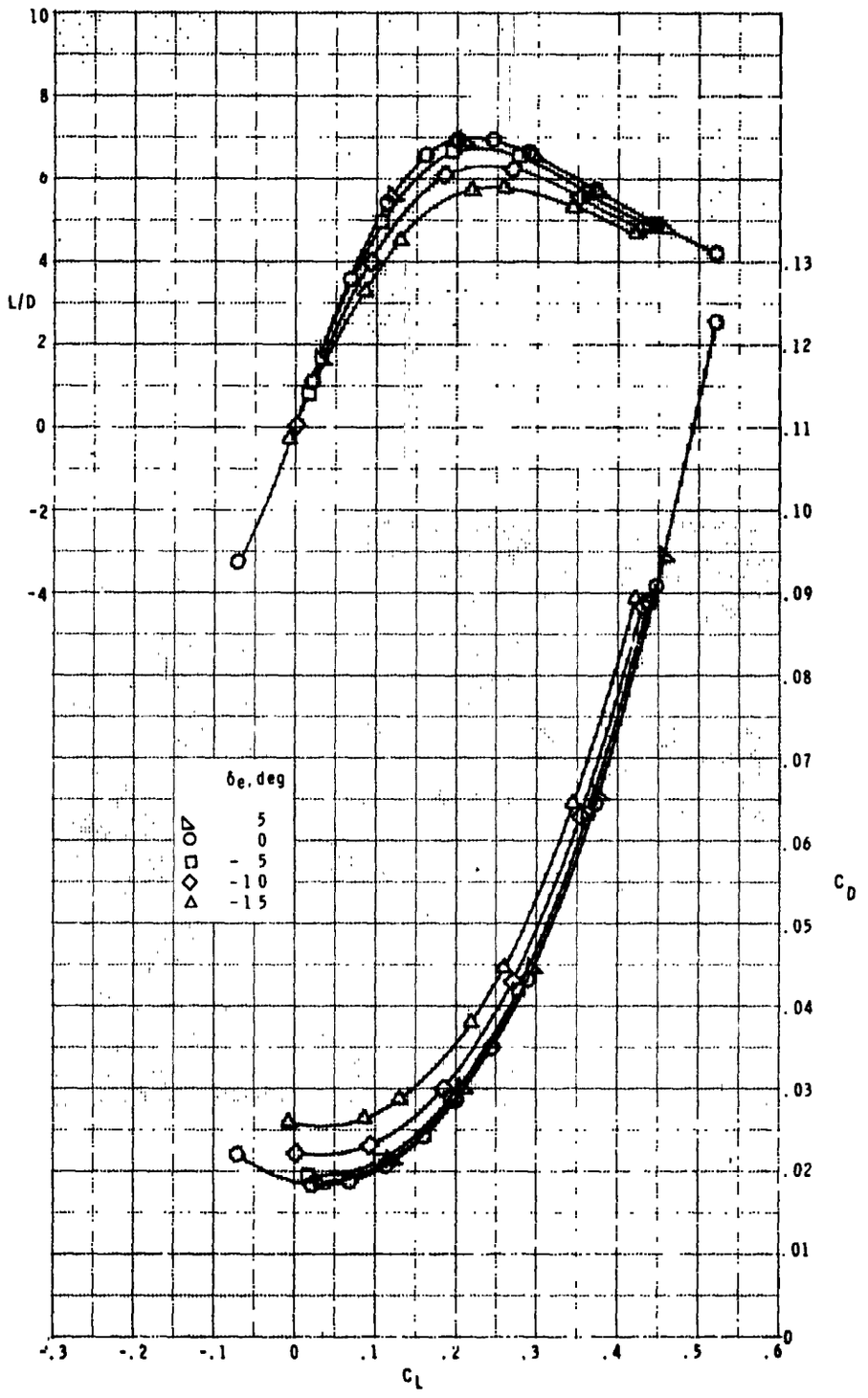

(f) Concluded.

Figure 7.- Continued.

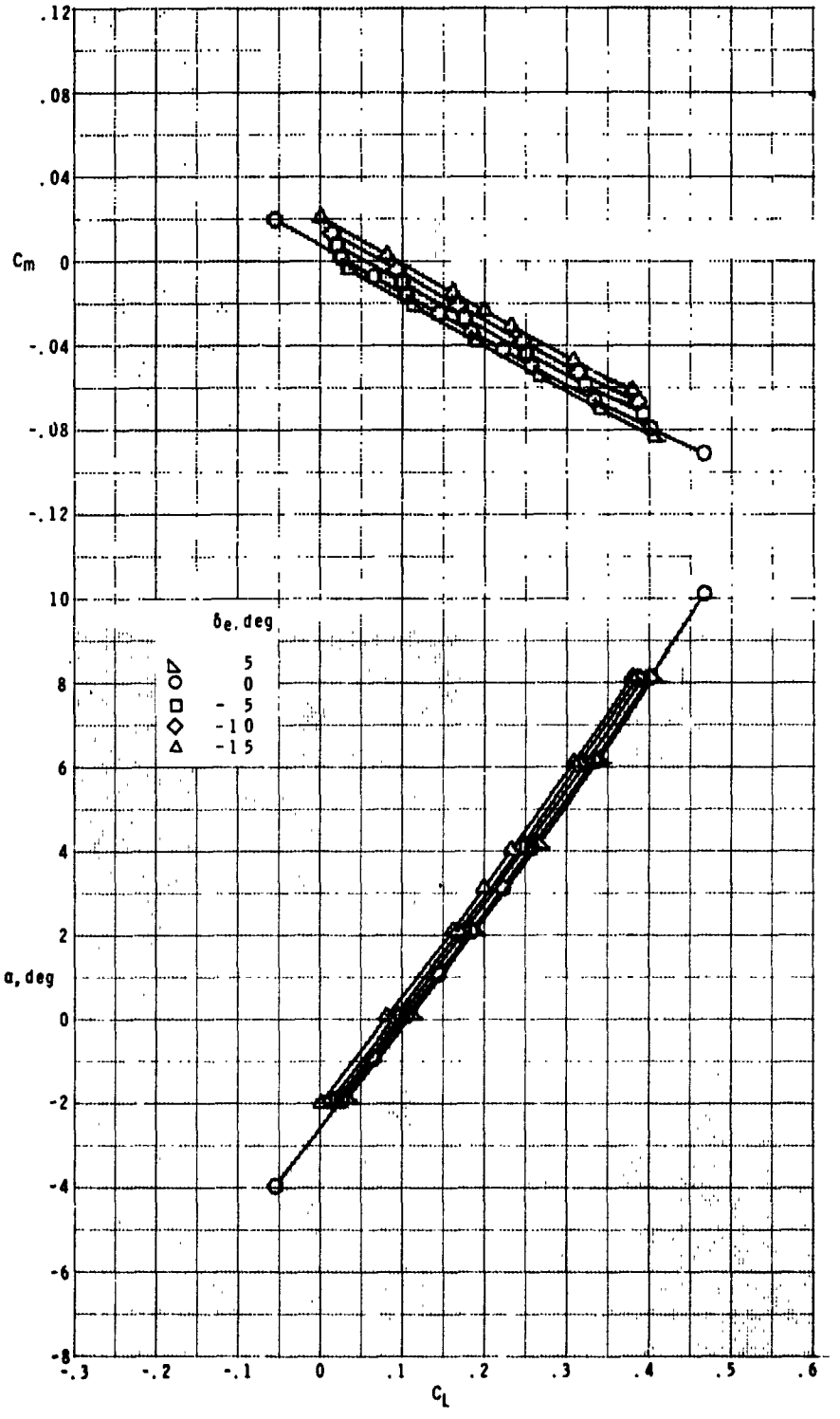

(g) M = 1.8.

Figure 7.- Continued.

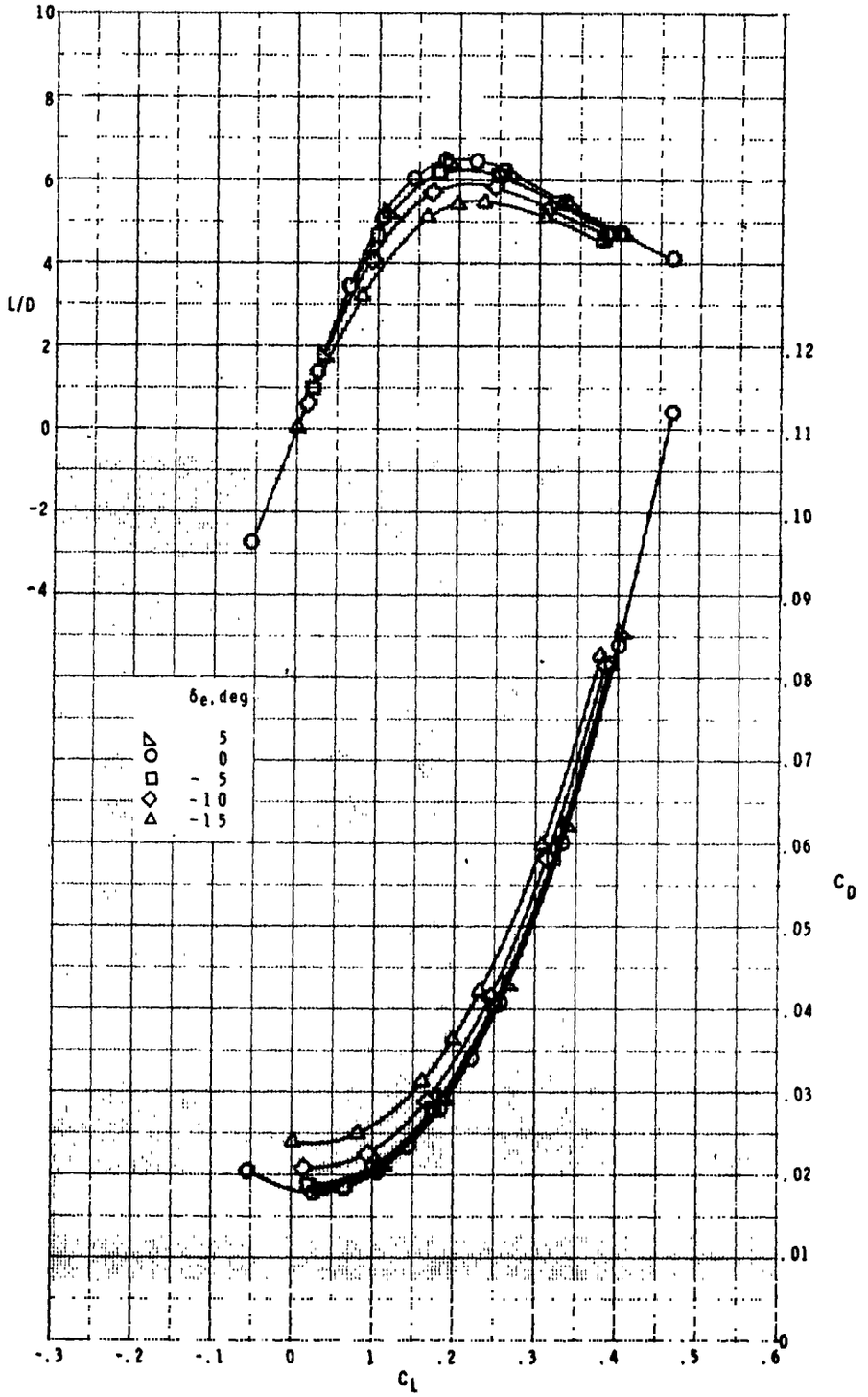

(g) Concluded.

Figure 7.- Continued.

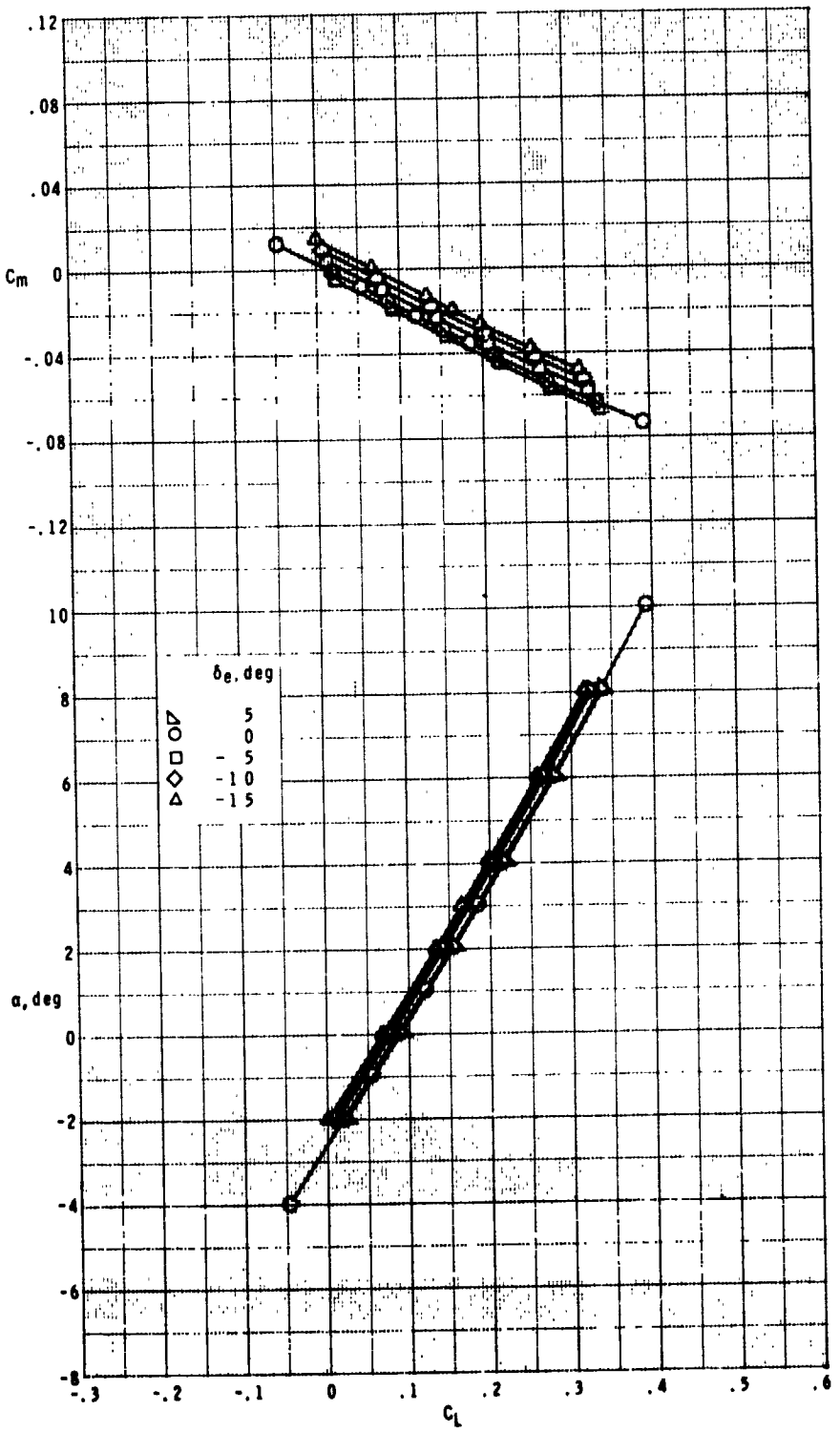

(h) M = 2.16.

Figure 7.- Continued.

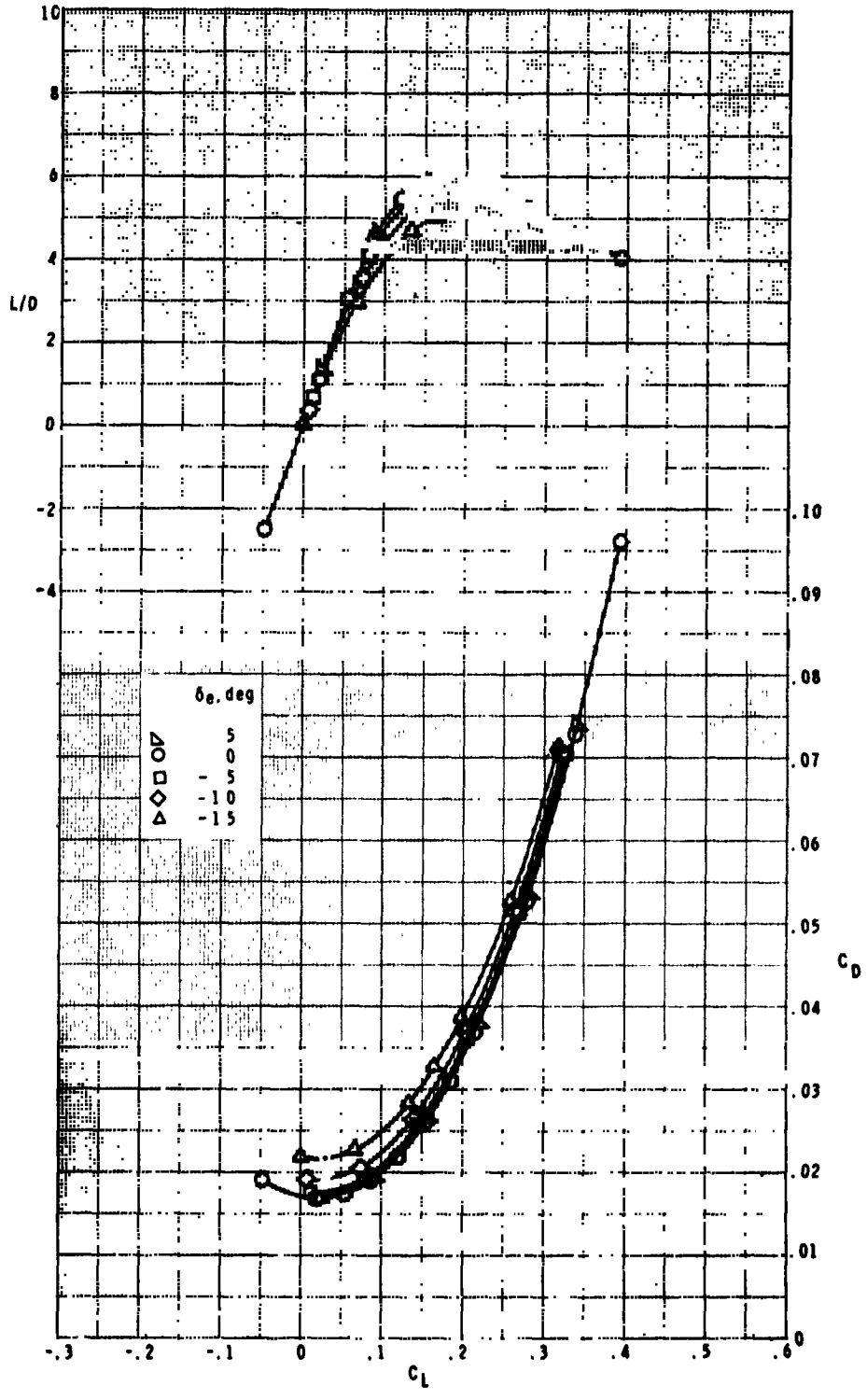

(h) Concluded.

Figure 7.- Concluded.

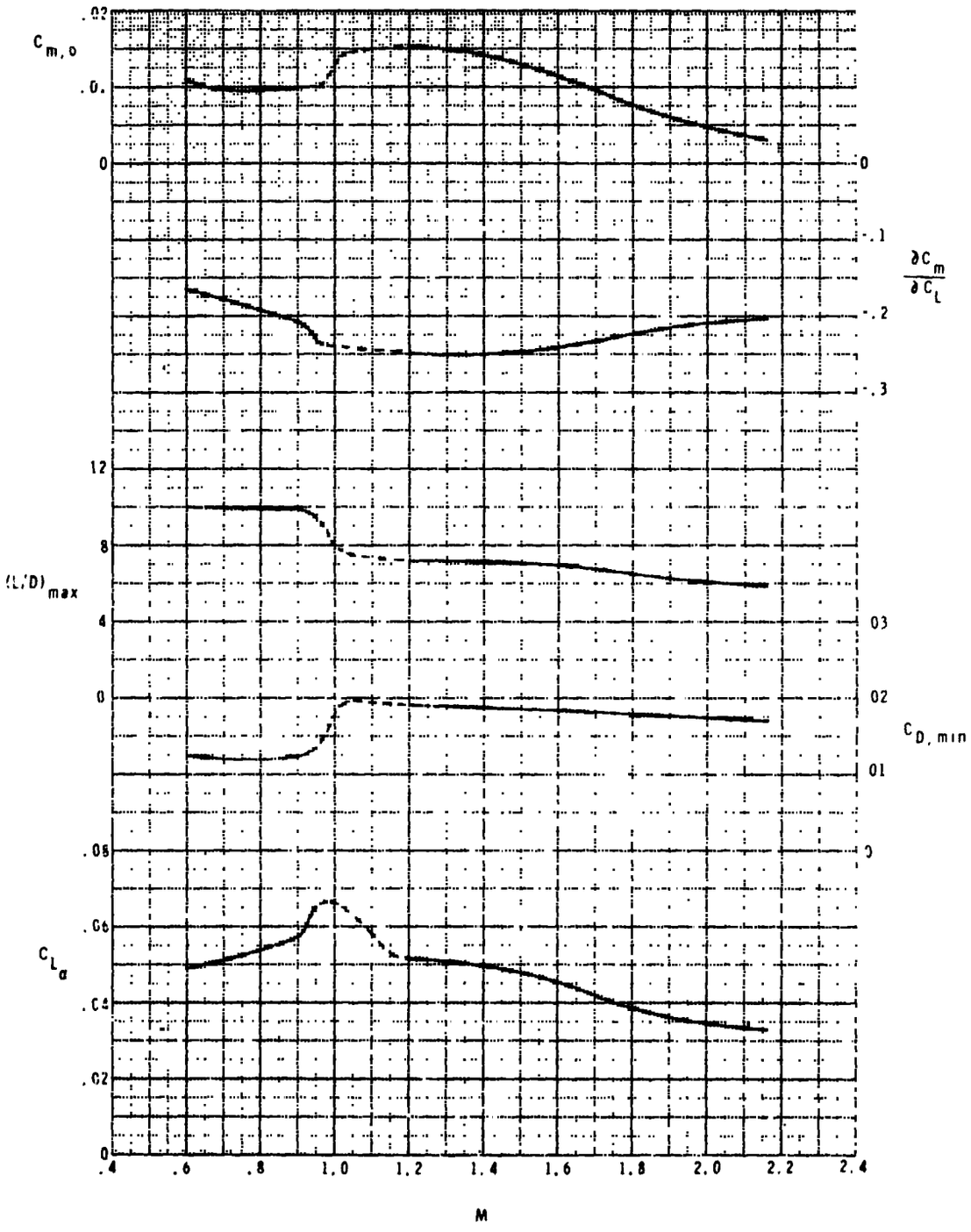

Figure 8.- Variation of some longitudinal parameters with Mach number. WBCVU, $\delta_e = 0^o$.

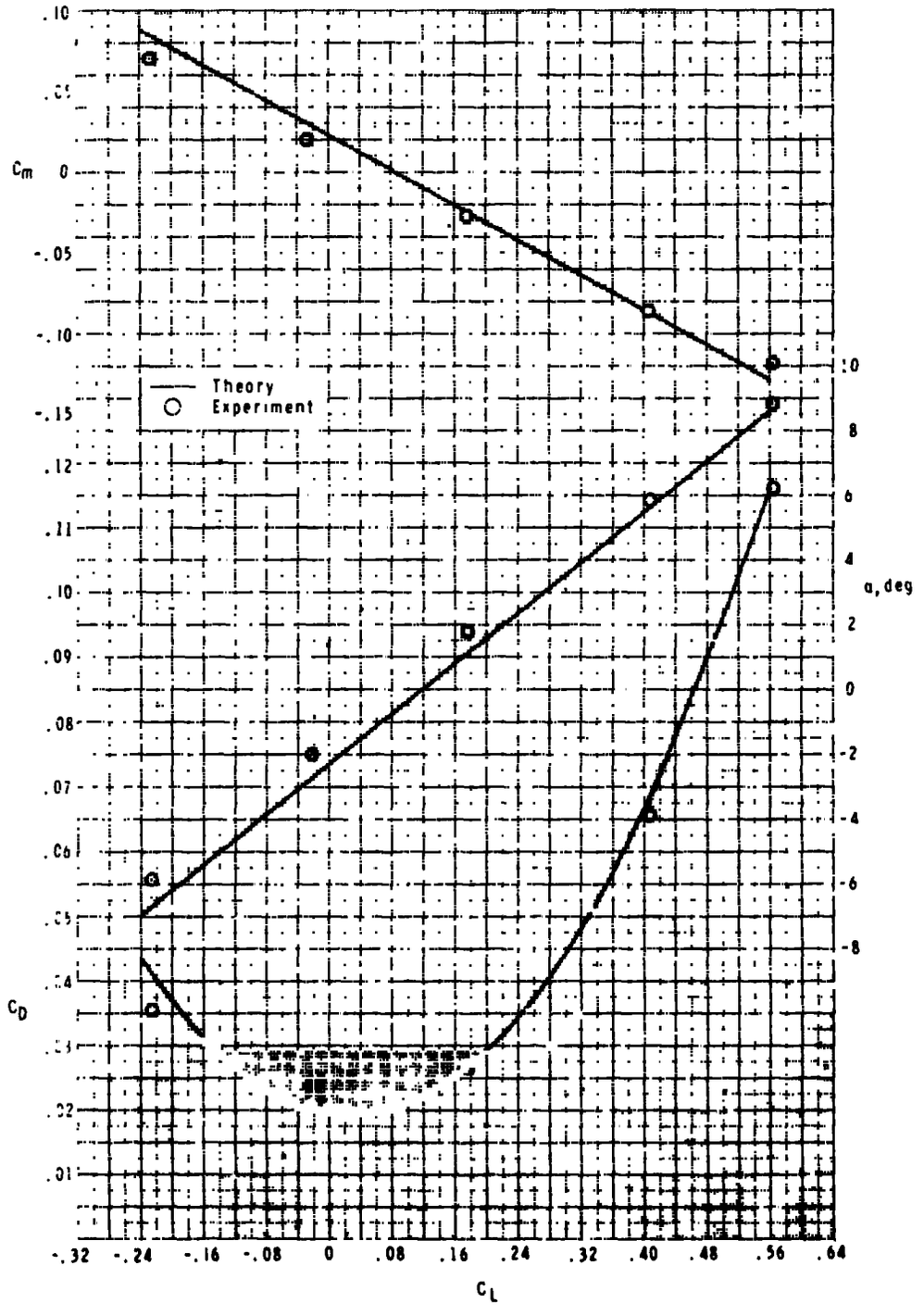

(a) M = 1.2.

Figure 9.- Comparison between theory and experiment at supersonic speeds. WBCVU, $\delta_e = 0^\circ$.

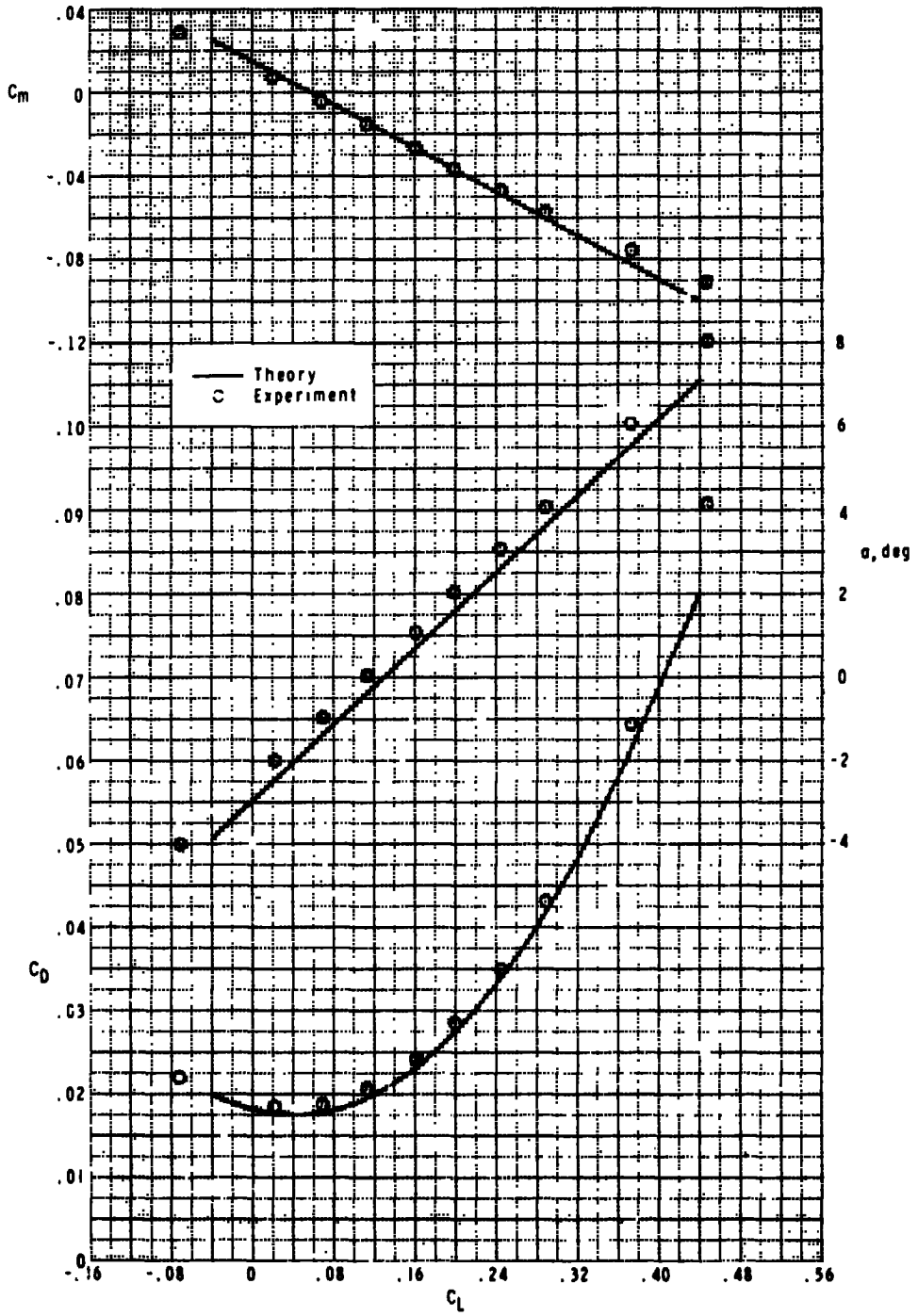

(b) M = 1.6.

Figure 9.- Continued.

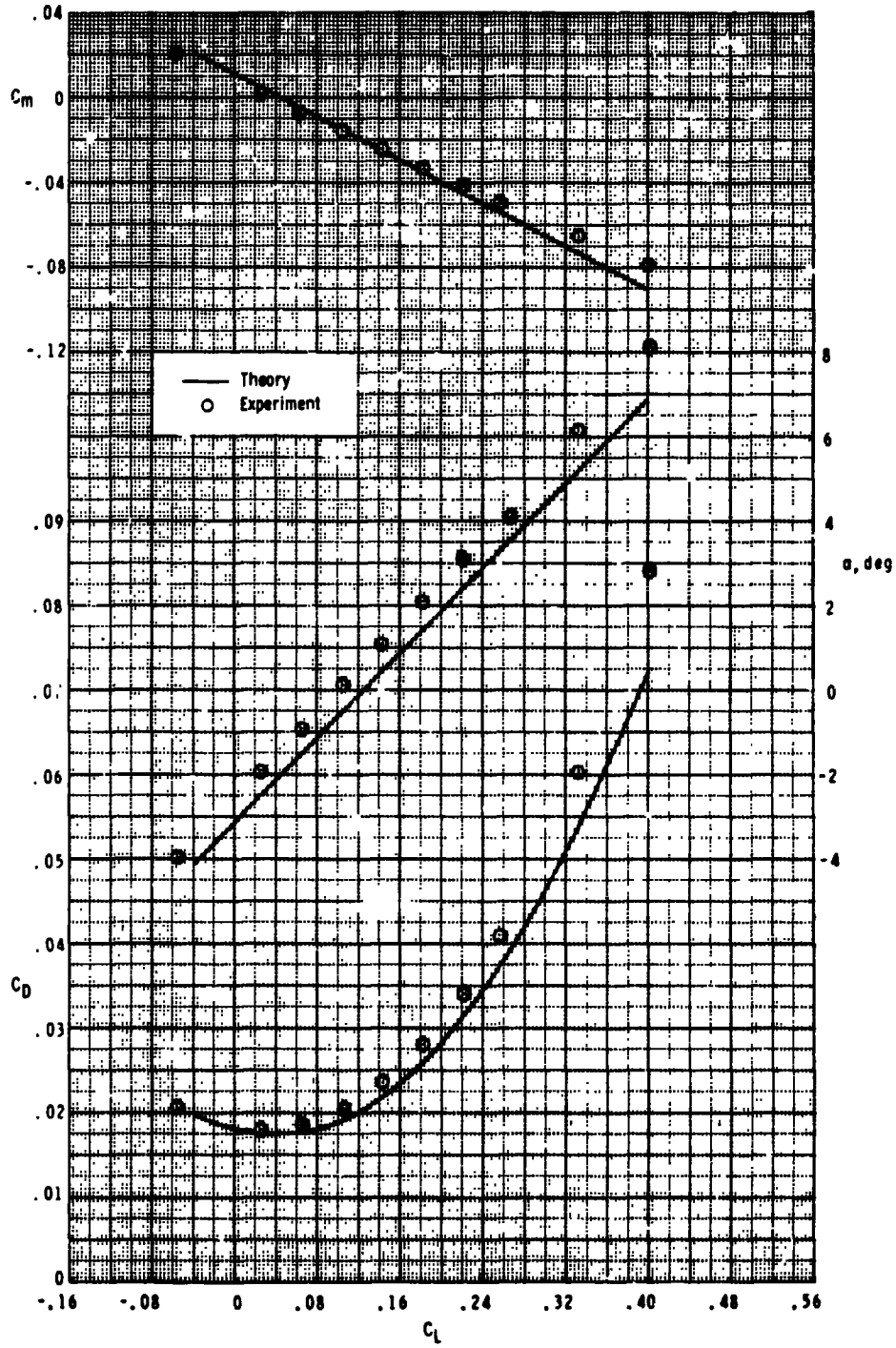

(c) M = 1.8.

Figure 9.- Continued.

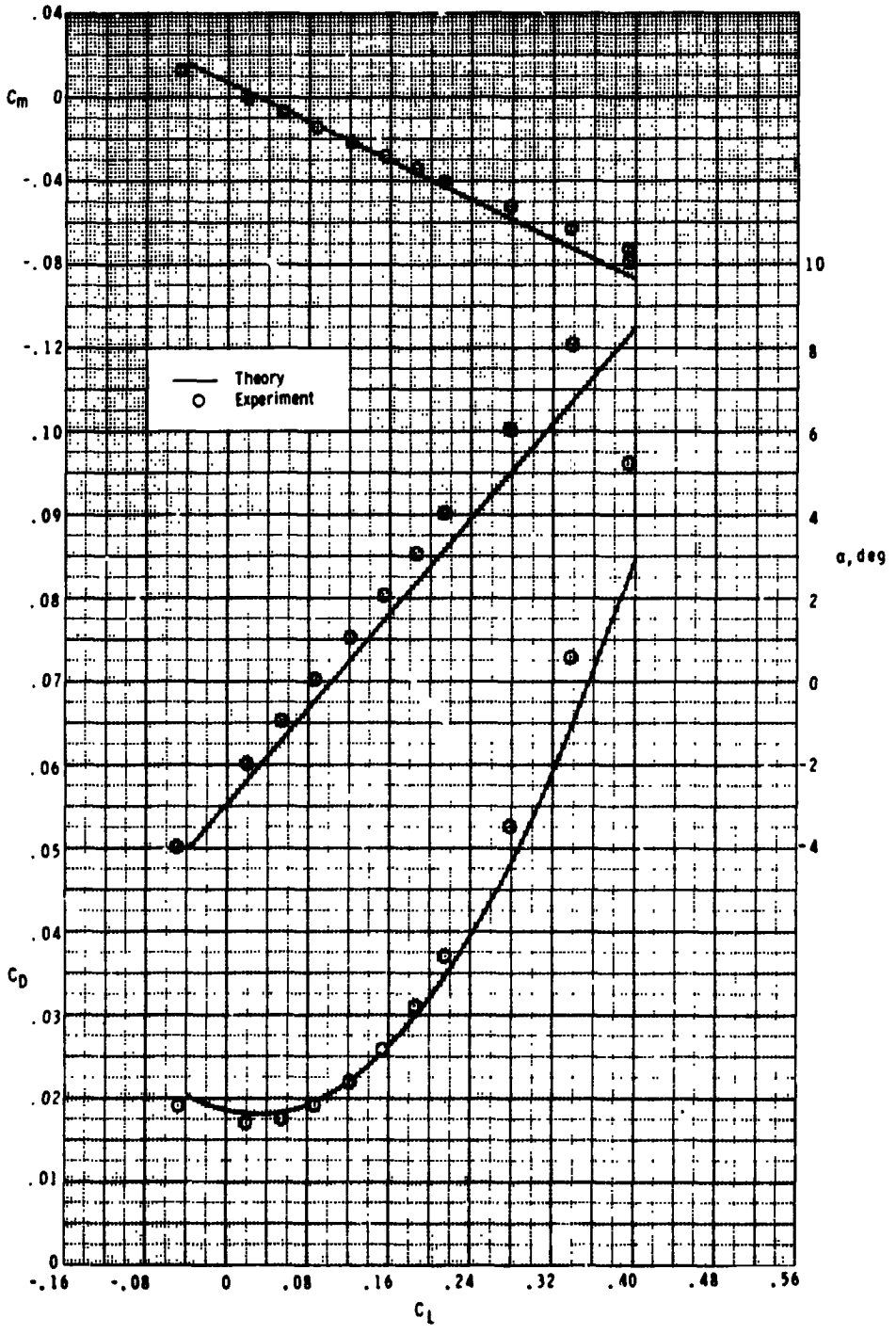

(d) M = 2.16.

Figure 9.- Concluded.

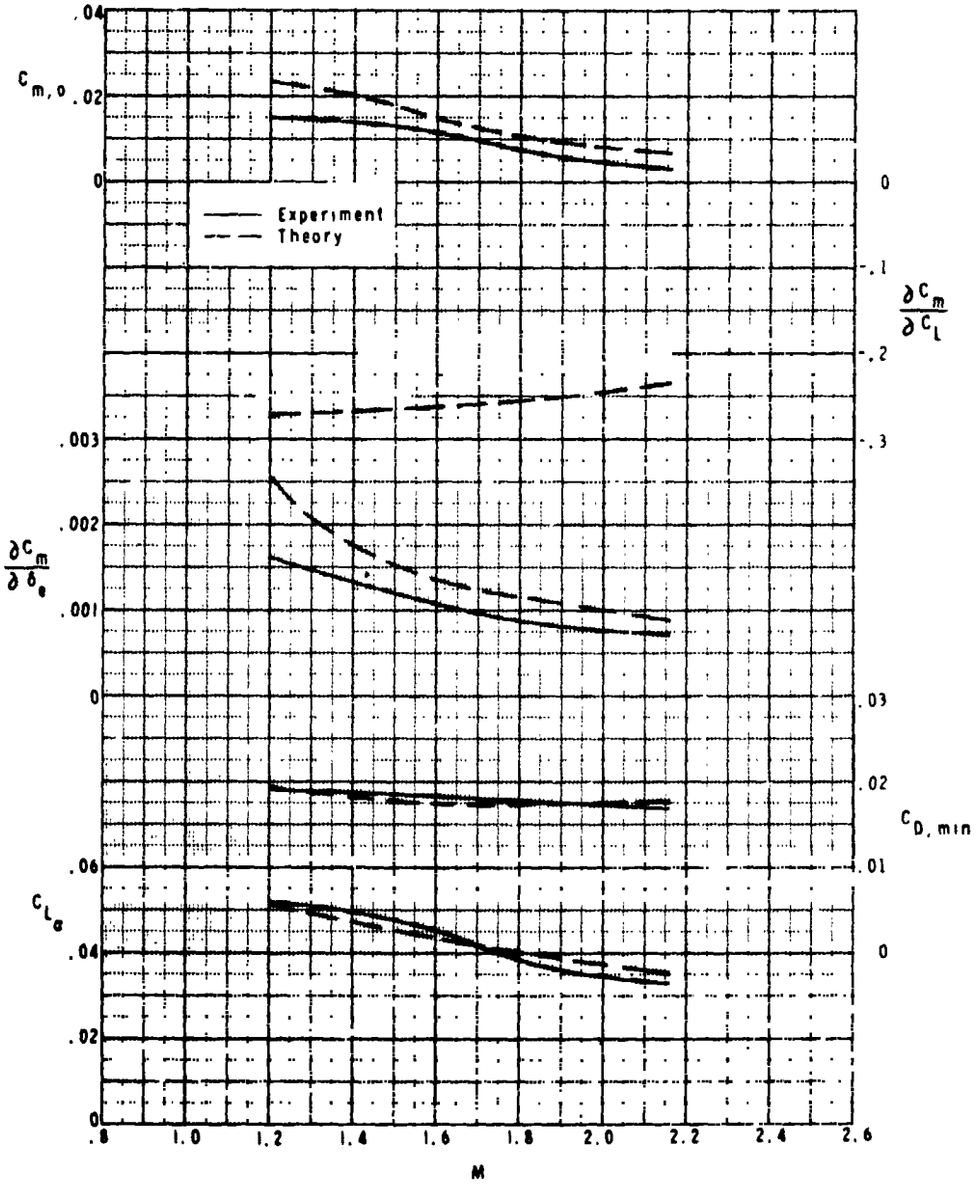

Figure 10.- Variation of some longitudinal parameters with Mach number at supersonic speeds. Comparison between theory and experiment. WBCVU.

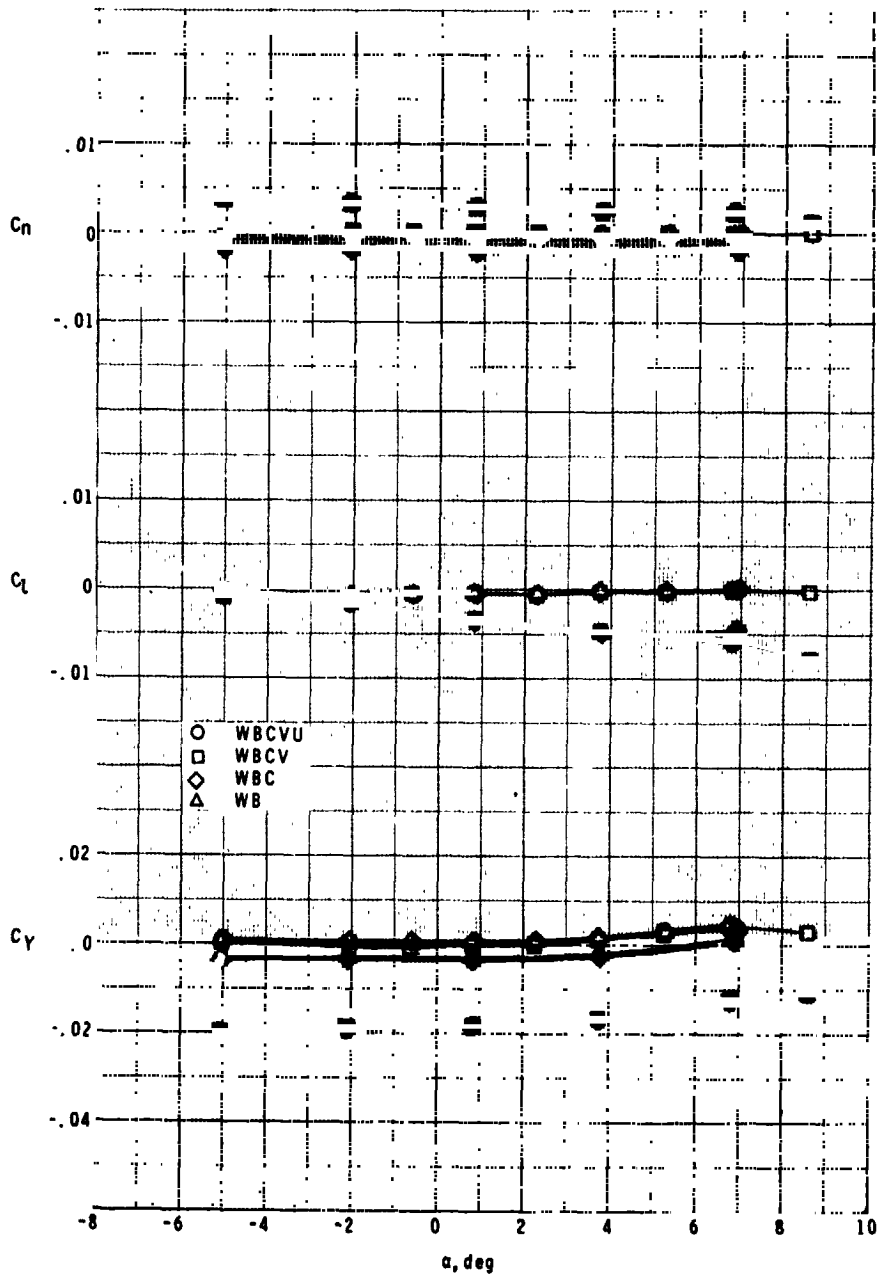

(a) M = 0.6.

Figure 11.- Effect of components on lateral-directional aerodynamic characteristics at subsonic-transonic speeds. $\delta_e = 0^o$. (Open symbols for $\beta = 0^o$, filled symbols for $\beta = 3^o$.)

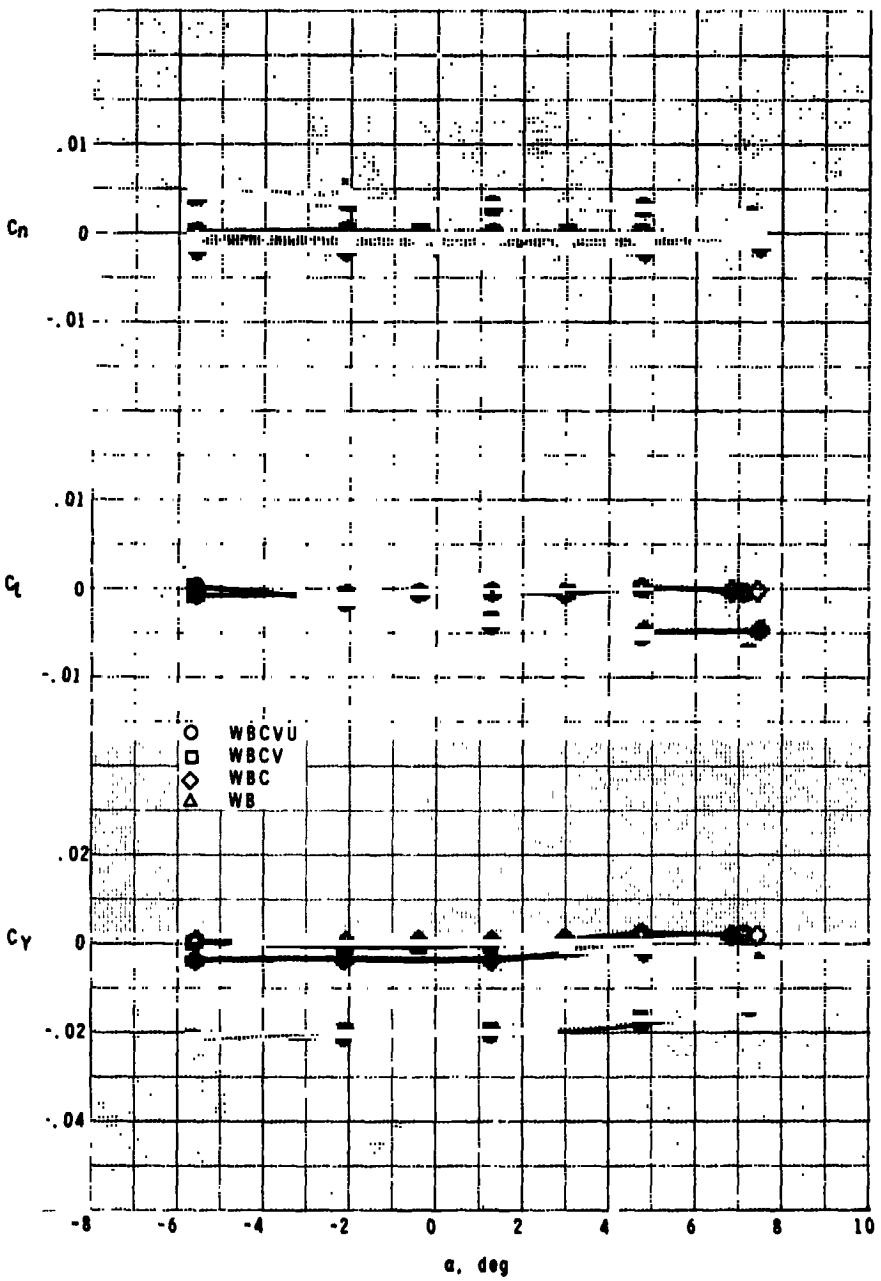

(b) M = 0.8.

Figure 11.- Continued.

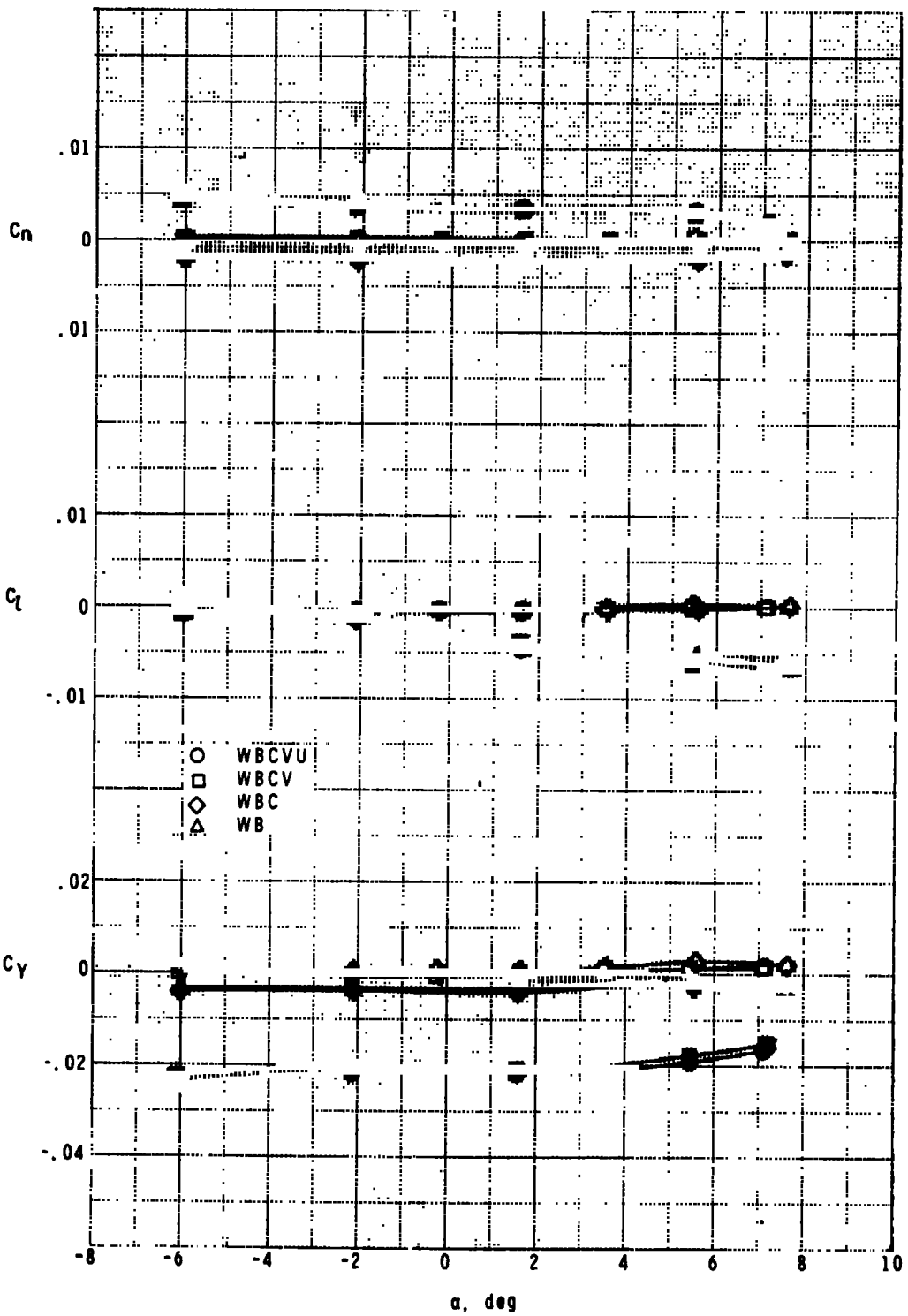

(c) M = 0.9.

Figure 11.- Continued.

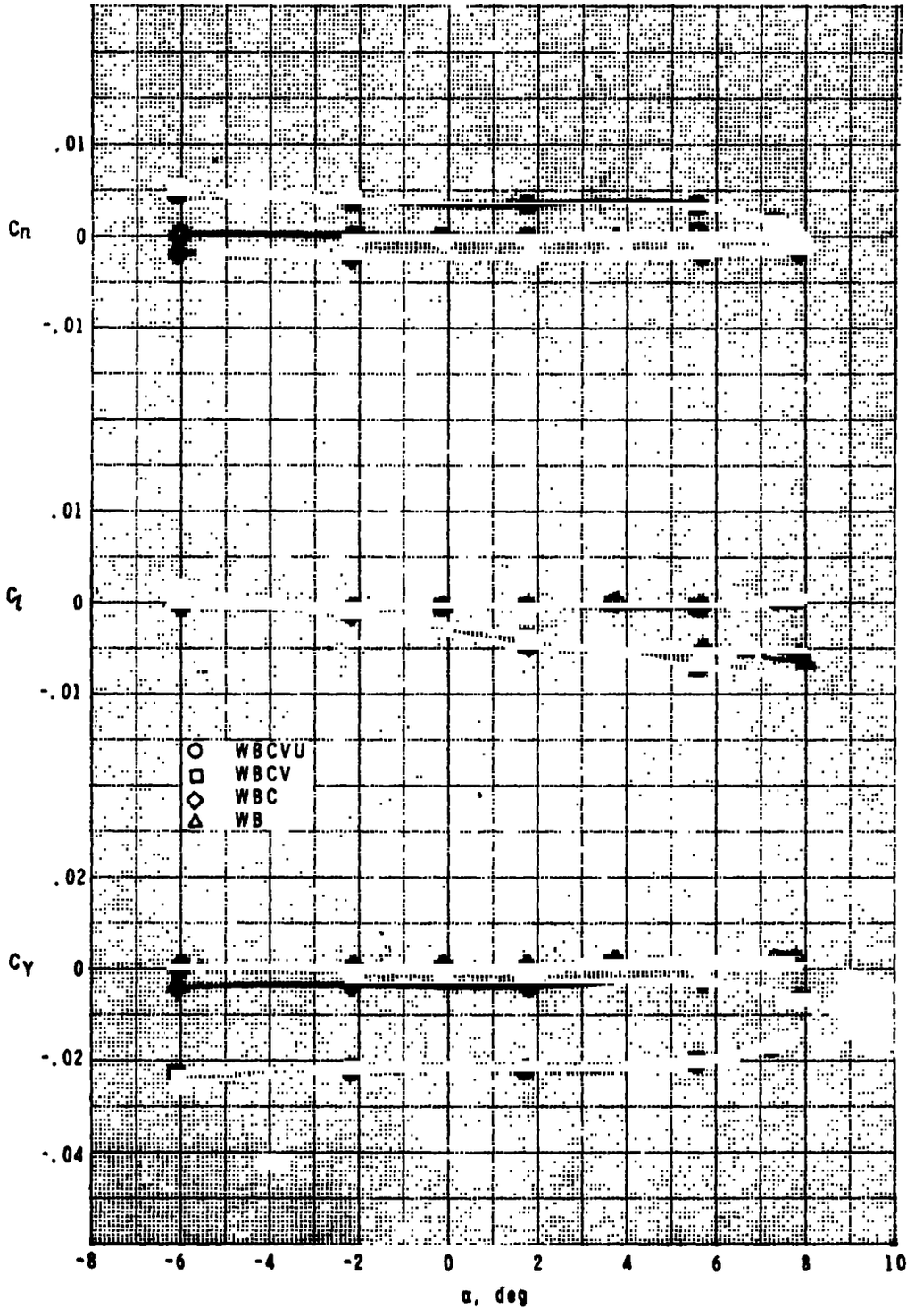

(d) M = 0.95.

Figure 11.- Continued.

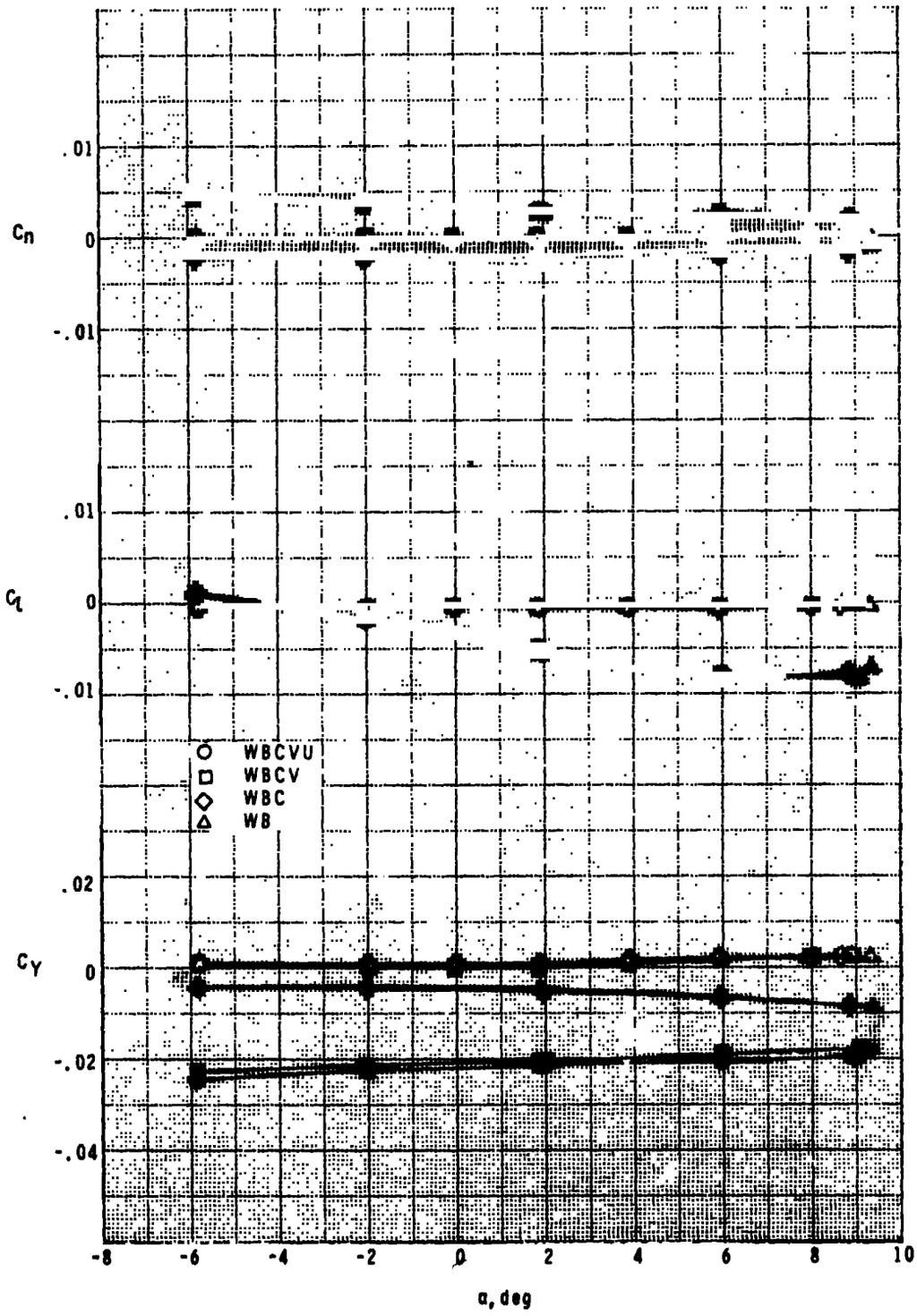

(e) M = 1.2.

Figure 11.- Concluded.

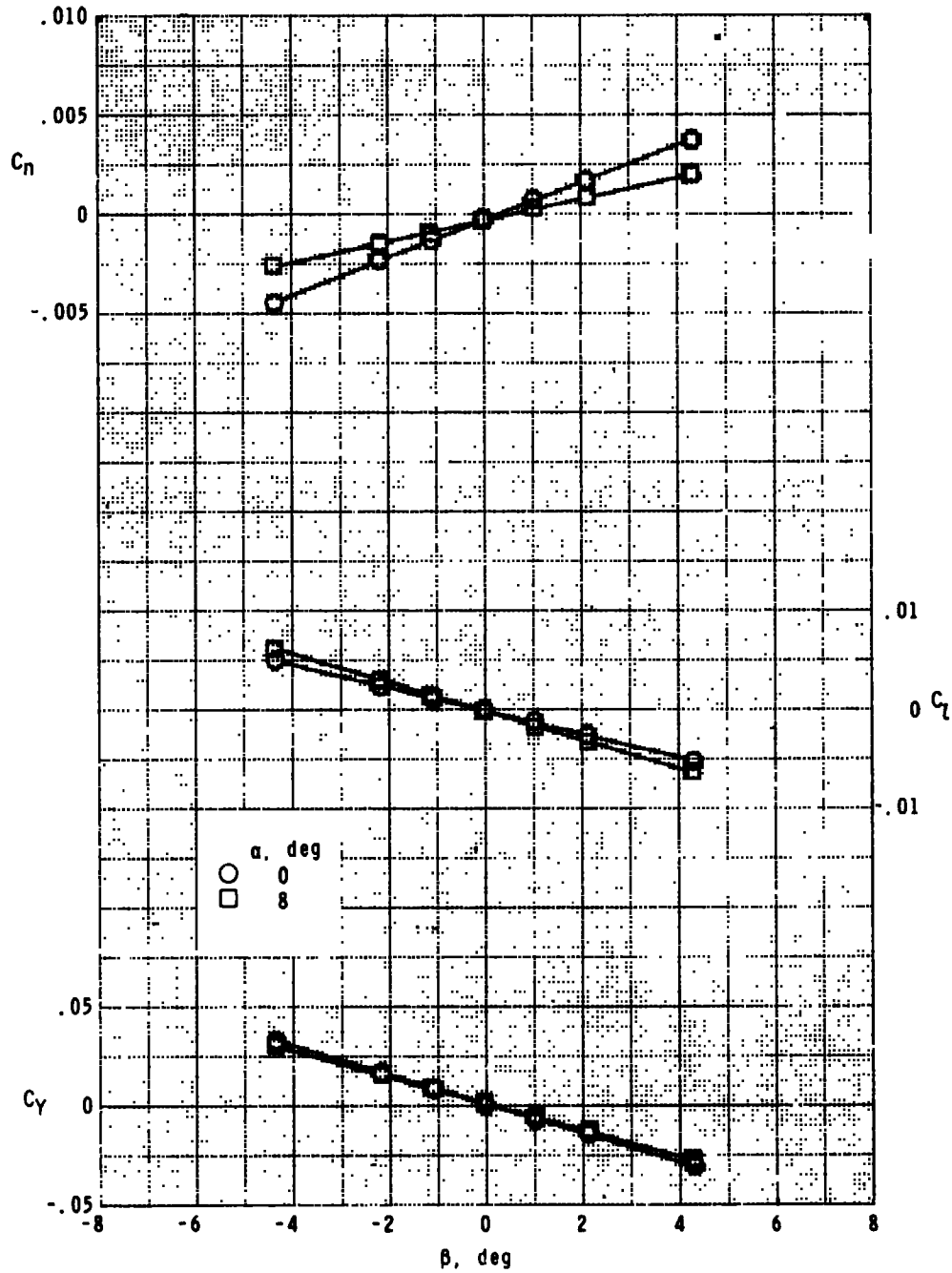

(a) M = 1.6.

Figure 12.- Variation of lateral-directional aerodynamic characteristics with sideslip angle at supersonic speeds. WBCVU, $\delta_e = 0^o$.

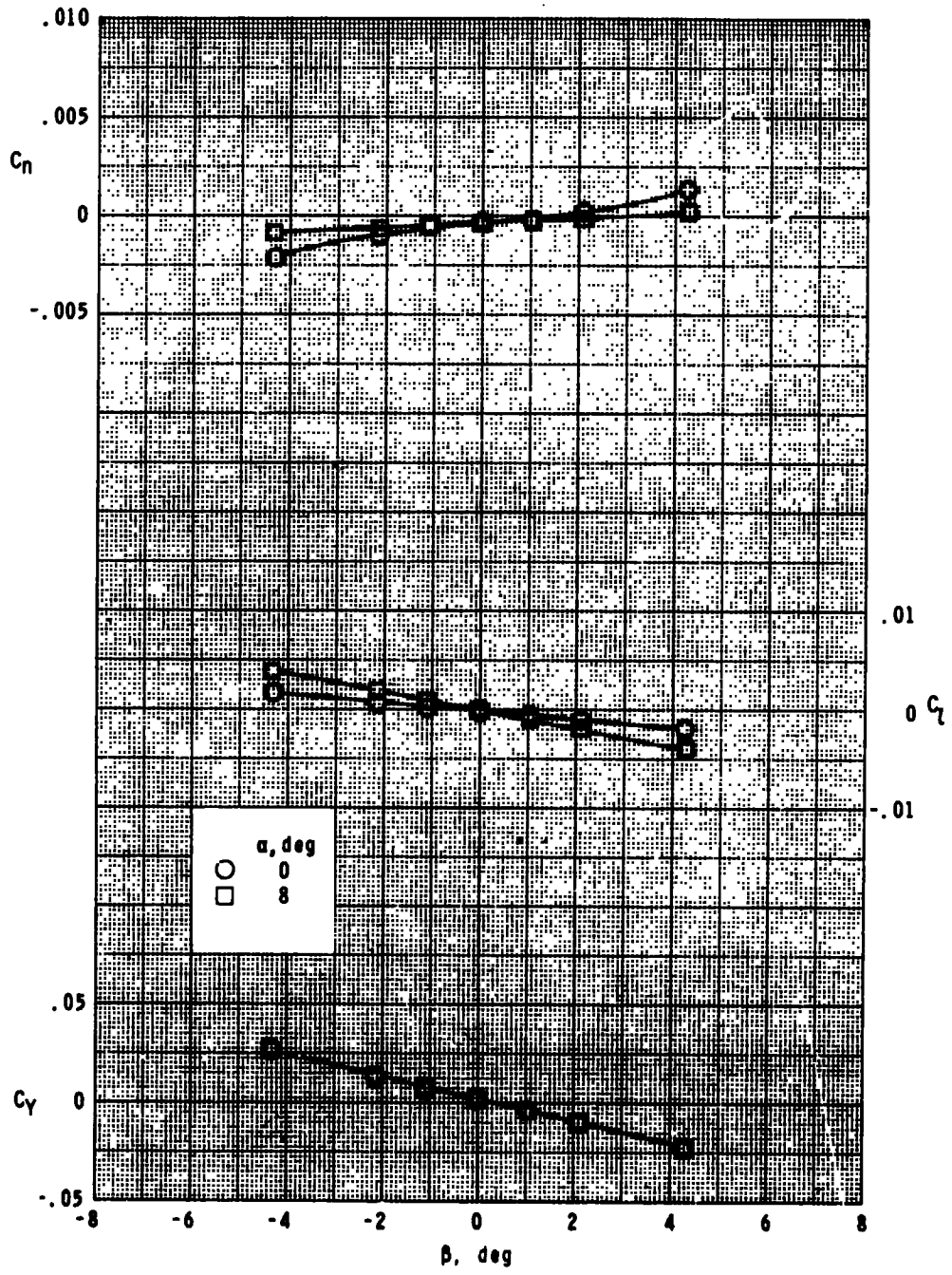

(b) M = 2.16.

Figure 12.- Concluded.

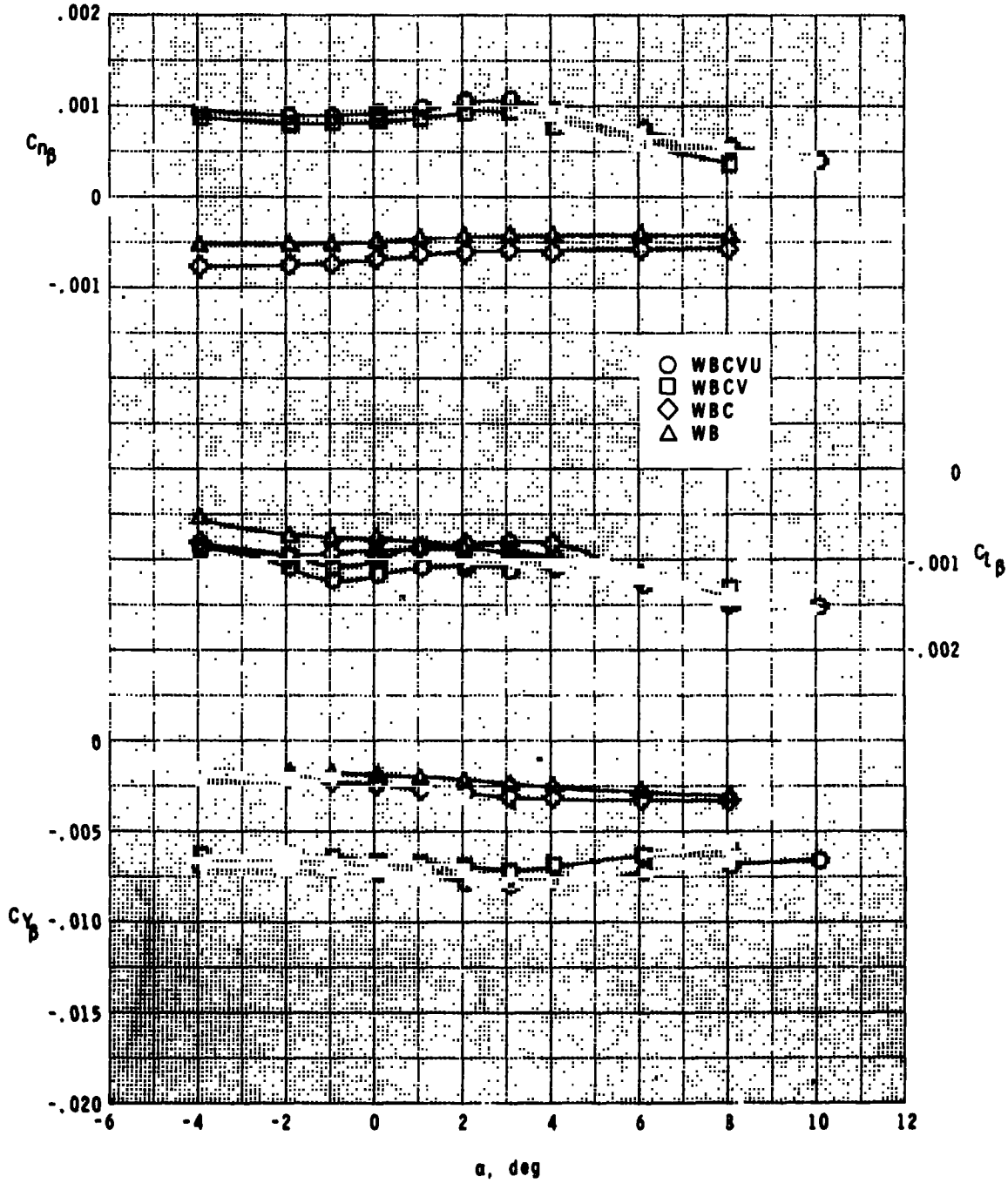

(a) M = 1.6.

Figure 13.- Effect of components on variation of sideslip derivatives with angle of attack at supersonic speeds. $\delta_e = 0^\circ$.

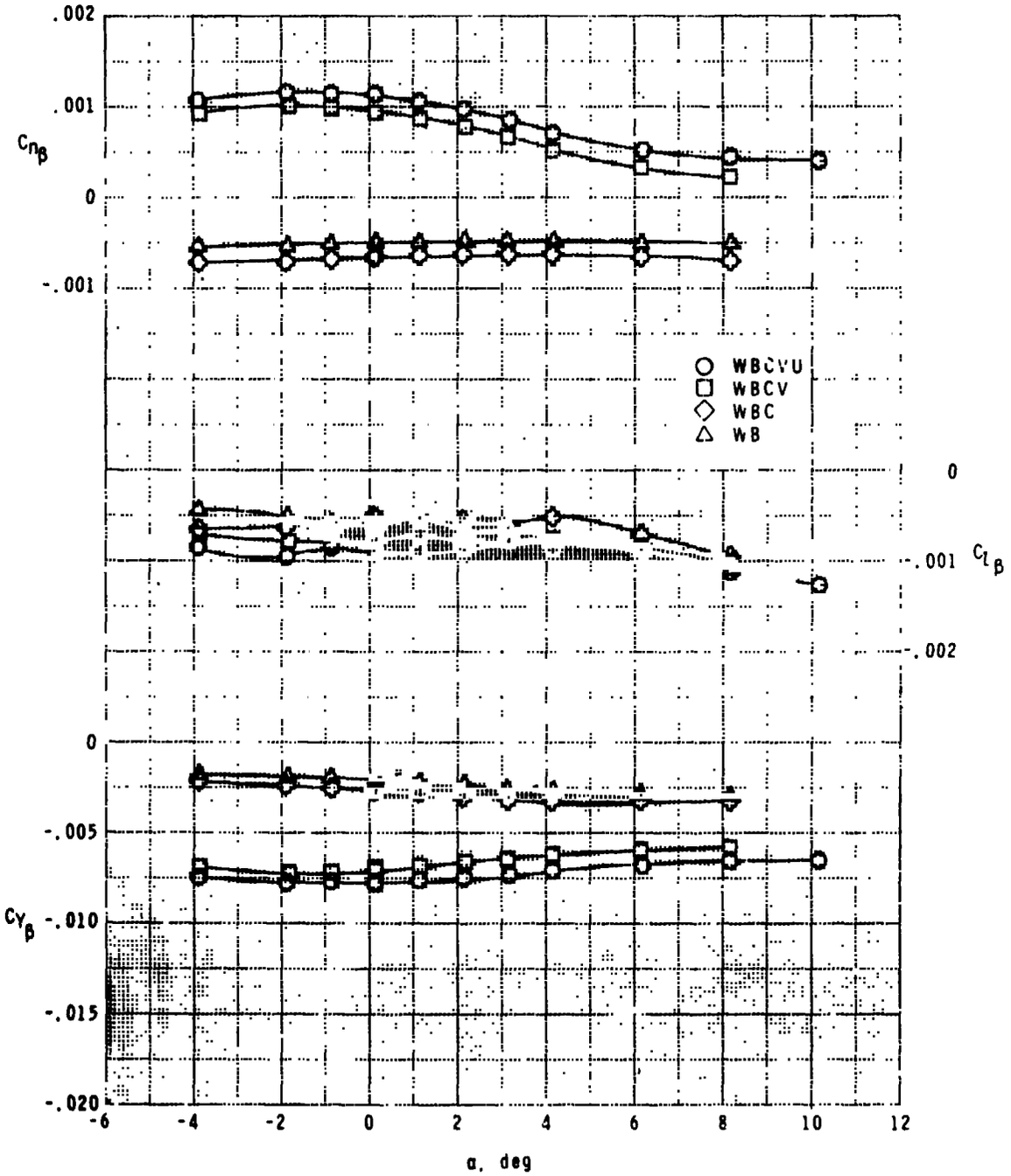

(b) M = 1.8.

Figure 13.- Continued.

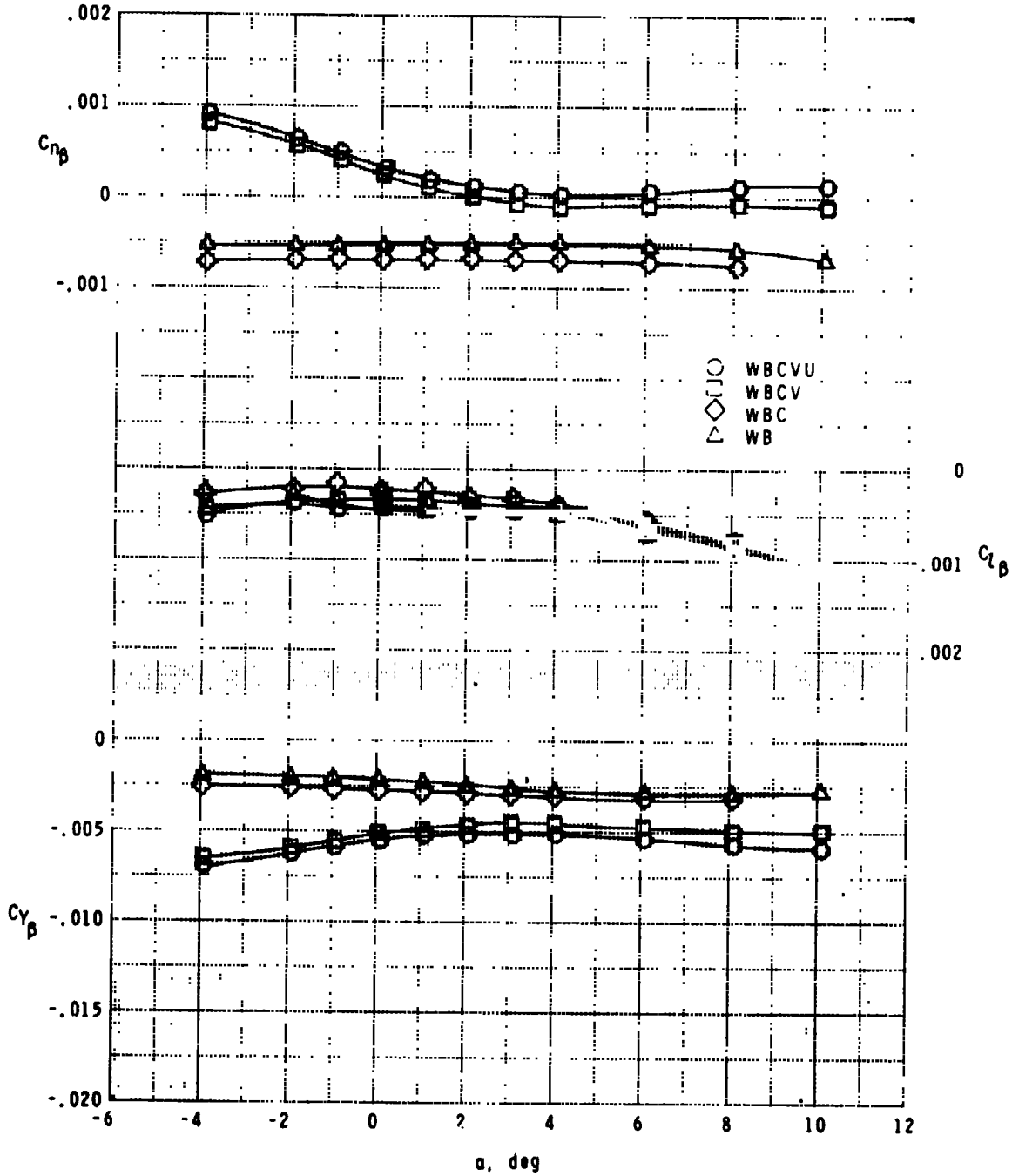

(c) M = 2.16.

Figure 13.- Concluded.